J O U R N A L

OF

MINING AND GEOLOGICAL SCIENCES

CONTENTS

СЪДЪРЖАНИЕ

RECOVERY THROUGH SURFACE-WELDING OF TOOTHED GEARS OF DRUM MILLS

Ivan Minin

University of Mining and Geology „St. Ivan Rilski", 1700 Sofia, E-mail: minin_ivan@abv.bg

ABSTRACT. The majority of the drum mills used in the mining industry have peripheral drive of the drum. This determines the presence of large-sized toothed gears with considerable size, weight and cost. After 8 to 10 years of service, the cog-wheels wear out on the one side of the teeth (depending on the direction of drum rotation), which results in deterioration of the teeth pair operational mode and risk of fracture and failure of the mill unit. Therefore, after expiration of the term of service, they are scrapped or recovered. This article shows a technology for recovery of worn out toothed gears through welding. The method for determining the electrical parameters of the electric arc welding is also explained, as an example it is applied to a gear of a mill type МШЦ 4,5 x 6. All other concomitant technological operations related to the restoration of toothed gears with parameters similar to a new one are also shown here.

Keywords: toothed gear, mill, surface-welding, electric arc

ВЪЗСТАНОВЯВАНЕ НА ЗЪБНИ ВЕНЦИ НА БАРАБАННИ МЕЛНИЦИ ЧРЕЗ НАВАРЯВАНЕ
Иван Минин
Минно-геоложки университет „Св. Иван Рилски", 1700 София, E-mail: minin_ivan@abv.bg

РЕЗЮМЕ. Голяма част от барабанните мелници, използвани в миннодобивната промишленост, са с периферно задвижване на барабана. Това обуславя наличие на едрогабаритни зъбни венци със значителни размери, тегло и цена. След 8-10 години служба зъбните венци се износват от едната страна на зъбите - в зависимост от посоката на въртене на барабана, което води до влошаване режима на работа на зъбната двойка и до опасност от счупване и отказ на мелничния агрегат. Поради това, след изтичане на срока им на служба, те биват бракувани или възстановявани. В настоящата статия е показана технологията за възстановяване на износени зъбни венци чрез наваряване. Обяснена е и методиката за определяне на електрическите параметри на електродъговото наваряване, като за пример тя е приложена на зъбен венец от мелница тип МШЦ 4,5 x 6. Показани са също и всички други съпътстващи технологични операции до получаването на възстановен зъбен венец със сходните параметри на нов.

Ключови думи: зъбен венец, мелница, наваряване, електродъгово.

Introduction

The toothed gears of the mills wear out one-sidedly by reducing the thickness of the tooth. Three methods are used for the gear`s restoration:
- replacement with a new one;
- recovery of the gear through surface-welding;
- correction of the toothed gear via the method of "Negative height correction".

The following has to be summarized about the recovery of toothed gears:
- it is advisable to create a stand with automatic surface-welding devices for worn teeth;
- an electrode or wire consumption is necessary, e.g.its quantity for a toothed gear of drum mill МШЦ 4,5x6 exceeds 1000kg;
- high electricity consumption, associated with the surface-welding of teeth;
- undetermined mechanical properties of the teeth, different from those of the main metal;
- difficulty in the mechanicl treatment (lathing and teeth-cutting) of the welded teeth, leading to further operation, namely temperature recovery in a furnace after the welding;
- thermal tensions between the weld layer and the base metal of the gear, resulting in a decrease of the teeth mechanical properties, variation in their geometric shapes, microcracks and lower reliability and term of service of the toothed gear.

To apply the "Negative Height Correction" method, we need to have the following prerequisites:
- the presence of a residual thick bandage of the toothed gear, allowing a negative height correction (pitting of the cutting contour at the teeth-cutting) without affecting the solidity and deformation characteristics of the gear;
- the possibility of displacement of the center-to-center distance of the gear.

The technology of toothed gear recovery through a "Negative height correction" has the following advantages:
- the geometrical and kinematic characteristics of the reconstructed gear are equivalent to the normal features of a new one;
- the teeth are made entirely of the gear's main metal;
- the mechanical treatment (lathing and teeth-cutting) is several times smaller in volume, than when making a new toothed gear;
- the exact calculation of the height correction allows very rapid and good recovery of the gear;
- the installation works, when replacing a repaired gear, are with lower labor costs than during the installation of a new toothed gear;

- the technology including a height correction can not be used in mills, where it is not possible to displace the center-to-center distance or there is a thin bandage.

The main question that may be set in the present study is about the possibility to recover a toothed gear through the surface-welding method and its economical justification.

Summary

The aim of the present study is to describe the activities of a vast recovery of large-scale toothed gears through surface-welding and to prove the quality of this technology.

Technology and equipment for toothed gears recovery through surface-welding. On the basis of what has been mentioned above and having in mind that the technology includng a height correction can not be used in all mills, a technology for recovery through surface-welding is proposed. This repairing technology covers a number of activities carried out in the following order:

Identification of the toothed gear. After removing it from the mill, the gear is stored in two or four parts (Fig. 1). The next step is testing after thoroughly cleaning of all contact surfaces (A_1, A_2) and the gear parts. The cleaning is performed with a metal brush and sandpaper in order to remove all mechanical contaminants and metal oxides on the co-mounting surfaces.
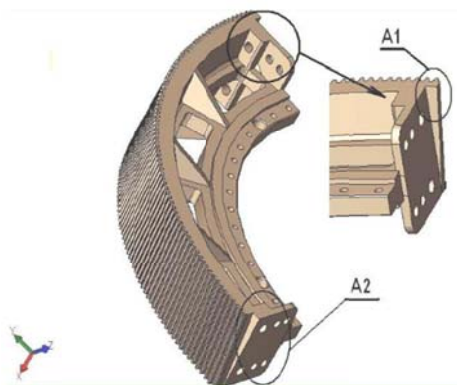
Fig. 1. One fourth of a toothed gear

The trial installation aims to establish the compliance and the affiliation of the separate parts of the gear. After that, the gear is separated and transported to the machine factories for a mechanical processing.

Preparation of a gear for surface-welding. When worn out parts are recovered, the place to be welded (the worn out part of the tooth) must be cleaned to a metallic gloss. This is done by sandblasting, technical brushes attached to a mechanized hand tool or by grinding with a DASH disk driven by an angle grinder. Regardless of the chosen mode, the cleaning should cover the welding area and in addition, 10-15mm around it.

During the recovering of the worn out part of the gear it is necessary to remove the top layer of metal from the working surface due to the danger of old cracks and other defects that can develop in depth of the part or in the welded layer. For this reason, these areas with defects are taken off in depth until they completely disappear. The area of the gear that is meant to be welded should not have sharp edges, so there should be made roundings with a radius over 3-4mm. Occasionally, when welding details with more complex shapes, a special bending (bed) for the welded metal is made, which takes into account the required thickness of the layer and the addition for the mechanical treatment, as well as the conditions for more convenient surface-welding.

When welding the toothed gear, the basic metal must be in inversely heated condition to have sufficiently high plasticity to absorb stresses and deformations.

The cleaning is done with metal brushes, sandpapers and sandblasting apparatus in order to remove all mechanical contaminants and metal oxides on the main metal onto which the surface-welded layer will be placed (Fig. 2).

In order to achieve a better quality of the coated layer and fewer defects, it is recommended the sectors of the toothed gear to be heated up to 150 degrees prior to the teeth welding.
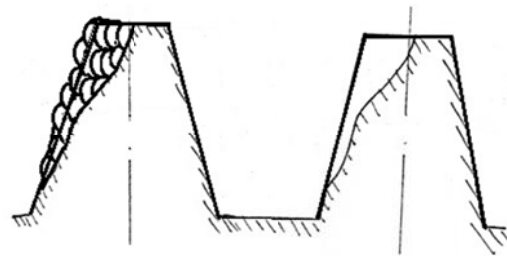
Fig. 2. A layer intended for surface-welding

Technological parameters of welding. The main parameters, determining the technological mode of welding are: the type of grease coating and the thickness of the electrode or electrode wire; the amperage, voltage and polarity; the length of the arc and the speed of movement of the electrode or the handle. These parameters determine the size and quality of the surface - welded layer as well as the character of the heat influenced area.

The welding should be done with a minimal arc length and without any interruptions. In order to avoid defects, the excitation as well as the break of the arc are as far away as possible from the welded layer. The surface-welding should be performed insuch a way that each subsequent transition overlaps from 1/3 to 1/2 of the previous one. The toothed sectors of the gear are placed in such a manner that the manual arc welding to be horizontal and comfortable for the welder (Fig. 3).

Fig. 3. A method of placing the gear at the welding

Selection of electrodes or wire for welding. Generally, the electrodes are selected with a basic thick grease coating, and the choice of electrodes and wire is determined by the chemical composition of the main material. In this case the rule is that the chemical composition of the electrode or wire corresponds as much as possible to the basic material. However, when it is necessary to increase the wear resistance of the parts, it is recommended to use alloyed materials, for example with a high content of manganese or chromium. Generally, the welding technology must be pursuant to the features of the basic material so that no structural changes occur in the part under the influence of the thermal welding mode.

At the manual welding, the electrode quality is of a great importance.

When there is a large difference in the compositions and properties of the base and the welded material, defects (cracks or flakes of the coated layer) may occur, so it is necessary to use the so-called intermediate layers.

Once an electrode or a wire is selected for welding according to their mechanical properties and chemical composition, the next step is the selection of the diameter of the electrode rod or the wire. This choice is determined by the required thickness of the welding layer and for this purpose the information presented in Table 1 is recommended.

Table 1.

Diameter of the electrode, mm	3	4-5	5-6
Thickness of the welded layer, mm	Up to 1.5	Up to 5	over 5
Number of welded layers	1	2	2 and more

When determining the overall thickness of the surface-welded layer, it is also necessary to provide an addition (2-3 mm), because subsequent mechanical processing is required.

Determination of the electrical parameters of the welding. The selection of amperages depending on the diameter of the electrode is based on the constant current loading of the electrode rod cross-section. The approximate amperage for electrodes with a diameter of 3 to 5 mm is determined by the formula:

$$I = k.d, A \tag{1}$$

where: d is the diameter of the electrode;

k - coefficient varying in the ranges from 30 to 50, proportional to the diameter of the electrode.

More precisely, the amperage, depending on the diameter of the electrode, is determined by the empirical formulas:

$$I = (20 + 6.d).d, A \tag{2}$$

$$I = (20 - 25).d^{1,5}, A \tag{3}$$

Based on the formulas 2 and 3, the indicative values of the current are calculated, depending on the standard diameters of the electrodes (Table 2).

Table 2.

Diameter of the electrode, mm	2.5	3.25	4	5	6
Current amperage, A	60	100	150	200	340

The data from Table 2 is indicative because the optimum values of the current depends, allthought to a lesser extent, on the chemical composition of the electrode, the type of grease coating, the length of the arc, the welding rate and other factors. When using wire feeders, only the diameter of the wire is set and the current is automatically determined by the welding machine.

A selection of the welding mode. It is recommended to be performed at a short arc, without interruptions and with minimal melting of the base material. The arc must be excited and interrupted, if possible, outside the working part of the welded layer. Table 3 shows the mode procedure at the surface-welding of a toothed gear of a mill type МШЦ 4,5 x 6.

Table 3.

El. d, mm	Pol.	I, A	U, V	t, s	L, mm	V, $mm.s^{-1}$
5	+ riverse	200	22	4-6	500	3.2-4.2

Technique of manual arc welding of the toothed gear. It differs from the welding mainly by the movement and inclination of the electrode or handle of the wire-feeding apparatus. The welding begins by tapping the electrode (vertically) onto the gear, causing the arc to ignite, then the electrode quickly retracts at a distance of 2-3mm and inclines at an angle of 20-30° to the vertical direction towards the direction of motion. With such an inclination, the drops of molten metal from the electrode fall into the melted area of the part.

In vertical position of the electrode (which should not be allowed) or if it is inclined to the vertical, but moves in the opposite direction of the above-described situation, it is possible the molten metal drops to fall on the surface of the detail, that is not yet melted, which is a prerequisite for weak bonding of the welded layer with the main metal of the part.

When welding, it is considered that the optimal depth of the molten area of the part should be about 30% of the total thickness of the welded layer. In the case of a larger molten area, carbon and other alloying elements of the part are burned, thereby reducing the mechanical properties of the base of the welded layer with the basic metal.

Welding should be performed in such a manner that each subsequent welding layer (transition) should overlap from 1/3 to 1/2 the previous one (Fig. 4a). Otherwise, slag inclusions may remain between the passages (Fig. 4b) and in case of multi-layer welding the quality of the welding may be coarsed. Fig. 5 shows a planar suface as the large-scaled toothed gear could be accepted for, because of its enormous radius. The welding often occurs without the oscillating movement of the electrode, which is characteristic of the joint-welding.
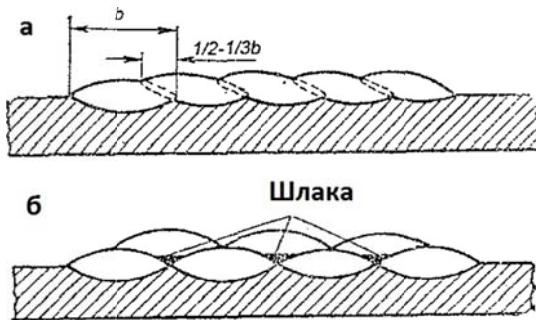
Fig. 4. Technique of surface-welding, used for recovery of a toothed gear

Apart from the above-described, the welding of planar surfaces can be done by a combined method, known as alternation of narrow and wide strips as shown at Figure 5. In this method, narrow strips without the oscillating movement of the electrode (3-5 times the diameter of the electrode) are initially welded, and then the intermediate distances are filled with oscillating motions of the electrode. The wide inter-layers should overlap from 1/3 to 1/2 of the narrow strips.
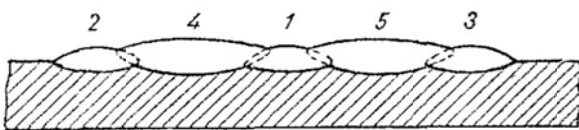
Fig. 5. Welding with narrow and wide strips

In the multi-strip welding of the surfaces of the gear, the welding of the next (upper) layers should be done after the surfaces of the lower ones are cleaned from the slag to a metallic gloss. In addition, each next (upper layer) is placed perpendicular to the lower one.

Assembly and annealing of the gear. The assembling is carried out in the company in which the thermal and mechanical processing of the toothed gear will be done.

The annealing is necessary due to the high hardness of the welded layer, that would result from the self-hardening, caused by the large mass of the bandage, leading to therapid cooling of the welded layer. This is done after the gear is assembled in a gas furnace. An exmplary thermal characteristic is shown on Figure 6.
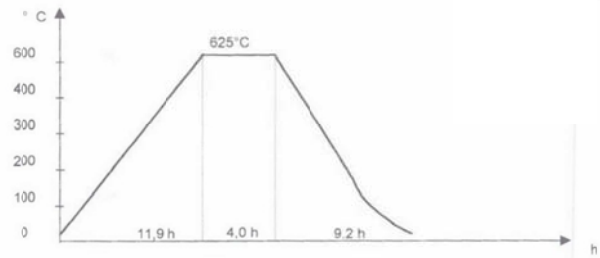
Fig. 6. Annealing characterisctics

Lathing of the toothed gear. The gear is placed on the planner rigger of the carousel lathe. In order to ensure a good result of the teeth-cutting, the lathing operation must be performed under conditions which ensure reliable setting and measurement bases. These bases are the internal diameter D_B, mm of the gear (setting) and the outer diameter D, mm (measuring). Thus, the accurate operation of the front and cylindrical surfaces is ensured and minimal radial and front beatings are guaranteed on them.

As the surface of the processed diameter serves as the basis for the alignment, this is done through an indicator clock with a sensitivity of $\delta = 0,01 mm$. In the case of available ellepticity on the centering (setting) diameter, the center of the planner rigger has to coincide with the geometric center of the gear. This is achieved if the measuring clock nozzle, attached to the spindle of the carousel lathe, describes a circle with a radius where *a* and *b* are relatively the both half-axes of the ellipse in the diameter hole.

The centering on the toothed gear front surface is also done with an indicator clock with a sensitivity of $\delta = 0,01 mm$. This centering follows the front beating, measured on the surface at both ends of two mutually perpendicular diameters of the toothed gear, and divides symmetrically (as divided into two) with respect to the horizontal plane.

The accuracy at the lathering of the outer diameter shall be of the seventh rate, where the tolerance for this diameter does not exceed 0.8 mm, and the beating of this diameter and the forehead with respect to the setting - not more than 0.08 mm.

All the base surfaces are processed to a roughness class not exceeding $R_Z = 20 \mu m (\Delta 5)$.

The obtaining of the new diameter of the repaired gear is achieved with a radial feed of the knife equal to l (Fig. 7).
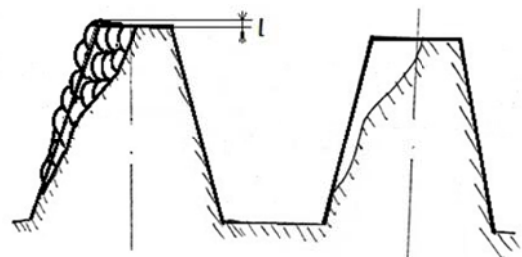
Fig. 7. Scheme of lathering

It is appropriate for the removal of the addition to happen in one transition at a rate of submission $v = 0,8 mm / min$.

The recommended speed for this typical continuous cut-off mode is from 30 to 90 m/min. It is assumed for it to be about $v_P = 60 m / \min$.

Teeth-cutting of the gear. The teeth-cutting of the gear can be performed on a worm gear hob by the touring method. The axial profile of the cutting section of the worm hob practically does not differ from the toothed gear, and therefore the cutting of the teeth with a worm gear hob can be represented as a splitting of an edge with a toothed wheel.

The working motion is ensured by the rotation of the hob 4 (Fig. 8). To ensure touring, the rotary movement of the worm hob and the toothed gear 3 must be coordinated in the same way, as the splitting of the worm 1 and worm gear 2. The rotation rate of the table with the gear must be less than the rotation rate of the hob, as the number of teeth of the toothed gear is greater than the number of hob cuts (in a single-cut hob the table rotates z times slowly than the hob).

When setting up the machine, the following operations are used: tuning of the machine's kinematic chains – gears lyra, feeding, dividing, differential; the toothed gear is put into place and centered, the hob is set to a specified cutting depth and the automatic cut-off or switching stops are set.

The machine has a differential mechanism that provides additional rotation of the gear when cutting the teeth because they are inclined.

Before the teeth-cutting, the toothed gear is adjusted to the front surface and the outer diameter.
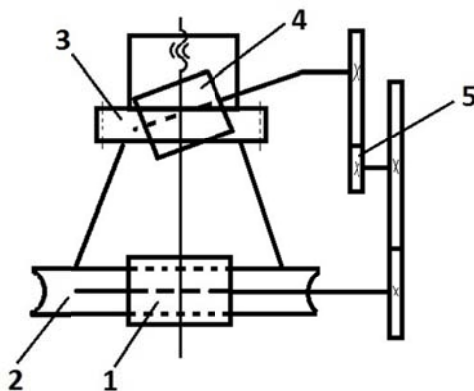
Fig. 7. Principle of operation of teeth-cutting hobs

The following rules must be observed when operating:
1. When attaching the toothed gear, gently clean all the centring and supporting surfaces from raspings and dirt.
2. Periodically check the radial beating of the work (centering) mandrel on the table.
3. Periodically check the front beating of the supporting bases of the setting device.
4. Place and screw up the toothed gear not to deform at the strongest tightenings, the screws are evenly tightened.
5. Check the radial and front beating of the gear before and after the machine is attached.
6. Due to the large sizes of the toothed gear, in order to reduce the internal stresses it is recommended to loosen the clamping screws after the rough machining process, re-tighten them prior to the clean processing and check the beating.

The outer surface of the gear ring serves as the base for adjusting the depth of hobbing. After switching on, the hob approaches the gear until its touching. In this position of the table and the stands, the linear or circular scale is reset to zero. The cutting-machine support is then lifted while the hob is over the toothed gear and then an additional radial alignment of the hob and the gear is performed to obtain the required cutting depth. The movement is detected with a ruler, a circle scale, or a measuring clock.

The sensitivity is checked with an indicator measuring clock with a sensitivity of $\delta = 0,01 mm$, in the same way as at the lathing operation.

Full tooth processing should be done for no more than 2-3 passes. Toothed gears of 7th rate of precision are cut into a slot-shaped modular hob and two clean passes with a worm gear hob.

The gear of 8th rate of precision are cut into a slot-shaped modular milling cutter and a single worm gear pass.

The cutting rate depends on the hardness of the material and it is selected as follows:

$$v = 18 m / \min \text{ at HB = 160;}$$

$$v = 15 m / \min \text{ at HB = 190;}$$

$$v = 12 m / \min \text{ at HB = 220.}$$

Due to the fact that a large part of the intermediate space is formed during the initial cutting of the gear, the removal of the basic amount of metal takes place through a drafting pass. Its depth should be determined in such a way so as to ensure that the worm hob is operated at the cleaning pass only with the side cutting edges. Therefore, it will only shape the evolvent profile of the working surfaces of the teeth, with minimal wear on the back surface of the teeth of the hob.

The control of the final phase of teeth-cutting can be done by measuring the total norm or by measuring the thickness of the tooth in different sections.

After the cutting, the gear is also controlled. This includes a profile error measurement. Deviations of the profile from the theoretical ones are recorded with a measuring clock or footprint. The universal evolvent-meter allows the profile of the tooth to be checked in different sections along its right and left sides without changing the position of the gear.

In addition, the basic step is also controlled, for example by a stationary universal tooth measuring device БВ-5060.

Conclusions

In conclusion, it can be stated that the chosen technology in this report is suitable for the recovery of the toothed gears of drum mills for ore grinding.

A new toothed gear is priced and available in the market at costs from 300 000 to 450 000 EUR, while the cost of the surface-welding recovery operations is no more than 50 000

EUR, which proves the great economic effect of the implementation of this technology. In addition, the material of the old restored gear is well trained and has better exploitational properties and fewer internal defects than these of a new one.

The qualitative performance of this technology can be increased considerably if a mechanical stand for automatic surface-welding of worn out teeth is designed and manufactured.

References

Вълков, К., „Електроди за заваряване и наваряване", Техника, С., 1985 г., (Vulkov, K. Elektrodi za zavaryavane i navaryavane. Tehnika, Sofia).

Мърхов Н., „Ремонт на минната механизация", Издателска къща МГУ "Св. Иван Рилски", С., 2011 г., (Murhov, N., Remont na minna mehanizatsiya. MGU, Sofia).

Сидеренко, А., И. Адам, „Производство крупньих зубчатых передач", Машгиз, М., 1961 г., (Siderenko, A., I. Adam, Proizvodstvo krupnih zubchatah peredach, Mashgiz, M., 1961)

Самолиев, С., „Технология тяжолого машиностроения", Машиностроение, М., 1967 г. (Samoliev, S., Tehnologiya tyazhologo mashinostroeniya, Mashinostroenie, M., 1967)

DETERMINATION OF THE FUNCTION OF RELIABILITY AND THE POSSIBILITY OF FAILURE-FREE OPERATION OF A JAW CRUSHER TYPE CJ615:01

Ivan Minin[1], Dimitar Mitev[2]

[1]*University of Mining and Geology „St. Ivan Rilski", 1700 Sofia, e-mail: minin_ivan@abv.bg*
[2]*University of Mining and Geology „St. Ivan Rilski", 1700 Sofia, e-mail: dimitar_i_radi@abv.bg*

ABSTRACT. The distribution of failures of an element or a machine from a specific technological line is an attempt for a mathematical description of their lifetime. The distribution mode affects the analytical form of this distribution. In the present study an attempt was made to determine the distribution of failures of the basic elements of a jaw crusher with complex swinging of the mobile jaw used for coarse crushing and to determine the probability of a faultless operation of the machine. In this case, the chosen crusher has six elements and in case of failure of any of them, its operation stops for repair works for its replacement. That is why, it is natural to consider the crusher as a system of six elements, connected in a series. This means, that if any of its components is damaged, there is a failure. The required number of statistic data has been collected and processed, which, after using some elements of the reliability theory, describes the behavior in regard to the reliability of its individual elements and the crusher as a whole. The possibility of failure-free operation of the whole crusher for a given quantity of processed ore is determined by the probability multiplication theorem, thus allowing the forecast of machine failures and the amount of spare lining plates necessary for the next year. The obtained results after the processing of the statistics unambiguously prove the correct choice of the jaw crusher under its conditions of operation.

Keywords: crusher, jaw, lining, reliability, failure.

ОПРЕДЕЛЯНЕ НА ФУНКЦИЯТА НА НАДЕЖДНОСТТА И ВЕРОЯТНОСТТА ЗА БЕЗОТКАЗНА РАБОТА НА ЧЕЛЮСТНА ТРОШАЧКА ТИП CJ615:01
Иван Минин[1], Димитър Митев[2]
[1]*Минно-геоложки университет „Св. Иван Рилски", 1700 София, e-mail: minin_ivan@abv.bg*
[2]*Минно-геоложки университет „Св. Иван Рилски", 1700 София, e-mail: dimitar_i_radi@abv.bg*

РЕЗЮМЕ. Разпределението на отказите на един елемент или една машина от дадена технологична линия е опит да се опише математически продължителността им на живот. Начинът на разпределението се отразява на аналитичния вид на това разпределение. В настоящата разработка е направен опит да бъде определено разпределението на отказите на основните елементи на челюстна трошачка със сложно люлеене на подвижната челюст използвана за едро трошене и да бъде определена вероятността за безотказна работа на машината. В настоящия случай избраната трошачката има шест елемента, като при повреда на всеки един от тях - спира да работи и започват ремонтни дейности по подмяната му. Ето защо е естествено трошачката да бъде разглеждана като система от шест елемента, които са последователно свързани. Това означава, че който и от елементите ѝ да се повреди, има наличие на отказ. Събрани са и са обработени необходимият брой статистически данни, които след използване на някои елементи от теорията на надеждността, описват поведението по отношение на надеждността на отделните ѝ елементи и на трошачката в съвкупност. Вероятността за безотказна работа на цялата трошачка за дадено количество преработена руда е определена от теоремата за умножение на вероятностите, като по този начин могат да бъдат прогнозирани отказите на машината и количеството на резервните облицовъчни плочи, необходими за година напред. Получените резултати след обработката на статистическите данни недвусмислено доказват правилния избор на челюстната трошачка за условията ѝ на експлоатация.

Ключови думи: Трошачка, челюстна, облицовка, надеждност, отказ.

Introduction

The object of the study is a jaw crusher type SANDVIK CJ615:01. The investigated jaw crusher has a complex swinging of the mobile jaw and works under extreme external conditions - high humidity and temperature underground in "Chelopech" mine. The sectional view of the 3D model of the machine, showing the main crusher nodes, is presented on Figure 1. The main elements and nodes that lead to the crusher outages (refusals) are: the mobile jaw lining 1, the stationary jaw lining 2, the lower lining plate on the left side 3, respectively the lower lining plate on the right side, the top lining plate on the left side 4, respectively - the top lining plate on the right side. This is due to the high abrasion of the ore and the relative vertical movement of the moving jaw towards the stationary one, leading to the grinding of the material in the crushing area, as well as the high quality of the design and production of the machine.

The main question that may be set in the present study is if there is a possibility to describe the behavior of a machine for the disclosure of mineral beads (jaw crusher) and to make a forecast of its failures for the planning of the necessary spare parts and upcoming repairs through the methods of the theory of probability and reliability.

The companies that exploit such machines are restocked with spare parts due to the fact that these machines are single and they determine the productivity of the whole enterprise in order to reduce the outages for the repairs. The mode of forecasting is brought to the arithmetic average of the required

number of input nodes and elements based on a previous year.
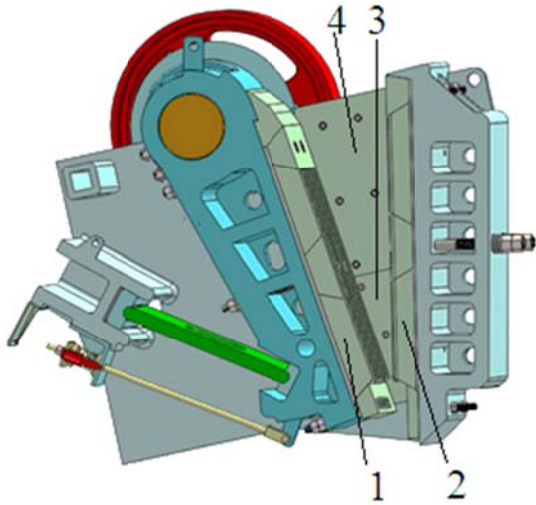
Fig. 1. A section of a jaw crusher type CJ615:01

The best solution in this case is to determine the parameters of the crusher's operational safety based on the reliability theory. A major problem for such a survey would appear during the statistics collection when the machine is supplied with spare parts and nodes from different manufacturers and of different quality. In the present study this problem is avoided.

It can be expected the present study to prove that the reliability theory can also be used to solve similar engineering tasks in the mining industry.

Summary

The aim of the present study is to investigate the regularities of altering the quality indicators over time by examining the effect of external and internal impacts on the operation of a machine for the disclosure of mineral beads - a jaw crusher, to create methods and means for forecasting the technical condition and to increase the reliability of such machines under operational modes.

Hypothesis of the research. In the present study are used some elements of the reliability theory to describe the behavior of the crusher in terms of the reliability of its separate elements.

In most cases in the literature the operational time without stops is accepted as an argument. Here, however, it is considered that it is more appropriate to choose the quantity of processed ore, indicated with q≥0 as an argument.

An element starts working at a zero initial quantity of processed ore and works until some quantity of ore is treated. Once a randomly selected quantity of ore is processed, a refusal occurs. It is assumed that the quantity of processed ore is a random variable, characterized by its distributional function $Q(q) = P(\chi < q)$. The probability of reliable operation of an element is expressed by the function $P(q) = 1 - Q(q)$. It is

called a function of reliability and expresses the probability (within a range of quantities of processed ore) not to occur a refusal $P(q) = 1 - Q(q)$. The graph of the probability of reliable operation is a monotonically decreasing function. Its boundary values are $P(0) = 1, P(\infty) = 0$.

The density of the distribution function will look like this.

$$f_X(q) = \lambda e^{-\lambda q} \tag{1}$$

The function of distribution itself is:

$$F_X(q) = \int_{-\infty}^{q} f_X(s)ds = \int_{0}^{q} f_X(s)ds = \int_{0}^{q} \lambda e^{-\lambda s} ds =$$

$$= -\int_{0}^{q} e^{-\lambda s} d(-\lambda s) = -\left(e^{-\lambda q} - e^{-\lambda 0}\right) = 1 - e^{-\lambda q}, q \geq 0 \tag{2}$$

The mathematical expectation (the first initial moment) of the random magnitude is:

$$M(X) = \int_{-\infty}^{\infty} s f_X(s)ds = \int_{0}^{\infty} s f_X(s)ds = \int_{0}^{\infty} s \lambda e^{-\lambda s} ds =$$

$$-\int_{0}^{\infty} s e^{-\lambda s} d(-\lambda s) = -\int_{0}^{\infty} s d\left(e^{-\lambda s}\right) = -s e^{-\lambda s}\Big|_{0}^{\infty} + \int_{0}^{\infty} e^{-\lambda s} ds =$$

$$= \int_{0}^{\infty} e^{-\lambda s} ds = -\frac{\lim\limits_{q \to \infty} e^{-\lambda q} - 1}{\lambda} = \frac{1}{\lambda} \tag{3}$$

The second initial moment is:

$$M(X^2) = \int_{-\infty}^{\infty} s^2 f_X(s)ds = \int_{0}^{\infty} s^2 f_X(s)ds = \int_{0}^{\infty} s^2 \lambda e^{-\lambda s} ds =$$

$$= -\int_{0}^{\infty} s^2 e^{-\lambda s} d(-\lambda s) = -\int_{0}^{\infty} s^2 d\left(e^{-\lambda s}\right) - s^2 e^{-\lambda s}\Big|_{0}^{\infty} + =$$

$$= +2\int_{0}^{\infty} s e^{-\lambda s} ds = -\frac{2}{\lambda}\int_{0}^{\infty} s d e^{-\lambda s} =$$

$$= -\frac{2}{\lambda} s e^{-\lambda s}\Big|_{0}^{\infty} + \frac{2}{\lambda}\int_{0}^{\infty} e^{-\lambda s} ds = -\frac{2}{\lambda}\frac{e^{-\lambda s}\Big|_{0}^{\infty}}{\lambda} = \frac{2}{\lambda^2} \tag{4}$$

Then the dispersion and the mean squared deviation are respectively: $D(X) = M(X^2) - M^2(X) = \frac{2}{\lambda^2} - \frac{1}{\lambda^2} = \frac{1}{\lambda^2}$;

$$\sigma(X) = \sqrt{D(X)} = \sqrt{\frac{1}{\lambda^2}} = \frac{1}{\lambda}.$$

In this case, the crusher has six elements, and in case of failure of any of them the machine stops working. Therefore, it is natural for the crusher to be considered as a system of six

elements that are bonded in a series. This means that if any of its components fails, the entire machine stops to operate. Therefore, the probability of faultless operation of the entire crusher for a given quantity of processed ore is determined by the probability multiplication theorem:

$$P_T(q) = P_1(q)P_2(q)P_3(q)...P_6(q) = \prod_{k=1}^{6} P_k(q) \qquad (5)$$

where $P_k(q)$ is the probability of faultless operation of the k-th element.

Further, the exponential distribution is perceived. In the case of exponential distribution law, the following expressions are used:

$$P_T(q) = e^{-\lambda_1 q} e^{-\lambda_2 q} e^{-\lambda_3 q} e^{-\lambda_4 q} e^{-\lambda_5 q} e^{-\lambda_6 q} = e^{-q\sum_{k=1}^{6} \lambda_k} \qquad (6)$$

For the statistical evaluation of each of the numbers according to the law of large numbers the arithmetic average of the measurements of failures of each detail of the crusher is used:

$$\frac{1}{\lambda_k} = \sum_{i=1}^{m_k} X_i^k \Rightarrow \lambda_k = \frac{1}{\sum_{i=1}^{m_k} X_i^k} \qquad (7)$$

$(k = 1,2,...,6)$ is the number of measurements for the k-th element of the jaw crusher.

Methodology used in processing the collected statistical information. The collected statistical data includes the quantity of processed ore up to the refusal of the relevant element and are shown in tables for each element separately. The recovery time is not taken into account, because it does not affect the parameters of the technological scheme in which the jaw crusher is included (the productivity of the crusher significantly exceeds that of the subsequent machine).

A new table is created for each element, where the following parameters are calculated:
$\overline{X}$ – quantity of processed ore;
f_i – frequencies of failures;
$P_i = \frac{f_i}{n}$ – probability in the selected range;
$C_i = \sum_{i=1}^{n} f_i$ - commutative frequencies;
$F_x(q) P_n = P_{n-1} + p_n$ – distribution function of the number of failures.

Finally, the mean squared processings of the relevant defected element $\sum_{i=1}^{n} \overline{X}$ are calculated and its frequency of failure $\lambda_i = \frac{1}{\frac{1}{n}\sum_{i=1}^{n} \overline{X}}$. The function of the failures distribution is then shown graphically.

Results

Table 1.
Processing to failure of the lining of the mobile jaw, t

260000	2588282	4751942
430000	2716170	4884806
741000	2853338	5040704
946000	3000961	5149226
1155000	3279603	5384500
1288222	3393323	5428150
1634000	3508533	5612515
1780400	3672893	5747326
1906672	3880059	5877240
2016404	3391411	5986908
2151443	4122638	6153689
2292018	4385294	6471889
2398073	4542166	

Table 2.
Processing of the data on the mobile jaw lining

$\overline{X}$	f_i	P_i	C_i	$F_x(q) P_n = P_{n-1} + p_n$
up to 100 thousands tones	0	0	0	0
100 -300	1	0.066667	1	0.026316
300 - 500	1	0.066667	2	0.052632
500 -700	0	0	2	0.052632
700 - 900	1	0.066667	3	0.078947
900 - 1100	1	0.066667	4	0.105263
1100 - 1300	2	0.133333	6	0.157895
1300 - 1500	0	0	6	0.157895
1500 - 1700	1	0.066667	7	0.184211
1700 - 1900	1	0.066667	8	0.210526
1900 - 2100	2	0.133333	10	0.263158
2100 - 2300	2	0.133333	12	0.315789
2300 - 2500	1	0.066667	13	0.342105
2500 - 2700	1	0.066667	14	0.368421
2700 - 2900	2	0.133333	16	0.421053
2900 - 3100	1	0.066667	17	0.447368
3100 - 3300	1	0.066667	18	0.473684
3300 - 3500	1	0.066667	19	0.5
3500 - 3700	2	0.133333	21	0.552632
3700 - 3900	1	0.066667	22	0.578947
3900 - 4100	1	0.066667	23	0.605263
4100 - 4300	1	0.066667	24	0.631579
4300 - 4500	1	0.066667	25	0.657895
4500 - 4700	1	0.066667	26	0.684211
4700 -4900	2	0.133333	28	0.736842
4900 - 5100	1	0.066667	29	0.763158
5100 - 5300	1	0.066667	30	0.789474
5300 - 5500	2	0.133333	32	0.842105
5500 - 5700	1	0.066667	33	0.868421
5700 - 5900	2	0.133333	35	0.921053
5900 - 6100	1	0.066667	36	0.947368
6100 - 6300	1	0.066667	37	0.973684
6300 - 6500	1	0.066667	38	1
over 6500	0	0	38	1

The mean squared processing of the lining of the mobile jaw is determined according to the expression:

$$\sum_{i=1}^{n} \overline{X_1} = 3289588t \qquad (8)$$

The frequency of failures of the mobile jaw lining is determined according to the expression:

$$\lambda_i = \frac{1}{\frac{1}{n}\sum_{i=1}^{n} \overline{X}} = \frac{1}{3289588} = 0,00000030399 \qquad (9)$$
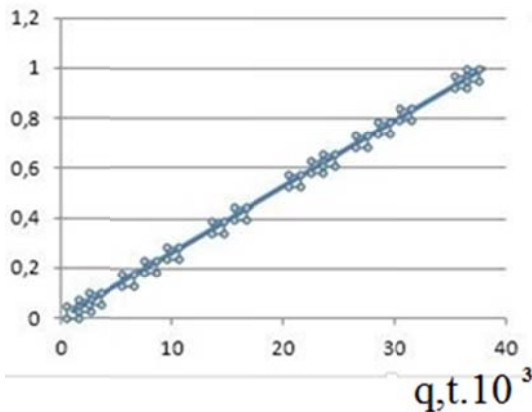
Fig. 2. Function of the failures distribution of the mobile jaw lining

Table 3.
Processing to failure of the stationary jaw lining, t

100000	2431687	4900638
170000	2507385	5009915
291000	2583882	5053807
390000	2653345	5074524
460000	2853338	5149226
600000	2938659	5223573
741000	3010407	5283548
831000	3183316	5360643
920000	3243216	5418268
998000	3307835	5486365
1088000	3367021	5543771
1155000	3424785	5603909
1222199	3496647	5671541
1288222	3551239	5723326
1380000	3632654	5797534
1453000	3704199	5859750
1520100	3787659	5223573
1589222	3875345	5903612
1653032	3959052	5956928
1734904	4038317	6020321
1823087	4122638	6074115
1901672	4203058	6145988
1922872	4279537	6208227
2016404	4347190	6348133
2071144	4439932	6377159
2134132	4502920	6440220
2193903	4578009	6499980
2262885	4658993	6567663
2321950	4746682	
2370520	4826970	

Table 4.
Processing of the data on the stationary jaw lining

$\overline{X}$	f_i	P_i	C_i	$F_x(q)\ P_n = P_{n-1}+p_n$
Up to 100 000 tones	1	0.011111111	1	0.011111111
100 -300	2	0.022222222	3	0.033333333
300 - 500	2	0.022222222	5	0.055555556
500 -700	1	0.011111111	6	0.066666667
700 - 900	2	0.022222222	8	0.088888889
900 - 1100	3	0.033333333	11	0.122222222
1100 - 1300	3	0.033333333	14	0.155555556
1300 - 1500	2	0.022222222	16	0.177777778
1500 - 1700	3	0.033333333	19	0.211111111
1700 - 1900	3	0.033333333	22	0.244444444
1900 - 2100	4	0.044444444	26	0.288888889
2100 - 2300	3	0.033333333	29	0.322222222
2300 - 2500	3	0.033333333	32	0.355555556
2500 - 2700	3	0.033333333	35	0.388888889
2700 - 2900	3	0.033333333	38	0.422222222
2900 - 3100	2	0.022222222	40	0.444444444
3100 - 3300	2	0.022222222	42	0.466666667
3300 - 3500	4	0.044444444	46	0.511111111
3500 - 3700	2	0.022222222	48	0.533333333
3700 - 3900	3	0.033333333	51	0.566666667
3900 - 4100	2	0.022222222	53	0.588888889
4100 - 4300	3	0.033333333	56	0.622222222
4300 - 4500	2	0.022222222	58	0.644444444
4500 - 4700	3	0.033333333	61	0.677777778
4700 -4900	3	0.033333333	64	0.711111111
4900 - 5100	3	0.033333333	67	0.744444444
5100 - 5300	3	0.033333333	70	0.777777778
5300 - 5500	3	0.033333333	73	0.811111111
5500 - 5700	3	0.033333333	76	0.844444444
5700 - 5900	3	0.033333333	79	0.877777778
5900 - 6100	4	0.044444444	83	0.922222222
6100 - 6300	2	0.022222222	85	0.944444444
6300 - 6500	4	0.044444444	89	0.988888889
over 6500	1	0.011111111	90	1

The mean squared processing of the stationary jaw lining is determined according to the expression:

$$\sum_{i=1}^{n} \overline{X_1} = 3450952t \qquad (10)$$

The frequency of failures of the stationary jaw lining is determined according to the expression:

$$\lambda_i = \frac{1}{\frac{1}{n}\sum_{i=1}^{n} \overline{X}} = \frac{1}{3450952} = 0,00000029 \qquad (11)$$

Table 5.
Processing until failure of the lower lining plate on the left side,t

330000	2016404	4077326
741000	2398073	4578009
1033000	2853338	5149226
1288222	3279603	5612515
1734904	3704199	6020321

Table 6.
Processing of the data on lower lining plate on the left side

$\overline{X}$	f_i	P_i	C_i	$F_x(q)\ P_n = P_{n-1} + p_n$
up to100 thousands tones	0	0	0	0
100 -300	0	0	0	0
300 - 500	1	0.0666667	1	0.066667
500 -700	0	0	1	0.066667
700 - 900	1	0.0666667	2	0.133333
900 - 1100	1	0.0666667	3	0.2
1100 - 1300	1	0.0666667	4	0.266667
1300 - 1500	0	0	4	0.266667
1500 - 1700	0	0	4	0.266667
1700 - 1900	0	0	4	0.266667
1900 - 2100	1	0.0666667	5	0.333333
2100 - 2300	0	0	5	0.333333
2300 - 2500	1	0.0666667	6	0.4
2500 - 2700	0	0	6	0.4
2700 - 2900	1	0.0666667	7	0.466667
2900 - 3100	0	0	7	0.466667
3100 - 3300	1	0.0666667	8	0.533333
3300 - 3500	0	0	8	0.533333
3500 - 3700	0	0	8	0.533333
3700 - 3900	1	0.0666667	9	0.6
3900 - 4100	1	0.0666667	10	0.666667
4100 - 4300	0	0	10	0.666667
4300 - 4500	0	0	10	0.666667
4500 - 4700	1	0.0666667	11	0.733333
4700 -4900	0	0	11	0.733333
4900 - 5100	0	0	11	0.733333
5100 - 5300	1	0.0666667	12	0.8
5300 - 5500	0	0	12	0.8
5500 - 5700	1	0.0666667	13	0.866667
5700 - 5900	0	0	13	0.866667
5900 - 6100	1	0.0666667	14	0.933333
6100 - 6300	0	0	14	0.933333
6300 - 6500	1	0.0666667	15	1
over 6500	0	0	15	1

Table 8.
Processing of the data on lower lining plate on the right side

$\overline{X}$	f_i	P_i	C_i	$F_x(q)\ P_n = P_{n-1} + p_n$
up to100 thousands tones	0	0	0	0
100 -300	0	0	0	0
300 - 500	1	0.0666667	1	0.066667
500 -700	0	0	1	0.066667
700 - 900	1	0.0666667	2	0.133333
900 - 1100	1	0.0666667	3	0.2
1100 - 1300	1	0.0666667	4	0.266667
1300 - 1500	0	0	4	0.266667
1500 - 1700	0	0	4	0.266667
1700 - 1900	0	0	4	0.266667
1900 - 2100	1	0.0666667	5	0.333333
2100 - 2300	0	0	5	0.333333
2300 - 2500	1	0.0666667	6	0.4
2500 - 2700	0	0	6	0.4
2700 - 2900	1	0.0666667	7	0.466667
2900 - 3100	0	0	7	0.466667
3100 - 3300	1	0.0666667	8	0.533333
3300 - 3500	0	0	8	0.533333
3500 - 3700	0	0	8	0.533333
3700 - 3900	1	0.0666667	9	0.6
3900 - 4100	1	0.0666667	10	0.666667
4100 - 4300	0	0	10	0.666667
4300 - 4500	0	0	10	0.666667
4500 - 4700	1	0.0666667	11	0.733333
4700 -4900	0	0	11	0.733333
4900 - 5100	0	0	11	0.733333
5100 - 5300	1	0.0666667	12	0.8
5300 - 5500	0	0	12	0.8
5500 - 5700	1	0.0666667	13	0.866667
5700 - 5900	0	0	13	0.866667
5900 - 6100	1	0.0666667	14	0.933333
6100 - 6300	0	0	14	0.933333
6300 - 6500	1	0.0666667	15	1
over 6500	0	0	15	1

The mean squared processing of the lining of the lower lining plate on the left side is determined according to the expression:

$$\sum_{i=1}^{n} \overline{X_1} = 29877743t \qquad (12)$$

The frequency of failures of the lower lining plate on the left side is determined according to the expression:

$$\lambda_i = \frac{1}{\frac{1}{n}\sum_{i=1}^{n}\overline{X}} = \frac{1}{29877743} = 0,000000335 \qquad (13)$$

The mean squared processing of the lining of the lower lining plate on the right side is determined according to the expression:

$$\sum_{i=1}^{n} \overline{X_1} = 3396065t \qquad (14)$$

The frequency of failures of the lower lining plate on the right side is determined according to the expression:

$$\lambda_i = \frac{1}{\frac{1}{n}\sum_{i=1}^{n}\overline{X}} = \frac{1}{3396065} = 0,000000294 \qquad (15)$$

Table 7.
Processing until failure of the lower plate on the right side, t

330000	2016404	3704199	5612515
741000	2398073	4077326	6020321
1033000	2853338	4578009	6359732
1288222	3279603	5149226	

Table 9.
Processing until failure of the upper lining plate on the left side, t

741000	3279603	6020321
1653032	4077326	
2398073	5149226	

Table 10.
Processing of the data on the upper lining plate on the left side

$\overline{X}$	f_i	P_i	C_i	$F_x(q)$ $P_n =$ $P_{n-1}+p_n$
Up to 100 thousands tones	0	0	0	0
100 -300	0	0	0	0
300 - 500	0	0	0	0
500 -700	0	0	0	0
700 - 900	1	0.142857	1	0.142857
900 - 1100	0	0	1	0.142857
1100 - 1300	0	0	1	0.142857
1300 - 1500	0	0	1	0.142857
1500 - 1700	1	0.142857	2	0.285714
1700 - 1900	0	0	2	0.285714
1900 - 2100	0	0	2	0.285714
2100 - 2300	0	0	2	0.285714
2300 - 2500	1	0.142857	3	0.428571
2500 - 2700	0	0	3	0.428571
2700 - 2900	0	0	3	0.428571
2900 - 3100	0	0	3	0.428571
3100 - 3300	1	0.142857	4	0.571429
3300 - 3500	0	0	4	0.571429
3500 - 3700	0	0	4	0.571429
3700 - 3900	0	0	4	0.571429
3900 - 4100	1	0.142857	5	0.714286
4100 - 4300	0	0	5	0.714286
4300 - 4500	0	0	5	0.714286
4500 - 4700	0	0	5	0.714286
4700 -4900	0	0	5	0.714286
4900 - 5100	0	0	5	0.714286
5100 - 5300	1	0.142857	6	0.857143
5300 - 5500	0	0	6	0.857143
5500 - 5700	0	0	6	0.857143
5700 - 5900	0	0	6	0.857143
5900 - 6100	1	0.142857	7	1
6100 - 6300	0	0	7	1
6300 - 6500	0	0	7	1
over 6500	0	0	7	1

The mean squared processing of the lining of the upper lining plate on the left side is determined according to the expression:

$$\sum_{i=1}^{n} \overline{X_1} = 333127t \tag{16}$$

The frequency of failures of the upper lining plate on the left side is determined according to the expression:

$$\lambda_i = \frac{1}{\frac{1}{n}\sum_{i=1}^{n} \overline{X}} = \frac{1}{333127} = 0,0000003 \tag{17}$$

Table 11.
Processing until failure of the upper lining plate on the right side, t

741000	3279603	6020321
1653032	4077326	
2398073	5149226	

Table 12.
Processing of the data on the upper lining plate on the right side

$\overline{X}$	f_i	P_i	C_i	$F_x(q)$ $P_n =$ $P_{n-1}+p_n$
Up to 100 thousands tones	0	0	0	0
100 -300	0	0	0	0
300 - 500	0	0	0	0
500 -700	0	0	0	0
700 - 900	1	0.142857	1	0.142857
900 - 1100	0	0	1	0.142857
1100 - 1300	0	0	1	0.142857
1300 - 1500	0	0	1	0.142857
1500 - 1700	1	0.142857	2	0.285714
1700 - 1900	0	0	2	0.285714
1900 - 2100	0	0	2	0.285714
2100 - 2300	0	0	2	0.285714
2300 - 2500	1	0.142857	3	0.428571
2500 - 2700	0	0	3	0.428571
2700 - 2900	0	0	3	0.428571
2900 - 3100	0	0	3	0.428571
3100 - 3300	1	0.142857	4	0.571429
3300 - 3500	0	0	4	0.571429
3500 - 3700	0	0	4	0.571429
3700 - 3900	0	0	4	0.571429
3900 - 4100	1	0.142857	5	0.714286
4100 - 4300	0	0	5	0.714286
4300 - 4500	0	0	5	0.714286
4500 - 4700	0	0	5	0.714286
4700 -4900	0	0	5	0.714286
4900 - 5100	0	0	5	0.714286
5100 - 5300	1	0.142857	6	0.857143
5300 - 5500	0	0	6	0.857143
5500 - 5700	0	0	6	0.857143
5700 - 5900	0	0	6	0.857143
5900 - 6100	1	0.142857	7	1
6100 - 6300	0	0	7	1
6300 - 6500	0	0	7	1
over 6500	0	0	7	1

The mean squared processing of the lining of the upper lining plate on the right side is determined according to the expression:

$$\sum_{i=1}^{n} \overline{X_1} = 3331226t \tag{18}$$

The frequency of failures of the upper lining plate on the right side is determined according to the expression:

$$\lambda_i = \frac{1}{\frac{1}{n}\sum_{i=1}^{n} \overline{X}} = \frac{1}{3331226} = 0,0000003 \tag{19}$$

Determination of the probability of failure of the jaw crusher. The probability of faultless operation of the entire crusher for a given quantity of processed ore is determined by the multiplication probability theorem:

$$P_T(q) = e^{-q\lambda_1}.e^{-q\lambda_2}.e^{-q\lambda_3}.e^{-q\lambda_4}.e^{-q\lambda_5}.e^{-q\lambda_6} =$$
$$= e^{-q\sum_{k=1}^{6}\lambda_k} \tag{20}$$

Therefore, there is obtained:

$$P_T(q) = e^{-q(0,00000034+0,00000029+0,00000335+ \atop +0,000000294+0,0000003+0,0000003)} = e^{-q(0,0000001823)} \tag{21}$$

The probability of failure of the entire jaw crusher in the average work until failure of the examined elements:

$$\sum_{i=1}^{n}\overline{X_i} = 3297800t \quad \text{- the processed ore equals to:}$$

$$P_T(q) = e^{-3297800(0,00000034+0,00000029+0,00000335+ \atop +0,000000294+0,0000003+0,0000003)} =$$
$$= e^{-3297800(0,0000001823)} = 0,548 \tag{22}$$

Conclusions

In conclusion, it can be said that through the methods of the theory of probability and reliability the behavior of machines for the disclosure of mineral beads (in this case jaw crusher) can be expressed, and the failures for planning of the necessary spare parts and upcoming repairs can be predicted.

From the last parameter it can be concluded that the probability of the crusher to fail in its annual operating is about 50%.

All this leads to the conclusion that this machine is very reliable and with high operational safety parameters and two sets of spare parts are necessary per year.

As a further task, heuristic algorithms and computer programs for analyzing and accumulating data, characterizing the life cycle of machines and systems used in the mining industry can be created.

References

Обрешков, Н. Теория на вероятностите. Наука и изкуство, София, 1963. (Obreshkov, N. Teoria na veroyatnostite, Sofia, 1963)

W.Feller, An Introduction to Probability Theory and its Applications. J.Wiley&Sons, New York, 1970. V.1, v.2.

Колмогоров, А. Н., И. Журбенко, А. Прохоров, Введение в теорию вероятностей. Москва, Наука, 1982. (Kolmogorov, A.N., I. Zhurbenko, A. Prohorov, Vvedenie v teoriyu veroyatnostei, Moskva, Nauka, 1982)

Гихман, И., А. Скороход, А. Ядренко, Теория вероятностей и математическая статистика. Висша школа, Киев, 1979. (Gihman, I., A. Skorohod, A. Yadrenko, Teoriya veroyatnostei i matematicheskaya statistika. Visha shkola, Kiev, 1979)Barlow, R., F. Proschan, Mathematical Theory of Reliability. SIAM, Philadelphia, 1996.

Димитров, К., Д. Данчев, Надеждност на строителни машини и системи. Техника, София, 1994. (Dimitrov, K., D. Danchev, Nadezhdnost na stroitelni mashini i sistemi. Tehnika, Sofia, 1994).

SPECIFYING THE METHODOLOGY FOR THE CALCULATION OF VIBRATORY FEEDERS

Hristo Sheiretov

University of Mining and Geology "St.Ivan Rilski" Sofia, sheiretov@abv.bg

ABSTRACT. A methodology for the calculation of vibratory feeders is developed. The frequency of the vibrations, the dimensions of the discharge section of the bin, the length of the feeder's chute, the width and the height of the feeder's chute, the material velocity, and the amplitude of the vibrations are determined. Motor-vibrators are chosen for feeder's drive. On the basis of the developed methodology a concrete example is solved.
The developed methodology may be useful for the students, and also for the specialists, working in the mining and processing industry.

Keywords: chute, vibration, frequency, amplitude, motor-vibrator

УТОЧНЯВАНЕ НА МЕТОДИКАТА ЗА ИЗЧИСЛЯВАНЕ НА ВИБРАЦИОННИ ЗАХРАНВАЧИ
Христо Шейретов
Минно-геоложки университет „Св.Иван Рилски", 1700 София, sheiretov@abv.bg

РЕЗЮМЕ. Разработена е методика за изчисляване на вибрационни захранвачи. Определят се честотата на трептенията, размерите на разтоварната част на бункера и дължината на улея на захранвача, ширината и височината на улея на захранвача, скоростта на транспортиране на материала и амплитудата на трептенията. Избират се мотор-вибратори за задвижване на захранвача. На базата на разработената методика е решен конкретен пример.
Разработената методика може да се използува както от студентите, така и от специалистите, които работят в миннодобивната и преработвателната промишленост.

Ключови думи: улей, трептене, честота, амплитуда, мотор-вибратор

Introduction

The vibratory feeder (fig.1) is an inclined chute, hanged on springs under the unloading outlet of the bin. The chute is carried out in reciprocating motion with the help of a vibrator. The material loaded in the chute accomplishes infinitely following one after another short movements forward with a definite velocity. The particles of the material move away from the bottom of the chute and move with micro jumps.

The vibratory feeders are driven by an electromechanical or electromagnetic vibrator, situated under the bottom of the chute, or by two synchronized motor-vibrators, attached to the both sides of the chute (Fig.1). In order to ensure the movement of the material in a definite direction the vibrators are mounted in such a way, so that the line of action of the excitation force is directed at a definite acute angle *α* toward the longitudinal axis of the chute.

The vibratory feeders are used for unloading the bins and uniformly feeding the material to crushers and belt conveyors (of dry, both fine and coarse materials); in the loading points of the open pit mines, the concentration and floatation plants - for feeding rock, ore and coal to the crushers and from the crushers to the belt conveyors; in the concrete stations - for feeding sand and gravel to the belt conveyors; in cement plants - for feeding limestone to the belt conveyors; in power stations - for feeding gypsum and slag to the crushers.

The advantages of the vibratory feeders are the simple and light construction, the small energy consumption and the small wearing out of the chute. The disadvantages are difficult transportation of wet, stick and dust materials and the transfer of the vibratory loads to the supporting structure.

Since the vibratory feeders are vibratory conveyors with small length, the methodologies for the calculation of the vibratory conveyors are used for their calculation. But the calculation of the vibratory feeders has some peculiarities.

The methodologies for the calculation of the vibratory conveyors are given in the literature, referring the mining transport and the transport machines with continuous action. However, a methodology for the calculation of vibratory feeders is not given. In some company manuals are given recommendations for the dimensioning and choice of some elements of the vibratory feeders.

In Jost vibratory feeders and Syntron heavy industry feeders are given the technical characteristics of the vibratory feeders, designed for tough work conditions in the mining and processing industry, schemes for determination of the dimensions of the unloading section of the bins and guides for the choice of the velocity of transportation.
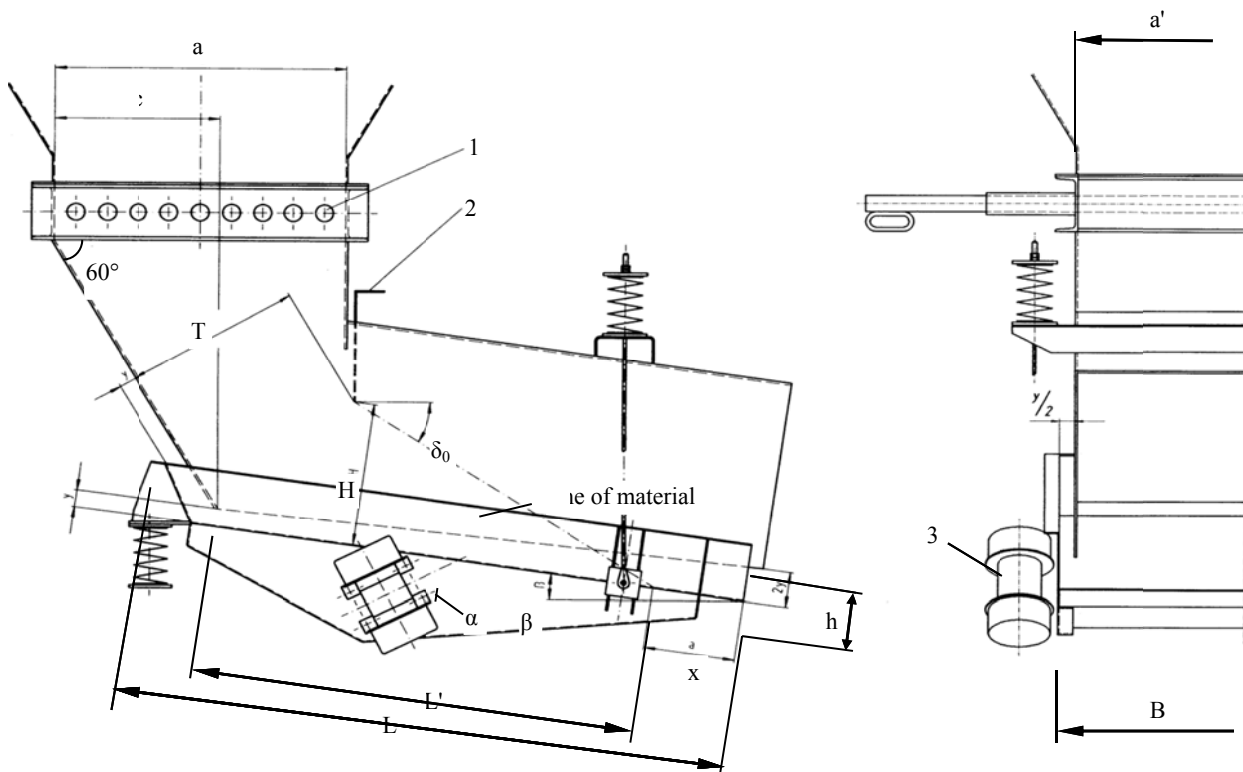
Fig.1. Scheme for the calculation of the vibratory feeder

L - length of the chute; *B* - width of the chute; *h* - height of the chute; *a*, *a'* - lengths of the sides of the bin's outlet; *H* - height of the outlet of the transitional section of the bin; *T* - height of the outlet of the transitional section of the bin; δ_0 - angle of repose of the material; *β* - angle of inclination of the feeder; *α* - angle between the line of action of the excitation force and the longitudinal axis of the chute; *x* - distance between the front end of the chute and the material; *y* - distance between the back wall of the chute and the bottom of the chute

1 - shutter for opening and closing the bin; 2 - shutter for regulating the thickness of the layer of the material; 3 - motor-vibrator
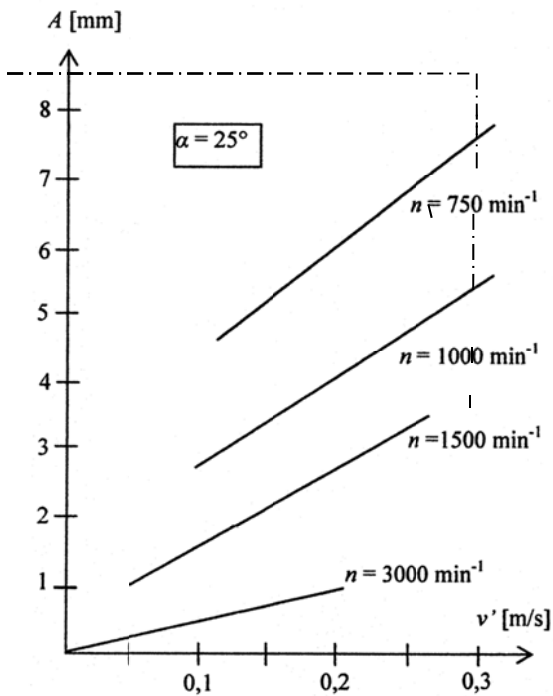

Fig. 2. Graphs for determination of the amplitude of the vibrations of the vibratory feeders

A - amplitude of the vibrations;
v' - velocity of material;
n - frequency of the vibrations;
α - angle between the line of action of the excitation force and the longitudinal axis of the chute

In Italvibras are given the technical characteristics of motor-vibrators and a methodology for their choice.

In Spivakovskii (1983) is given the theory of determination of the working regime (subresonant and overresonant) of the vibratory conveyors and a methodology for their calculation.

The aim of the present work is, on the basis of these references, a complete methodology for the calculation of vibratory feeders to be developed. A concrete example for a vibratory feeder with two motor-vibrators is solved.

Input data

The input data for the feeder's calculation is:
- Kind of the transporting material - crushed bauxite, sized;
- Density of the material ρ = 1.3 t/m³;
- Angle of repose of the material δ_0 = 30°;
- Maximum size of the materials particles a_{max} = 75mm;
- Angle of inclination of the feeder β = -8° (β = -5 ÷ -10°);
- Necessary output of the feeder Q' = 650 t/h;
- Bin's outlet dimensions $a = a'$ = 950mm = 0.95m.

Frequency of the vibrations

The frequency of the vibrations n is chosen from Table 1 according to the size of the material.

Table 1.
Recommended frequency of the vibrations of the vibratory feeders (Syntron heavy-industry feeders)

Maximum size of the particles of the material a_{max} [mm]	< 10	10 - 100	> 100
Frequency of the vibrations n [min⁻¹]	1500; 3000	1000; 1500	750; 1000

Length of the chute of the feeder

The length of the chute L is determined graphically by the scheme, showed in Fig.1, according to the angle of repose δ_0 and the height of the outlet H of the transitional section of the bin. The height H is dependent on the size of the bin's outlet a. The drawing is done in the following sequence (according to Jost and Syntron):
- The size $c=(0.3÷0.6).a=0.56.950=530$mm is determined and a vertical line is passed on the distance c from the beginning of the bin's outlet;
- An inclined line is produced at an angle 60° toward the horizontal line to the intersection with the vertical line. An intercept is obtained, which refers to the bin's back wall;
- A vertical intercept is produced from the end point of the bin's outlet to a point, which is at a distance T from the bin's back wall, where $T=560$mm ≥ $4.a_{max}=4.75=300$mm for sized material and $T≥ 2.a_{max}$ for unsized material;
- From the end point of the vertical intercept an inclined line is produced at an angle $\delta_0=30°$. This line determines the position of the material;
- An inclined line is produced, which is at an angle $\beta=8°$ to the horizontal line, and is at a distance y from the point, corresponding to the end of the bin's back wall. This line corresponds to the bottom of the chute. The minimum distance

y is recommended to be chosen (Jost vibratory feeders): y_{min}=30mm при n=3000min⁻¹; y_{min}=40mm при n=1500min⁻¹; y_{min}=60mm при n=1000min⁻¹; y_{min}=80mm при n = 750min⁻¹. For the calculated example it is accepted that $y=y_{min}$=60mm;
- The minimum length of the chute is determined $L_{min}=L'+x=1440+300=1740$mm=1.74m, where L' is the distance between the intersection point of the line of the bottom of the chute and the line of material and the point, corresponding to the end of the bin's back wall. The distance L' is obtained graphically according to the scheme on Fig.1. The distance x is accepted to be $x=300$mm ≥ 150mm;
- A check is made $T/H=560/490 = 1.14 = 0.7÷1.25$. The height of the outlet H = 490mm is obtained according to the scheme on Fig. 1. A standard length of the chute is accepted from Table 2 $L = 2$m > L_{min} = 1.74m.

Table 2.
Chute's dimensions and mass of the vibratory feeders
(Jost vibratory feeders)
With two electromechanical motor-vibrators (L = 1÷2.5m)

B [m]	0.4	0.5	0.6	0.8
h [m]	0.15	0.15	0.2	0.2
L [m]	1; 1.5; 2	1; 1.5; 2	1; 1.5; 2	1; 1.5; 2
m [kg]	155; 190; 250	165; 205; 280	180; 250; 300	650; 760; 1140
B [m]	1	1.2	1.4	1.6
h [m]	0.2	0.2	0.2	0.2
L [m]	1; 2; 2.5	1.5; 2; 2.5	1.5; 2; 2.5	2; 2.5
m [kg]	730; 1010; 1150	810; 1130; 1380	1340; 1750; 1960	1730; 1920; 2350

With two electromechanical motor-vibrators (L = 3÷6m)

B [m]	0.4	0.5	0.6	0.8
h [m]	0.25	0.25	0.25	0.25
L [m]	3; 4; 5; 6	3; 4; 5; 6	3; 4; 5; 6	3; 4; 5; 6
m [kg]	365; 525; 750; 855	470; 635; 800; 890	505; 680; 855; 1090	650; 770; 1090; 1245

B [m]	1		1.2	1.4
h [m]	0.25		0.25	0.25
L [m]	3; 4; 5; 6		3; 4; 5; 6	3; 4; 5; 6
m [kg]	725; 1040; 1235; 1390		800; 1150; 1365; 1810	1140; 1590; 1890; 2400

With an electromagnetic vibrator (L = 0.75÷2.5m)

B [m]	0.2	0.4	0.6
h [m]	0.2	0.2	0.2
L [m]	0.75; 1; 1.25; 1.5	1; 1.25; 1.5; 1.75	1.25; 1.5; 1.75; 2
m [kg]	82; 110; 115; 125	125; 185; 195; 205	210; 300; 315; 330
B [m]	0.8	1	1.2
h [m]	0.25	0.25	0.25
L [m]	1.5; 1.75; 2; 2.25	1.5; 2; 2.25; 2.5	1.5; 2; 2.25; 2.5
m [kg]	355; 395; 420; 670	390; 675; 710; 735	660; 775; 1440; 1490

B - width of the chute; h - height of the chute; L - length of the chute; m - mass of the feeder including the mass of the vibrator.

Width and height of the chute of the feeder

The width of the chute B=1.2m and the height of the chute h = 0.2m are chosen from Table 2. The following conditions must be satisfied:

$$B = 1200 \text{ mm} \geq a' + y = 950 + 60 = 1110 \text{ mm} \qquad (1)$$

$$Q = 3600.v.\rho.\psi.k_\beta.B.h \geq Q' , \text{ t/h} \qquad (2)$$

$$Q = 3600.0,23.1,3.2.1,3.1,2.0,2 = 670 \text{ t/h} > Q' = 650 \text{ t/h} ,$$

where: v [m/s] - velocity of transportation of the material for a horizontal chute (it is chosen from Table 3; when a_{max} = 75mm and a drive with two motor-vibrators it is accepted v=0.23m/s); ψ - chute filling coefficient (ψ=2; it is assumed, that the height of the material's layer is two times greater than the height of the chute); k_β - coefficient, which refers to the increasing of the transportation velocity with the increasing of the inclination of the chute (it is accepted from Table 4; (Spivakovskii, 1983) when β = -8° k_β = 1.3).

Table 3.
Recommended velocities for transportation of the material on a horizontal chute v [m/s] for the vibratory feeders (Syntron heavy-industry feeders)

Maximum size of the pieces of the material a_{max} [mm]	< 10	10 - 100	> 100
For an electromagnetic vibrator	0.15	0.13	0.11
For an electromechanical vibrator or two electromechanical motor-vibrators	0.25	0.23	0.19

Table 4.
Coefficient, which refers to the increase of the output of the feeder with the increase of the angle of inclination (Spivakovskii)

β [°]	0	- 5	- 8	- 10	- 12
k_β	1	1.2	1.3	1.4	1.5

Amplitude of vibrations

The amplitude of vibrations A [mm] is determined from the graphs shown on Fig.2 depending on the frequency of the vibrations n [min⁻¹] and the velocity of transportation $v' = v.k_\beta = 0,23.1,3 = 0,3$m/s. When n = 1000min⁻¹ and v' = 0.3m/s A = 5.5mm.

The graphs are drawn at an angle between the line of action of the excitation force and the longitudinal axis of the feeder α = 25°. It is recommended for bin feeders to take α = 25°, and for screens – α = 35 or 45° (Italvibras).

Choice of motor-vibrators

The motor-vibrators are chosen from Table 5 according to the frequency of vibrations n [min⁻¹] and the necessary kinetic moment $M'_к$ [kg.mm]:

$$M'_к = 0,5.m.A = 0,5.1130.5,5 = 3110 \text{ kg.mm}, \qquad (3)$$

where: m [kg] - mass of the feeder (it is given in Table 2 for the chosen dimensions of the chute; when B = 1.2m, h = 0.2m and L = 2m the mass is m = 1130kg).

Motor-vibrators are chosen with the following parameters: frequency of the vibrations (synchronous frequency of rotation of the electric motor) n = 1000min⁻¹; kinetic moment $M_к$ = 5838kg.mm > $M'_к$ = 3110kg.mm; power of the electric motor $P_{дв}$ = 4.3kW.

Table 5.
Characteristics of the motor-vibrators (Italvibras)

n= 3000min⁻¹	$M_к$ [kg.mm]	153; 179; 205; 230; 344; 387; 515; 895
	$P_{дв}$ [kW]	1.4; 2; 2.2; 2.2; 4; 4; 5; 9.3
n= 1500min⁻¹	$M_к$ [kg.mm]	163; 219; 286; 415; 561; 715; 958; 962; 1507; 1526; 1990; 2598; 3260; 2246; 4544
	$P_{дв}$ [kW]	0.3; 0.3; 0.525; 0.55; 0.9; 1.1; 1.6; 1.6; 2.2; 2.2; 3.6; 6; 7; 7.5; 10
n =1000min⁻¹	$M_к$ [kg.mm]	163; 286; 457; 723; 1012; 1443; 1464; 2309; 2326; 3422; 2658; 5838; 6083; 7197; 7752; 8673; 10996; 12662; 15500; 20025
	$P_{дв}$ [kW]	0.18; 0.35; 0.35; 0.68; 0.75; 1.1; 1.1; 1.96; 1.96; 2.5; 3.8; 4.3; 5; 7; 7.5; 7.6; 9; 10.6; 13; 19
n = 750min⁻¹	$M_к$ [kg.mm]	163; 286; 458; 722; 1012; 1443; 1464; 2309; 2326; 3421; 4658; 5838; 7197; 12390; 13816; 17946; 21337; 28633
	$P_{дв}$ [kW]	0.23; 0.28; 0.35; 0.4; 0.4; 0.95; 0.95; 1.5; 1.5; 2; 2.8; 4; 3.9; 6.8; 7.6; 9.2; 10.4; 12.5

n - frequency of the vibrations (synchronous frequency of rotation of the electric motor); $M_к$ - kinetic moment; $P_{дв}$ - power of the electric motor.

Conclusions

In the present paper, a methodology for the calculation of vibratory feeders is developed, based on several references, which consider the vibratory conveyors and the vibratory feeders.

The developed methodology may be useful for the students, and also for the specialists, working in the mining and processing industry.

References

Спиваковский, А.О., В.К. Дьячков. Транспортирующие машины. М., Машиностроение, 1983. (Spivakovskii, A.O. Transportiruyushtie Mashini", Moskva)

Italvibras. General catalogue, available at: http://www.italvibras.it/user/upload_inc_scelta_motovibratore/upload_inc_cataloghi/catalogo_generale_FR.pdf (accessed on 26 June, 2017).

Jost vibratory feeders. Catalogue, available at: https://www.joest.com/en/products/charging-feeding/hopper-discharge-feeder-unbalance-channel/ (accessed on 26 June, 2017).

Syntron heavy industry feeders. FMC Technologies. Catalogue, available at: http://www.tristateelectricmc.com/pdf/FMC%20Technologies%20Syntron%20Heavy%20Industry%20Feeder.pdf (accessed on 26 June, 2017).

CALCULATION OF THE MECHANISM FOR THE STRETCHING AND RETRACTING OF THE BOOM OF A TRUCK MOUNTED CRANE

Hristo Sheiretov

University of Mining and Geology "St.Ivan Rilski" Sofia, sheiretov@abv.bg

ABSTRACT. A methodology for the calculation of the mechanism for the stretching and retracting of the telescopic boom of a truck mounted crane is developed. The necessary force of the piston rod of the hydraulic cylinder for the stretching of the boom is determined using the principle of mechanics for the possible displacements of the telescopic boom with the load. Two cases are considered - at maximum and minimum angle of inclination of the boom, and at maximum angle a greater force is obtained. At first the problem is solved when the friction forces between the separate sections of the boom and the resistance in the rollers of the lifting polyspasts are ignored, and after that the obtained forces are corrected by the relevant coefficients. The necessary diameter of the piston and the necessary displacement of the hydraulic cylinder for the stretching and retracting of the boom are determined, and after that a hydraulic cylinder is chosen. The working liquid consumption of the hydraulic cylinder is determined. The maximum forces in the ropes of the polyspasts for the stretching and retracting of the upper section of the boom are determined and ropes are chosen.
On the basis of the developed methodology a concrete example is solved for the crane KC-45717, mounted on the truck chassis KamAZ.

Keywords: telescopic boom, tackle block, hydraulic cylinder, cable

ИЗЧИСЛЯВАНЕ НА МЕХАНИЗМА ЗА РАЗПЪВАНЕ И ПРИБИРАНЕ НА СТРЕЛАТА НА АВТОМОБИЛЕН КРАН
Христо Шейретов
Минно-геоложки университет „Св.Иван Рилски", 1700 София, sheiretov@abv.bg

РЕЗЮМЕ. Разработена е методика за изчисляване на механизма за разпъване и прибиране на телескопичната стрела на автомобилен кран. Определена е необходимата сила на буталния прът на хидроцилиндъра за разпъването на стрелата, като се изхожда от приципа на механиката за възможните премествания на телескопичната стрела с товара. Разгледани са два случая - при максимален и при минимален ъгъл на наклон на стрелата, като по-голяма сила се получава при максимален ъгъл на наклон. Първоначално задачата е решена като се пренебрегват силите на триене между отделните секции на стрелата и съпротивлението при въртенето на ролките от подемния полиспаст, след което получените сили се коригират чрез съответните коефициенти. Определени са необходимият диаметър на буталото и необходимият ход на хидроцилиндъра за разпъване и прибиране на стрелата, след което е избран хидроцилиндър. Определен е разходът на работна течност на хидроцилиндъра. Определени са максималните сили във въжетата на полиспастите за разпъване и прибиране на горната секция на стрелата и са избрани въжета.
На базата на разработената методика е решен конкретен пример за кран КС - 45717, монтиран на автомобилно шаси КамАЗ.

Ключови думи: телескопична стрела, полиспаст, хидроцилиндър, въже

Introduction

The methodologies for the calculation of the mechanisms for hoisting, traveling, slewing and boom inclination of the cranes are given in the textbooks, referring to the load lifting machines, but a methodology for the calculation of the mechanism for the stretching of the boom is not given.

In Reutov (2013) equations for the calculation of the forces in the hydraulic cylinder and the cables for the stretching and retracting of the boom of a truck mounted crane are obtained. Calculations with and without the regard to the friction forces between the sections and the resistances in the hoisting tackle block is done.

In Sharipov (2002) a methodology for the calculation of the hydraulic drives is given. In „Kran strelovoi avtomobilnai KS 45717K-1" the design and the technical parameters of the calculated crane are given. In "Kanat dvoinoi svivki (GOST)"

the Russian standard for the cables, used in the truck cranes, is given.

The aim of the present work is the development of a methodology for the calculation of the mechanism for the stretching and retracting of the boom on the basis of these references. With the help of this methodology a concrete example is solved.

The boom of the crane KS-45717 (Fig.1) (Kran strelovoi avtomobilnai KS 45717K-1) is three sectional telescopic. It consists of a base section 4, a middle stretching section 2 and an upper stretching section 1. The mechanism for the stretching and retracting is mounted on the boom.

The sections of the boom have rectangular welded construction. In the front and back end of the movable sections are mounted the plastic plates 9, which guide the sections during their movement.
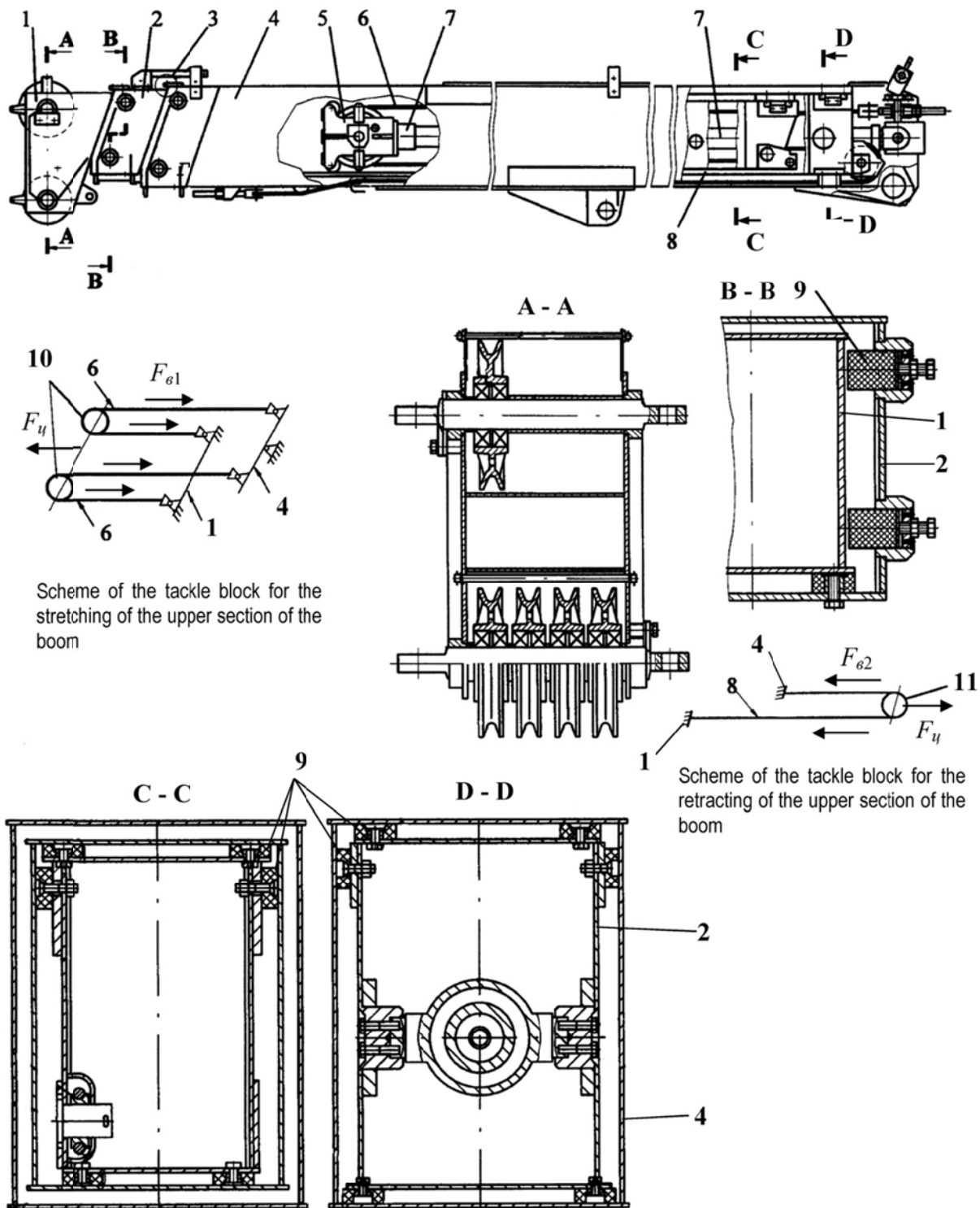
Fig. 1. Telescopic boom of the truck mounted crane KS-45717

1 - upper section; 2 - middle section; 3 - frame-restrictor of the hoisting cable; 4 - base section of the boom; 5 - bracket of the hydraulic cylinder; 6 - cables for the stretching of the upper section; 7 – hydraulic cylinder for stretching and retracting the boom; 8 - cable for the retracting of the upper section; 9 - plastic plates; 10, 11 - tackle blocks

$F_{в1}$ - tension in the cable for the stretching of the upper section of the boom; $F_{в2}$ - tension in the cable for the retracting of the upper section of the boom; $F_ц$ - force of the piston rod or the hydraulic cylinder for the stretching or retracting of the boom

The mechanism for the stretching and retracting of the sections of the boom consists of the hydraulic cylinder 7 and two cable tackle blocks. The cylinder ensures the movement of the middle section of the boom and the tackle blocks - the synchronic movement of the upper section of the boom when the middle section is moved.

The piston rod of the hydraulic cylinder 7 is attached to the back of the base section 4. The cylinder is attached to the back of the middle section 2. On the front end of the hydraulic cylinder 7 is mounted the bracket 5 with the blocks 10.

The tackle block for the stretching of the boom consists of the blocks 10 and the two cables 6. One of the ends of the cables 6 is attached to the back of the upper section 1 and the other - to the back of the base section 4.

The tackle block for the retracting of the boom consists of the block 11, mounted on the back of the middle section 2, and the cable 8. One of the ends of the cable 8 is attached to the back of the upper section 1 and the other - to the front end of the base section 4.

The length of the boom in unstretched position is 9m. When the middle section is moved toward the base section at a distance of 6m, which is equal to the stroke of the hydraulic cylinder, the upper section is moved toward the base section at a distance of 12m. This is, because the stretching tackle block has a ratio 2 and the upper section will move two times quicker than the middle section. In such a way the maximum stretched boom will have a length of 21m (9+12=21).

The retracting tackle block has also a ratio 2. When the cylinder retracts to the starting position the upper section will move backward 12m and the middle section - 6m.

Input data

The input data for the calculation of the mechanism is (Kran strelovoi avtomobilnii KS 45717K-):
- length of the boom L=9÷21m;
- angle of inclination of the boom β=5÷75°;
- lifting capacity of the crane at L=21m and β=75° Q_1=6.35t;
- lifting capacity of the crane at L=21m and β=5° Q_2=0.9t;
- mass of the upper section of the boom $m_в$=657 kg;
- mass of the middle section of the boom m_c=642 kg;
- mass of the hook block $m_{pб}$=306 kg;
- ratio of the tackle block of the hoisting mechanism m=8;
- velocity of stretching (retracting) of the boom v_{pc}=18m/min;
- nominal pressure of the working liquid in the hydraulic system of the cylinder for stretching of the boom $p_н$=20MPa;
- group of the working regime of the mechanism - 1.

Necessary force of the hydraulic cylinder for the stretching of the boom

With the purpose of simplifying the problem, the friction forces between the boom sections and the rolling resistances of the blocks of the hoisting tackle block are disregarded. We proceed with the principle from mechanics for the possible movements of the telescopic boom with the load. The work, which the piston rod of the hydraulic cylinder accomplishes, is

equal to the sum of the works, which the gravity forces of the middle and the upper sections of the boom and the hook block with the load accomplish. Then during the stretching of the boom the following equation is valid (fig.2):

$$F'_ц . s_ц = G_c . s_c . sin\beta + G_в . s_в . sin\beta + (G_m + G_{pб}) . s_m , \qquad (1)$$

where: $F'_ц$ [kN] - necessary force of the piston rod of the hydraulic cylinder for overcoming the gravity forces of the middle and the upper section of the boom, the load and the hook block;
$s_ц$ [m] - stroke of the piston rod of the hydraulic cylinder;
G_c [kN] - gravity force of the middle section of the boom;
s_c [m] - stroke of stretching of the middle section of the boom;
$G_в$ [kN] - gravity force of the upper section of the boom;
$s_в$ [m] - stroke of stretching of the upper section of the boom;
G_m [kN] - gravity force of the load;
$G_{pб}$ [kN] - gravity force of the hook block;
s_m [m] - distance of the movement of the hook block with the load.

As the piston rod of the cylinder is connected with the middle section of the boom and the upper section of the boom is connected with the middle section by a velocity tackle block with ratio m' (the upper section moves quicker than the middle section during the stretching of the boom) the following equations are valid:

$$s_ц = s_c ; \qquad s_в = m' . s_c \qquad (2)$$

The movement of the load during the stretching of the boom is determined by solving the equations (3÷6) together:

$$s_m = H_2 - H_1 \qquad (3)$$

$$H_1 = L_1 . sin\beta - h_1 \qquad (4)$$

$$H_2 = (L_1 + s_в) . sin\beta - h_2 \qquad (5)$$

$$h_1 - h_2 = \frac{s_в}{m} \qquad (6)$$

where: H_1, H_2 [m] - heights of the load toward the axis of the hanging of the boom before and after the stretching of the boom;
L_1 [m] - length of the boom before the stretching;
h_1 , h_2 [m] - distance between the top of the boom and the load before and after the stretching.

The following equation is obtained for the movement of the load:

$$s_m = s_в . \left(sin\beta + \frac{1}{m} \right) \qquad (7)$$

After the substitution of the equations (7) and (2) in the equation (1), the following equation is obtained for the necessary force of the piston rod of the cylinder:

$$F'_ц = (G_c + m' . G_в) . sin\beta + m' . (G_m + G_{pб}) . \left(sin\beta + \frac{1}{m} \right) \qquad (8)$$

The case when the boom is stretched from L_{min}=9m to L_{max}=21m at maximum angle of inclination (β=75°)
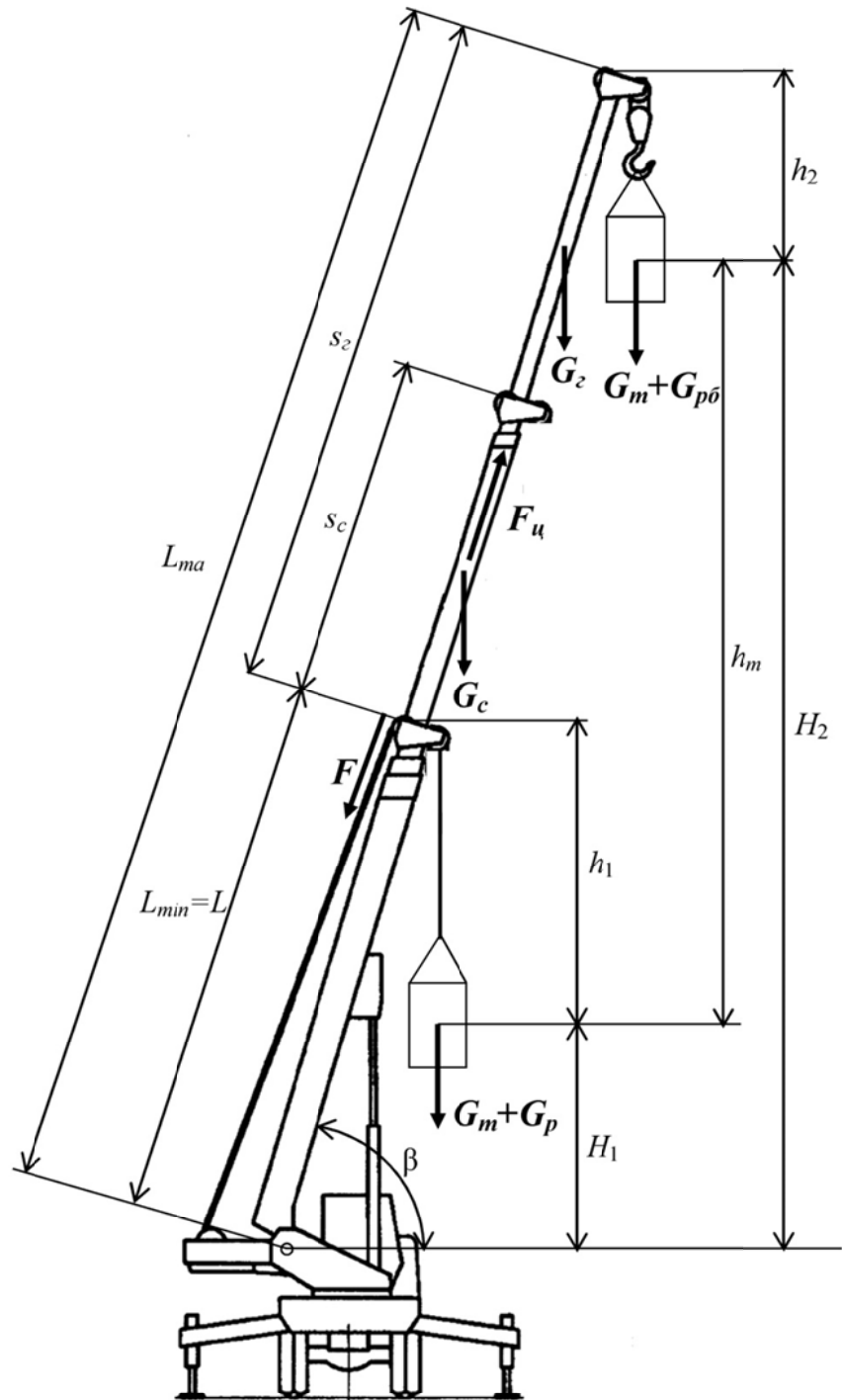
Fig. 2. Scheme for the calculation of the mechanism for the stretching and retracting of the boom

s_g, s_c - strokes of the upper and the middle section of the boom; L_{max}, L_{min}, β - maximum length, minimum length and angle of inclination of the boom; L_1 - length of the boom before the stretching; G_m, $G_{p\delta}$, G_g, G_c - gravity forces of the load, the hook block, upper section of the boom and the middle section of the boom; F - tension in the hoisting cable; H_1, H_2 - heights of the load toward the axis of the hanging of the boom before and after the stretching of the boom; h_1, h_2 - distances between the top of the boom and the load before and after the stretching of the boom; F_u - force of the piston rod of the hydraulic cylinder for the stretching of the boom

with load, equal to the maximum permissible for $L=21$m and $\beta=75°$, i.e. at lifting capacity $Q=Q_1=6,35$t is considered. The ratio of the tackle block for the stretching of the upper section of the boom is assumed to be $m'=2$. Then, the following equations are obtained:

$$F'_{\text{ц}}=(6,3+2.6,45).sin75+2.(62,3+3).\left(sin75°+\frac{1}{8}\right)=160 \text{ kN (9)}$$

where: $G_c = 0,001.m_c.g = 0,001.657.9,81 = 6,45$ kN (10)

$$G_e = 0,001.m_e.g = 0,001.642.9,81 = 6,3 \text{ kN} \qquad (11)$$

$$G_m = Q_1.g = 6,35.9,81 = 62,3 \text{ kN} \qquad (12)$$

$$G_{p6} = 0,001.m_{p6}.g = 0,001.306.9,81 = 3 \text{ kN} \qquad (13)$$

After the calculations with the regard to the friction forces between the sections (the coefficient of friction is $f=0.15$) and the rolling resistances of the blocks of the tackle the following is found out (Reutov, 2013): the resistance from the friction forces at maximum angle of inclination of the boom ($\beta=75°$) is 13% from the total resistance and at minimum angle of inclination of the boom ($\beta=5°$) - 80%; the rolling resistances of the blocks are 2.7% at $\beta=75°$ and 0.9% at $\beta=5°$. Then, the following equation for the necessary force of the hydraulic cylinder for the stretching of the boom is obtained:

$$F_{\text{ц}} = k_m.F'_{\text{ц}} = 1,19.160 = 190 \text{ kN} , \qquad (14)$$

where: k_m - coefficient, regarding the resistance of the friction forces between the sections of the boom and the rolling resistance of the blocks of the hoisting tackle during the stretching of the boom (it is determined by equations (15) and (16));

$$k_m=\frac{100}{100-(k_1+k_2)}=\frac{100}{100-(13+2,7)}=1,19 \quad \text{at } \beta=75° \qquad (15)$$

$$k_m=\frac{100}{100-(k_1+k_2)}=\frac{100}{100-(80+0,9)}=5,24 \quad \text{at } \beta=5° \qquad (16)$$

where: k_1 [%], k_2 [%] - percentage components of the resistance of the friction forces between the sections of the boom and the rolling resistance of the blocks of the hoisting tackle from the total resistance during the boom extension.

Now a second case is considered when the boom is stretched from $L_{min}=9$m to $L_{max}=21$m at a minimum angle of inclination ($\beta=5°$) with a load, equal to the maximum permissible for $L=21$m and $\beta=5°$, i.e. at lifting capacity $Q=Q_2=0.9$t. For this case the following equation is obtained:

$$F'_{\text{ц}}=\left(G_c+m'.G_e\right).sin\beta+a'.\left(G_m+G_{p6}\right).\left(sin\beta+\frac{1}{m}\right) \qquad (17)$$

$$F'_{\text{ц}} = (6,3 + 2.6,45).sin5° + 2.(8,8 + 3).\left(sin5° + \frac{1}{8}\right) = 6 \text{ kN}$$

$$F_{\text{ц}} = k_m.F'_{\text{ц}} = 5,24.6 = 31 \text{ kN} , \qquad (18)$$

where: $G_m = Q_2.g = 0,9.9,81 = 8,8$ kN (19)

From the equations (14) and (18) is seen that force, obtained at a maximum angle of inclination of the boom is greater, i.e. $F_{\text{ц}}=190$kN.

Necessary diameter of the piston of the hydraulic cylinder for the stretching and the retracting of the boom

$$d'_{\text{ц}} = \sqrt{\frac{4.S'_{\text{ц}}}{\pi}} = \sqrt{\frac{4.11904}{3,14}} = 123 \text{ mm} \qquad (20)$$

where: $S'_{\text{ц}}$ [mm²] - necessary area of the cross section of the cylinder (it is determined by equation (21));

$$S'_{\text{ц}} = \frac{1000.F_{\text{ц}}}{\Delta p.\eta_{\text{цм}}} = \frac{1000.190}{16,8.0,95} = 11904 \text{ mm}^2 , \qquad (21)$$

where: Δp [MPa] - pressure drop in the hydraulic cylinder (it is determined by equation (22)); $\eta_{\text{цм}}$ - mechanical coefficient of efficiency of the hydraulic cylinder ($\eta_{\text{цм}}=0.9\div0.95$);

$$\Delta p=p_{ex}-p_{u3x}=17-0,2=16,8 \text{ MPa} , \qquad (22)$$

where: p_{ex} [MPa] - pressure of the working liquid at the inlet of the hydraulic cylinder (it is determined by equation (23)); p_{u3x} [MPa] - pressure of the working liquid at the outlet of the hydraulic cylinder (it is assumed $p_{u3x}=0.2\div0.3$MPa);

$$p_{ex} = (0,8\div0,9).p_{\text{н}} = 0,85.20 = 17 \text{ MPa} \qquad (23)$$

Necessary stroke of the piston of the hydraulic cylinder for the stretching and the retracting of the boom

$$s'_{\text{ц}} = \frac{L_{max} - L_{min}}{m'} = \frac{21-9}{2} = 6 \text{ m} , \qquad (24)$$

where: L_{max} и L_{min} [m] - maximum and minimum length of the boom (see fig.2).

Selection of a hydraulic cylinder for the stretching and the retracting of the boom

The hydraulic cylinder is chosen according to the necessary diameter of the piston $d'_{\text{ц}}$ [mm] and the necessary stroke of the piston $s'_{\text{ц}}$ [mm]. The conditions (25 and 26) must be fulfilled:

$$d_{\text{ц}}=125 \text{ mm} \geq d'_{\text{ц}}=123 \text{ mm} \quad (25); \quad s_{\text{ц}}=6 \text{ m} = s'_{\text{ц}}=6 \text{ m} \qquad (26)$$

where: $d_{\text{ц}}$ [mm] - diameter of the piston of the cylinder; $s_{\text{ц}}$ [mm] - stroke of the piston of the cylinder.

The hydraulic cylinder KC-45717.63.900-1 is chosen with the following parameters: - diameter of the piston $d_\text{ц}$=125mm; - diameter of the piston rod $d_\text{ц1}$=100mm; - stroke or the piston rod $s_\text{ц}$=6000mm; - nominal pressure $p_\text{ц}{}^\text{н}$=20MPa.

Working liquid consumption of the hydraulic cylinder for the stretching and the retracting of the boom

$$Q_\text{ц} = \frac{0,06.S_\text{ц}.v_\text{ц}}{\eta_\text{цо}} = \frac{0,06.12265.0,15}{0,95} = 116 \text{ dm}^3/\text{min} , \quad (27)$$

where: $S_\text{ц}$ [mm^2] - cross section area of the hydraulic cylinder (it is determined by equation (28));
$v_\text{ц}$ [m/s] - necessary velocity of the piston rod of the hydraulic cylinder (it is determined by equation (29));
$\eta_\text{цо}$ - volumetric coefficient of efficiency of the hydraulic cylinder ($\eta_\text{цо}$=0,95).

$$S_\text{ц} = \frac{\pi.d_\text{ц}^2}{4} = \frac{3,14.125^2}{4} = 12265 \text{ mm}^2 \quad (28)$$

$$v_\text{ц} = \frac{v_{pc}}{60.m'} = \frac{18}{60.2} = 0,15 \text{ m/s} \quad (29)$$

Selection of cables for the stretching of the upper section of the boom

The size of the cables is chosen according to the necessary breaking strength. The following condition must be satisfied:

$$F_\text{разк} = 165 \text{ kN} \geq k.F_\text{в1} = 3,55.38 = 135 \text{ kN} , \quad (30)$$

where: $F_\text{разк}$ [kN] - breaking strength of the cable (it is dependent on the diameter of the cable d and the tensioning strength of the wires σ_B [N/mm^2]). At d=16mm and σ_B=1770N/mm^2 $F_\text{разк}$=165kN;
k - safety coefficient of the rope (it is determined from Table 1). At group of the regime of work or the mechanism 1, k=3.55;
$F_\text{в1}$ [kN] - maximum tension in the cable (see Fig.2) (it is determined by equation (29));

Table 1.
Safety coefficient or the cables k

Group of the regime of work of the mechanism	1	2	3	4	5	6
k	3.55	4	4.5	5.6	7.1	9

$$F_\text{в1} = \frac{F'_\text{ц} - \left(G_c + G_в + G_m + G_\text{рб}\right).sin\beta - F}{z_в}$$

$$F_\text{в1} = \frac{160+30-(6,3+6,45+62,3+3).sin75°-8,3}{2} = 38 \text{ kN} , \quad (31)$$

where: F [kN] - tension in the hoisting cable (Fig.2) (it is determined by equation (32)); $z_в$ - number of the cables for the stretching of the upper section of the boom ($z_в$ = 2);

$$F = \frac{G_m + G_\text{рб}}{\eta_n.m} = \frac{62,3 + 3}{0,933.8} = 8,3 \text{ kN} \quad (32)$$

where: η_n - coefficient of efficiency of the tackle block (it is determined by equation (33));

$$\eta_n = \frac{1-\eta_{po}^m}{\left(1-\eta_{po}\right).m} = \frac{1-0,98^8}{(1-0,98).8} = 0,933 , \quad (33)$$

where: η_{po} - coefficient of efficiency of one block (η_{po} = 0.98).
A cable type LK-RO (Kanat dvoinoi svivki LK-RO) 16-G-V-ZH-N-R-1770 GOST 2669-80 with diameter d=16mm, load (G), model of the wires V, with zinc-coated wires with surface density type ZH, non-twisting (N), balanced (R), with tensile strength of the wires σ_B=1770N/mm^2 and breaking strength $F_\text{разк}$=165 kN is chosen.

Selection of a cable for the retracting of the upper section of the boom

The size of the cable is chosen according to the necessary breaking strength. The following condition must be satisfied:

$$F_\text{разк} = 122 \text{ kN} \geq k.F_\text{в2} = 3,55.30 = 107 \text{ kN} , \quad (34)$$

where: $F_\text{разк}$ [kN] - breaking strength of the cable (at d=15mm and σ_B=1670N/mm^2 $F_\text{разк}$ = 122kN);
$F_\text{в2}$ [kN] - preliminary tension of the cable for the retracting of the upper section of the boom, necessary for the compensation of the pressure force to the cable when the boom is retracted (see Fig.2) (when the angle of inclination of the boom is large the retracting of the boom is done under its own weight) (it is assumed $F_\text{в2}$ = 30kN).

A cable type LK-R (Kanat dvoinoi svivki LK-R) 15-G-VK-ZH-N-R-1670 GOST 2669-80 with diameter d=16mm, tensile strength of the wires σ_B = 1670N/mm^2 and breaking strength $F_\text{разк}$ = 122 kN is chosen.

Conclusions

A methodology for the calculation of the mechanism for the stretching of the boom is developed, which will be useful for the specialists dealing with the design and exploitation of mobile cranes.

The maximum forces in the hydraulic cylinder and the cables of the mechanism are obtained at a maximum angle of inclination of the boom with a maximum permissible load.

References

Канат двойной свивки ЛК-Р и ЛК-РО конструкции 6х39 и 6х36. Государственный стандарт ГОСТ 7669-80, Kanat dvoinoi svivki LK-R i LK-RO konstruktsii 6x39 i 6x36 available at: https://znaytovar.ru/gost/2/GOST_766980_Kanat_dvojnoj_sviv.html (accessed 26 June 2017)

Кран стреловой автомобильный КС45717К-2. Руководство по эксплуатации, Kran strelovoi avtomobilnai KS457117K-2. Rukovodstvo po ekspluatatsii available at: http://www.uks76.ru/upload/docs/Rukovodstvo_po_ekspluatatsii_KS-45717K-2.pdf (accessed 26 June 2017)

Реутов, А.А. Расчет усилий механизма выдвижения телескопической стрелы. Вестник Брянского государственого технического университета 2013, №3 (39), Reutov, A.A. Raschet usilii mehanizma vaidvizheniya teleskopicheskoi strelai. Vestnik Bryanskogo gosudarstvenogo tehnicheskogo universiteta 2013, N3, available at: https://elibrary.ru/item.asp?id=20341615 (accessed 26 June 2017)

Шарипов, В.М. Проектирование механических, гидродинамических и гидрообъемных передач тракторов. М.: МГТУ "МАМИ", 2002, 300 с., Sharipov, V.M. Proektirovanie mehanicheskih, gidrodinamicheskih i gidroobemnaih peredach traktorov. M.: MGTU "MAMI", 2002, p. 300, available at http://window.edu.ru/resource/734/78734/files/mami_auto34.pdf (accessed 26 June 2017)

The article is reviewed by Assoc. Prof. Dr. Antoaneta Yaneva and Assist. Prof. Dr. Jivko Iliev.

WEAR AND MALFUNCTIONS OF GEARBOXES IN THE MINE LOCOMOTIVES FOR UNDERGROUND TRANSPORTATION

Lyuben Tasev

University of Mining and Geology "St. Ivan Rilski", 1700 Sofia, e-mail: nrbmo94@gmail.com

ABSTRACT. The paper examines the impact loads on the wheels of the underground mining locomotives derived from the dynamic loads and the impact they exert on the gearbox. The dependencies for the emergence and change of the forces are shown. Ways of wear reduction are suggested.

Keywords: Underground mine locomotives, wear, impact loads.

ИЗНОСВАНИЯ И ПОВРЕДИ В РЕДУКТОРИТЕ НА РУДНИЧНИТЕ ЛОКОМОТИВИ ЗА ПОДЗЕМЕН ИЗВОЗ
Любен Тасев
Минно-геоложки университет "Св. Иван Рилски",1700 София, e-mail: nrbmo94@gmail.com

РЕЗЮМЕ. В статията се разглеждат ударните натоварвания върху колооста на рудничните локомотиви за подземен извоз, получени от динамичните натоварвания, и въздействието, което оказват върху опорните точки на редуктора. Изведени са зависимости за появата и изменението на силите. Посочени са пътищата за ограничаване на износването.

Ключови думи: локомотиви за подземен извоз, износване, ударно натоварване

Introduction

The trend in the development of underground mining locomotives is increasing the speed of movement and traction power (Mateev, 1961). Restrictions on the dimensions of mining locomotives remain virtually unchanged, the development and modernization of these locomotives remain primarily related to the possibilities of creating powerful and compact drives. The development of the non-adjustable power drives for individual propulsion in the arm-suspension of the traction motor naturally takes place in accordance with the general trends in the mining locomotive (Volotkovskii S., 1981). Contemporary electric locomotives for underground mine transport have an increased rotation speed of the traction motor rotor. This allows more powerful motors to be mounted in the limited space. In most cases, the motor is positioned longitudinally (Figure 1). Maintaining the allowed speed of movement of the locomotive (12 km/h) in this way requires a corresponding increase in the gear ratio. As a result most of the modern mining electric locomotives are equipped with two-stage cylindrical gears with transverse traction (4.5 АРП2М, 5АРП и 7АРП) and conical-cylindrical wheels - with the longitudinal traction motor (see Figure 1) with (К10М1У,К7М1 РКЛ-7А, РКЛ-10А, РАЛ-8А, АМ8Д, etc.) These gearboxes are enclosed into a solid massive shell, made from cast steel or welded structure. The gearboxes houses both the engagement and the centering of the electric motor, as well as the bearing and transmission of the torque of the driven wheel.
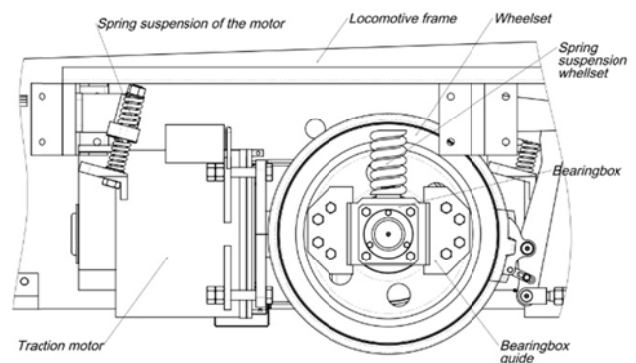
Exposition

Fig. 1. Longitudinal power drive РКЛ-10А

In its movement the locomotive experiences longitudinal, transverse and vertical loads caused by road irregularities, curves and conicity of the wheel bracelets. These loads are also transmitted to the gearbox through the drive wheels. All electrically-operated undercarriages are equipped with gearboxes mounted on the wheelset and spring-mounted via the frame motor (Figure 1). There are permanent and impact loads on the gear unit. The last ones are obtained from the accelerations (positive and negative) of the locomotive and the passage of the wheelset through the rail joints, the different types of arrows and other unevenness on the road.

With this kinematic coupling scheme, which is dominant for almost all railroad electric transport, the most powerful load is absorbed by the wheelset and all its components directly connected to it - the wheels, the shafts, the gear housing and the bearingbox. The reason for this is that the kinematic element is unsuspended and absorbs all traction and braking loads and assumes the dynamic loads from the unevenness of the road and the available gaps in the kinematic scheme. Such gaps are the technological loopholes that are in the sliding elements - the guide and the bearingbox. The links between the rails are particularly influential. The difference in heights and the gap between the two rails causes a shock load.

Fig. 2. Wear bearing housing

My studies have shown that the wear and deformation of the gearbox bearings as well as their housing (Figure 2) takes the most damages. There are some differences when we have a rolling or a plane bearing. Studies show that, in the primarily used rolling bearings, the process begins with gap formation in the gearbox body. In my opinion, this gap is due to plastic deformations caused by the different types of loads and, most of all, the impact ones. The appearance of the gap creates conditions for obtaining internal impact loads in the gear housing as well. At the beginning, the material splashes and further increases the gap. In the end, it gets such dimensions that the loads reach values exceeding the strength of the shell of the bearing. This leads to its destruction (Figure 3). This is an emergency state that blocks the wheelset, and the locomotive respectively.

In the plain bearing, there is a technological gap in the bearing itself, which is designed to provide lubrication of the bearing. This gap, mainly due to impact loads, is progressively increasing. This leads to deterioration of the lubrication of the bearing. It also leads to a change in the tooth spacing and worsening of the grip in the tooth.

Fig. 3. Destruction wheelset roll bearing K10M

The process continues until the kinematic connection between the gears is broken. In this process, the bearing bush (Figure 4) and also part of the gear housing are worn to the end. Although such a level of weariness seems absurd, I have found a significant number of such cases in our practice.

Fig. 4. Wear of plain bearing bush АМ8Д

The change in the center distance of the tooth pair leads to abnormal contact of the teeth and, respectively, to their intensive wear (Figure 5).

Fig. 5. Gear wear АМ8Д

Forces that act on the bearings, respectively the gear housing, will mainly be divided into static, dynamic and percussion. The static loads are determined by the weight of the gearbox and the engine coupled to it, as well as by the constant force produced by the wheelset - traction or braking, taking into account the center of gravity, the position of the motor suspension and the position of the bearings. Bearings, by construction, are arranged to be evenly loaded by this force, which means that each bearing takes up half of the load. In the drives I have studied, the center of gravity is located very close to half the distance between the engine suspension and the

gear axis. Under these conditions, each bearing will be loaded with the following force:

$$P_{cm} = \frac{\sum m_i}{2}, N; \qquad (1)$$

where: $\sum m_i$ is the sum of the masses of the involved elements.

The maximum traction effort is determined by the engine torque, the gear ratio and the traction coefficient (Mateev, 1961):

$$F_T = \psi \frac{2iM_{\partial в}}{D_k}, N; \qquad (2)$$

where: $M_{\partial в}$ - the rated torque of the engine;

i - the gear ratio of the power transmission;

D_k - the diameter of the traction wheel;

ψ - the traction coefficient.

Dynamic loads are caused by the change in speed in the longitudinal and transverse directions. Longitudinal accelerations are caused by the change in train speed. The accelerations obtained in the gearbox depend on the traction effort generated by the drive wheels and the total mass of the single drive, their size is being determined by the formula:

$$F = \frac{dv}{dt}(m_p + m_{\partial в}), N; \qquad (3)$$

where: m_p - mass of the gearbox;

$m_{\partial в}$ - mass of the traction motor.

The equation above is true in the absence of a technological and non-technological gap in the kinematic scheme of the gearbox and the machine (between the bearingbox and its guide - Fig. 6). In the presence of gaps (technological and non-technological) we have initial acceleration of the gear unit together with the motor until it is removed. When the gap is seized, the wheelset stops its movement, causing a stroke between the bearingbox and its guide. At the same time, the gearbox continues its movement until the technological and non-technological gaps in the bearing assembly are closed. Under these conditions, impact loads are obtained in the bearing housings of the hull and the bearings themselves. The magnitude of this impact is determined by the kinetic energy of the gearbox. Obviously, the wider the gap and the longer the drive's travel are, the higher the speed will be. It can be determined by the following equation:

$$E_{y\partial} = \frac{1}{2}v^2(m_p + m_{\partial в}), J; \qquad (4)$$

The ultimate speed of the single drive is determined by the force applied to it and the gap between the jack and the driver. Assuming the motion is equally accelerated, it can be written:

$$a_p = \frac{F_T}{m_p + m_{\partial в}}, m/s^2; \qquad (5)$$

and the ultimate speed will be:

$$v = a_p t$$
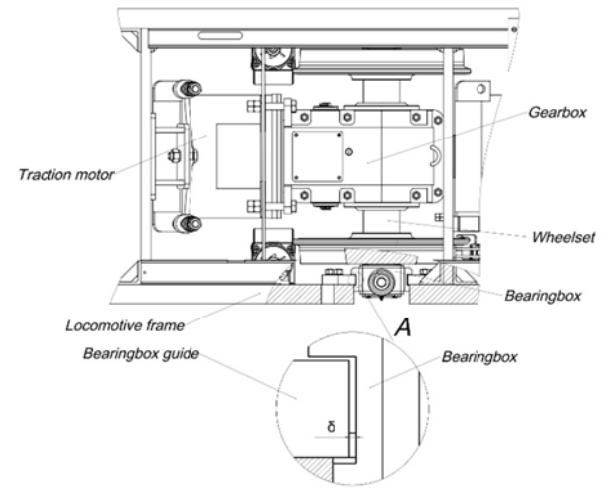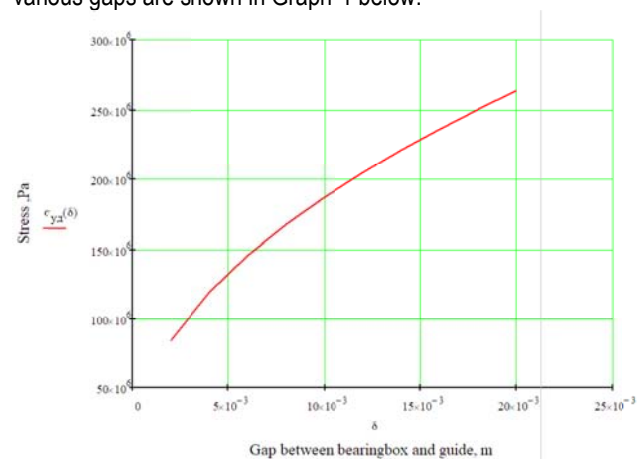$$F_{max} = P_{cц}\psi \qquad (6)$$

Fig. 6. Technological gaps of the power drive

Then the force of the impact, can be calculated based on (Kisyov, 1979):

$$k_{\partial} = 1 + \sqrt{1 + \frac{2\delta}{\Delta_{cm}}\frac{P_{ез}}{P_{ез} + G_{red}}} \qquad (7)$$

where: $\delta = \dfrac{v^2}{2a_{max}}$ is the gap between the bearingbox and its guide.

The stresses resulting from the above dependency for various gaps are shown in Graph 1 below.

Graph 1. Relationship between the gap and stress

It can be seen from the graph that at normal values of the gap of 5-10mm, the stresses have acceptable values of 180MPa. Similar stresses are also produced at the gear unit bearing. Hertz's calculated tensions are one and a half to two times greater. These high stresses lead to compacting, and

then to plastic deformations as shown in the above-mentioned figures. Additionally, the situation is complicated by obtaining a non-technological gap between the bearing and the bearing body. This clearance creates the conditions for an additional internal impact between the wheelset and all the elements attached to it and the gear housing. This impact stress initially leads to rapid increase of the gap and subsequently when the size is enough to destruction of the bearing.

Analogical impact loads are obtained by passing the wheelset through unevenness on the track, mainly the joints between the rails. These will be a topic of another paper.

Conclusion

This study aims to determine the magnitude of the impact forces that eventually lead to wear of the locomotive, and in some instances, to its failure. In my opinion, the limitation of the size of these forces is most likely to be achieved by extinguishing part of the energy of the impact.

In conclusion I can say that the grounded reason for getting gaps in the bearing assembly are the impact loads in a horizontal and vertical direction. The reduction of these loads in the horizontal direction can be constructively limited by the introduction of a damping element in the guiding drivers of the locomotive. The damping could be made of rubber elements to provide the necessary elasticity and mobility of the element, while attenuating the impact loads. To some extent, they reduce the impact loads in the vertical direction as they add the

entire mass of the locomotive to the dynamics of the process. Unfortunately, these constructions have a short operating life, which limits the application. Attempts to absorb such elements are made by various companies. At this stage, these elements have a limited resource, finding them applied to smaller machines. In the R & D base of the University of Mining and Geology "St. Ivan Rilski" under my leadership a similar damping mechanism is being developed. It is designed to take on loads of seven-tonne locomotives that are common in Bulgarian mines. It is of great importance to increase the resources of the existing locomotives to maintain the margin in the boundaries defined by the constructor, and to increase their repairs over the limit.

References

Матеев М., Руднична локомотивна тяга, Техника, Sofia, 1961; (Mateev M., Rudnichna lokomotivna tyaga, Tehnika, Sofia, 1961).

Волотковский С., Рудничная электровозная тяга, «Недра», Москва, 1981; (Volotokovskii S., Rudnichnaya elektrovoznaya tyaga, Nedra, Moskva, 1981

Кисьов И., Наръчник на инженера, Техника, София, (Kisyov I., Naruchnik na inzhenera, Tehnika, Sofia),1979.

AN APPROACH FOR DETERMINING THE INTERNAL FORCES IN A KNIFE BUCKET

Raina Vucheva[1], Violeta Trifonova – Genova[2]

[1] *University of Mining and Geology "St. Ivan Rilski", 1700 Sofia, r.wutschewa@abv.bg,*
[2] *University of Mining and Geology "St. Ivan Rilski", 1700 Sofia, violeta.trifonova@yahoo.com*

ABSTRACT: The article examines the internal forces in a knife bucket. It is modeled as a broken space frame. Its two ends are tilted. Furthermore it is supported by four-point rods. Most of the frame lies in one plane. The load on the teeth of the knife is asymmetric. It is located on the local axis of the section and is composed of two groups. The first group includes transvers forces and moments, lying in the plane. The second group load is composed of forces, lying in the plane and moments, perpendicular to it. A case is reviewed, in which the first group load is significantly higher than the second. This leads to solving the plane-space frame. A method of forces is used to determine the internal forces. The basic frame is obtained after removal of the unnecessary connections. For this frame linear equations and its relevant coefficients are described. By solution of the equations the reaction forces and the diagrams in the frame are obtained.
In the paper analytical expressions of bending and torsional moments in limited points of segments are given. These expressions are two groups. The first group of expressions is determined due to the action of the unit forces and moments, applied in excess ties, imposed on the system. The second group of expressions is obtained by external loads, composed of external forces and moments. The paper presents only a part of the developed methodology to determine the internal forces in a knife bucket of an excavator.

Keywords: knife bucket, method of forces, broken space frame

ЕДИН ПОДХОД ЗА ОПРЕДЕЛЯНЕ НА ВЪТРЕШНИТЕ СИЛИ В НОЖ НА КОФА НА БАГЕР
Райна Вучева[1] , Виолета Трифонова – Генова[2]
[1] *Минно-геоложки университет "Св. Иван Рилски", 1700 София, r.wutschewa@abv.bg,*
[2] *Минно-геоложки университет "Св. Иван Рилски ", 1700 София, violeta.trifonova@yahoo.com*

РЕЗЮМЕ: В статията се изследват вътрешните сили в конкретен нож на кофа на багер. Той е моделиран като начупена пространствена рамка. Двата й края са запънати. Освен това в четири точки тя е подпряна с пръстове. По-голямата част от рамката лежи в една равнина. Натоварването върху зъбите на ножа е несиметрично. То е разположено върху локалните оси на рамката и се състои от две групи. Първата група включва напречни сили и моменти, лежащи в равнината. Втората група натоварване се състои от сили, лежащи в равнината, и моменти, перпендикулярни на нея. Тук се разглежда случай, при който първата група натоварване е значително по-голяма от втората. Това води до решаване на равнинно-пространствена рамка. За определяне на вътрешните сили в неопределимата рамка се използва силов метод. След отстраняване на излишните връзки е определена основната система. За нея са описани каноничните уравнения и съответните коефициенти. От решението на тези уравнения са получени реакциите и диаграмите в рамката.
В работата са дадени аналитичните изрази за огъващите и усукващите моменти в гранични точки на участъците. Тези изрази са две групи. Първата група изрази са определени вследствие на действието на единичните сили и моменти, приложени в излишните връзки, наложени на системата. Втората група изрази са получени от външното натоварване, състоящо се от външни сили и съсредоточени моменти. В настоящата работа са представени само част от етапите на разработена методика за определяне на вътрешните сили в нож на кофа.

Ключови думи: нож на кофа, силов метод, пространствена рамка.

Introduction

The finite element method is often used to solve mechanical problems. According to it, the continuum body is presented as discrete models, interacting with each other. This method is described in many books for beams, plates and shells. It has led to the development of many powerful software products which facilitate the engineers' work. The implementation requires on the one hand, time to get acquainted with it and on the other hand, good preparation of the constructors to analyse the results. The exact description of the model's geometry is also important. It concerns the knife bucket of an excavator SRS 4000 (Dinev, 2016).

One of the criteria for reliability of the numerical method results is to compare them with their model tasks solved with classical methods. The approach of these methods to studying the behavior of structural elements consists in obtaining equilibrium equations for an infinite little element, establishing ratios between individual variables and solving these equations.

One such analytical method is the method of forces. The obtaining of (Dinev, 2016) the computational scheme of knifes will be explored. The load on the teeth consists of asymmetric forces. Typical of the frame is that it is for the most part plane.

One possible case of loading with forces is described here. It includes transverse concentrated forces and moments, lying in the plane of the frame. The purpose of the work is to describe with analytical expression the internal forces in boundary points of share in the frame.

Exposition

1. Application of the problem

Current computational scheme with dimensions according to Fig. 1 by (Dinev N., 2016) is considered. The load consists by force P_i^*, which is perpendicular to the plan $y_* z_*$, bending and torsional moments (M_{y_i} and M_{x_i}), which lie in the same plane and are applied in points A_i ($i = 1 \div 4$). In sections A_* and B_* the frame is fixed and is supported by four point rods.

2. Reactions forces

The load determines the approach to obtaining the internal forces. It is a broken and indefinable plane-space frame.

To build the diagrams it is necessary to determine the unnecessary connections imposed on the frame (fig.1). Their total number is 7. In this case, supports B_y, $M_{B,y}$, $M_{B,x}$, H_y, F_y, $A_{2,y}$, $A_{3,y}$ are suppressed and the basic frame is determined. There is a broken frame with hammock idler A.

The external loads and the reaction forces of the suppressed supports are applied. That's how the equivalent frame is obtained. The reaction forces must have such values, that the displacements in their directions of equivalent frame are zero. In this way a linear equation is obtained. This number is equal to the suppressed supports (Kisyov, 1978):

$$\sum_{j=1}^{7} \delta_{ij} X_j = \Delta_{i,P} \quad i = 1 \div 7 . \tag{1}$$

Here δ_{ij} is the displacement to direction i of the basic frame by the unit force, loaded instead of and towards X_j and Δ_{iP} is the displacement to the direction of unit force X_i, in basic frame loaded with a given load (P).

Equation (1) can be presented as follows:

$$[A]\{X\} = \{B\} , \tag{2}$$

Where:

$$\{X\}^T = \{X_1 \quad X_2 \quad X_3 \quad X_4 \quad X_5 \quad X_6 \quad X_7\}^T ;$$
$$\{B\}^T = \{\Delta_{1,P} \quad \Delta_{2,P} \quad \Delta_{3,P} \quad \Delta_{4,P} \quad \Delta_{5,P} \quad \Delta_{6,P} \quad \Delta_{7,P}\}^T ;$$

The basic frame is loaded only by an external load and only unit forces are applied in the suppressed supports. The reaction forces and diagrams of M_x^I, M_x^{II}, M_y^I, M_y^{II} are determined for each scheme. They correspond to two cases of load.
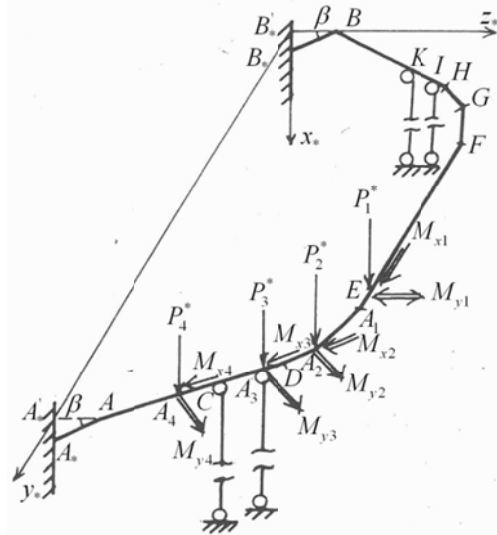

Fig. 1. Computational scheme

$$[A] = \begin{bmatrix} \delta_{11} & \delta_{12} & \delta_{13} & \delta_{14} & \delta_{15} & \delta_{16} & \delta_{17} \\ \delta_{21} & \delta_{22} & \delta_{23} & \delta_{24} & \delta_{25} & \delta_{26} & \delta_{27} \\ \delta_{31} & \delta_{32} & \delta_{33} & \delta_{34} & \delta_{35} & \delta_{36} & \delta_{37} \\ \delta_{41} & \delta_{42} & \delta_{43} & \delta_{44} & \delta_{45} & \delta_{46} & \delta_{47} \\ \delta_{51} & \delta_{52} & \delta_{53} & \delta_{54} & \delta_{55} & \delta_{56} & \delta_{57} \\ \delta_{61} & \delta_{62} & \delta_{63} & \delta_{64} & \delta_{65} & \delta_{66} & \delta_{67} \\ \delta_{71} & \delta_{72} & \delta_{73} & \delta_{74} & \delta_{75} & \delta_{76} & \delta_{77} \end{bmatrix} .$$

Then the coefficients of the system (1) can be determined by the expression:

$$\delta_{ij} = \delta_{ij}^1 + \delta_{ij}^2 ; \qquad \Delta_{iP} = \Delta_{iP}^1 + \Delta_{iP}^2 , \tag{3}$$

Where:

$$\delta_{ij}^1 = \sum_{k=1}^{m} \frac{1}{EJ_{y,k}} \int_{l_i} M_{y,i} M_{y,j} dx ;$$

$$\delta_{ij}^2 = \sum_{k=1}^{m} \frac{1}{EJ_{x,k}} \int_{l_k} M_{x,i} M_{x,j} dx ;$$

$$\Delta_{iP}^1 = \sum_{k=1}^{m} \frac{1}{EJ_{y,k}} \int_{l_k} M_{y,i} M_{y,P} dx ;$$

$$\Delta_{iP}^2 = \sum_{k=1}^{m} \frac{1}{EJ_{x,k}} \int_{l_k} M_{x,i} M_{x,P} dx .$$

Here m is the number of segment, i is the index of unknown support ($i = 1 \div 7$) and l_k is the length of segment.

Ready tables are constructed according to the rules, given by Vereshtchaguin (Trifonova-Genova, 2017). According to them two diagrams with same or different form are multiplied. These forms can be rectangular, triangular, trapezial and a combination of them.

The equations of equilibrium to the other reaction forces are described. They consist of: a sum of projected forces by axis x_* and equations for moments by axis y_* and z_*.

3. Diagrams of moments by load

3.1. Diagrams of unit forces

The segment i between points j and k has length (Fig. 2):

$$l_i = \sqrt{\left(\overline{y}_{ot,i}\right)^2 + \left(\overline{z}_{ot,i}\right)^2} \, , \tag{4}$$

Where:

$$\overline{y}_{ot,i} = y_*^k - y_*^j ; \overline{z}_{ot,i} = z_*^k - z_*^j \, .$$
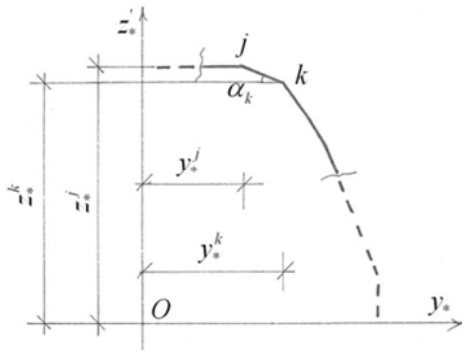

Fig. 2. The coordinates of points by the segment i

In equation (4) y_*^j and z_*^j are the coordinates of point j, but y_*^k and z_*^k are the same of point k.

The slope of section i with regard to the horizon is calculated by the expression:

$$\alpha_i = arctg \frac{\overline{y}_{ot,i}}{\overline{z}_{ot,i}} \, . \tag{5}$$

The arm of moment in point k by force applied in point j is determined by the expression (Fig.3a) (Valkov et al., 2013; Valkov, 2011) :

$$d_k^j = \sqrt{\left(\overline{y}_{ot,i}^*\right)^2 + \left(\overline{z}_{ot,i}^*\right)^2} \, . \tag{6}$$

Here $\overline{y}_{ot,i}$ is the width and $\overline{z}_{ot,i}$ is the height of the segment i.
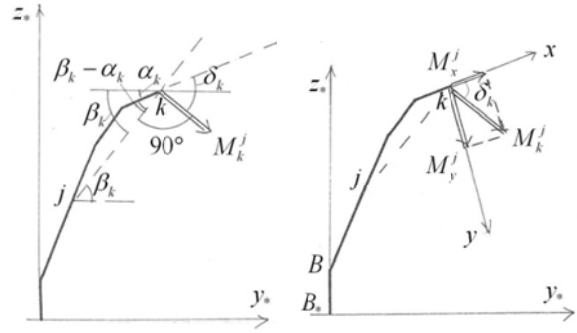

Fig. 3a   **Fig. 3б**

Fig. 3. The components of moment in point k, by the unit force in point j (left part of frame).

The slope of arm by horizontal axis is written in:

$$\beta_k = arctg \frac{y_{ot,k}^*}{z_{ot,k}^*} \, . \tag{7}$$

The method of forces is applied in this analysis. The components of moments by unit force applied in point j and perpendicular to the plane of frame are determined by two steps. In the first step M_k^j is determined:

$$M_k^j = 1.d_k^j = d_k^j \, , \tag{8}$$

This moment is perpendicular by arm.

In the second step this moment is resolved by local axis of section (Fig.3b):

$$M_y^j = M_k^j \sin \delta_k ; \ M_z^j = M_k^j \cos \delta_k \, , \tag{9}$$

In this expression the angle is determined by two methods. The angle to the points found on the left of the axis of symmetry, is calculated by (Fig.3a and Fig.3b)

$$\delta_k = 90 - \left(\alpha_k - \beta_k\right) \, . \tag{10}$$

When the angle to the points found on the right of the axis of symmetry, is calculated by

$$\delta_k = 90 - \left(\alpha_k + \beta_k\right). \tag{11}$$

In the points B_*, K, I, A_3 „ C unit forces are applied (Fig.1) and the diagrams $M_{x,i}^j$, $M_{y,i}^j$ are obtained. In these formulas i is the segment number, but the number $j = 1,4,5,6,7$. The numbering starts at segment B_*B ($i = 1$) and goes to segment AA_* ($i = 15$).
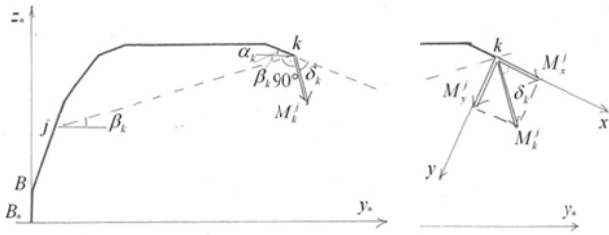
Fig. 4a   **Fig. 4b**

Fig. 4. The components of moments in point k **, by unit force applied in point** j **(right part of frame)**

3.2. Diagrams of unit moments

The components of moment in the current segment, when the frame is loaded by unit moments by axis y_* (Fig.6) are given as follows:

$$M^2_{x,i} = \varsigma \sin \alpha_i; \ \ M^2_{y,i} = \cos \alpha_i. \qquad (12)$$

The coefficient ς has two values. For points located to the left of the axis of symmetry $\varsigma = -1$ (fig.6a). The second value is $\varsigma = 1$ (fig.6b).
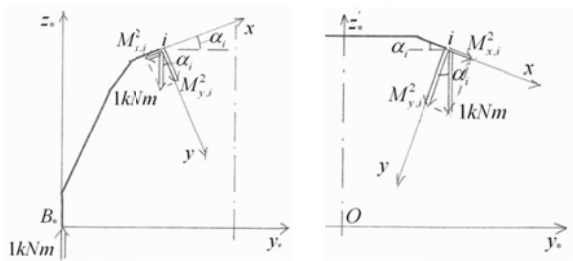

Fig.6a   **Fig.6b**

Fig. 6. The Components of moment in point k **, by unit vertical moment, applied in point** B_*

In the case when the basic frame is loaded by unit moment by axis y_*, the components of moments are expressed:

$$M^3_{x,i} = \cos \alpha_i; \ M^3_{y,i} = \varsigma \sin \alpha_i. \qquad (13)$$

The coefficient ς has a point value 1 for points located to the left of the axis of symmetry (Fig.7a), and the value -1 for the others (Fig.7b).

4. Diagrams by external load

The diagrams of forces (P^{*I}_i), applied in point A_i ($i = 1 \div 4$), are described in paragraph 3. The external moments of Figure 8 are projected on the local axis of each segment.
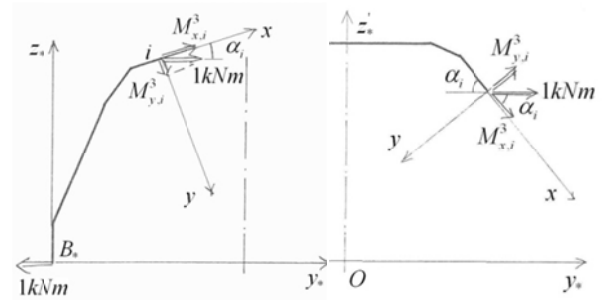

Fig. 7a   **Fig. 7b**

Fig. 7. Component of moment in point k **, by unit horizontal moment, applied in point** B_*
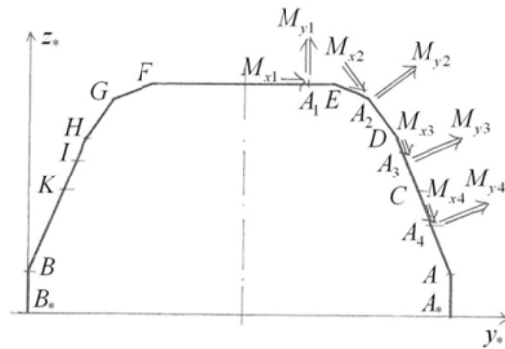

Fig. 8. External load in the plane of the frame

Then, their components can be written as:

$$M_{x,i} = \sum_{l=1}^{m_1} M^l_{x,i}; \qquad M_{y,i} = \sum_{l=1}^{m_1} M^l_{y,i}, \qquad (14)$$

where

$$M^l_{x,i} = -M_{xl} \cos \alpha_{ol,i} + M_{yl} \sin \alpha_{ol,i};$$
$$M^l_{y,i} = M_{xl} \sin \alpha_{ol,i} + M_{yl} \cos \alpha_{ol,i}.$$

In expressions (14) m_1 takes values, given in Table 1, depending on the number of segment.

Table 1
Values of constant m_1

m_1	1	2	3	4
section	8 и 9	10 и 11	12 и 13	14 и 15

The angle in expression (14) has the appearance (Fig.9):

$$\alpha_{o1,i} = \alpha_i \qquad \rightarrow \quad 8 \leq i \leq 15; \qquad (15)$$
$$\alpha_{o2,i} = \alpha_i - \alpha_{10} \quad \rightarrow \quad 10 \leq i \leq 15;$$
$$\alpha_{o3,i} = \alpha_i - \alpha_{11} \quad \rightarrow \quad 11 \leq i \leq 15;$$
$$\alpha_{o4,i} = \alpha_i - \alpha_{11} \quad \rightarrow \quad 14 \leq i \leq 15.$$
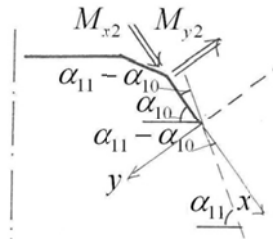
Fig. 9. External load in segment 10 and 11

4. The reactions of forces in indefinable frame

After solving the system (1) the reaction forces are determined. The principle of independent action by the forces is used (Kisyov, 1978):

$$R_j = R_{j,P} + \sum_{i=1}^{7} R_{j,i}^l X_i . \qquad (16)$$

In this expression R_j is the reaction force in the direction j of arbitrary support from the equivalent frame;

$R_{j,P}$ is the reaction force in direction j of support by the external load in basic frame only from the specified load;

$R_{j,i}$ is the reaction force in direction j of the same support by unit force in basic frame.

For the other reaction forces (B_x, B_{z_*}, M_{Bz_*}) equilibrium equations are recorded.

5. Diagrams in indefinable frame

The same principle is applied for determining the diagrams of moments. They are a sum of the algebraic ordinates of the diagrams by external load (P) with the ordinates of all single diagrams, multiplied by the respective unknown values X_j in each segment. Following this rule, in an arbitrary section of the system, the diagrams M_x and M_y are built by (Kisyov, 1978):

$$M_x = M_{x,P}^{**} + \sum_{i=1}^{7} M_{x,i} X_i ;$$

$$M_y = M_{y,P}^{**} + \sum_{i=1}^{7} M_{y,i} X_i . \qquad (17)$$

In these expressions $M_{x,P}^{**}$ and $M_{y,P}^{**}$ are the ordinates from the corresponding diagrams in an arbitrary segment, but $M_{x,i}$ and $M_{y,i}$ are the ordinates in a diagram unit with number i in the same segment.

6. Key findings

The expressions for internal forces are used to develop algorithms and programs for their automated determination. These results represent an extension of the solution given in (Kisyov, 1978) for a rectangular plane space frame.

Conclusion

A part of the developed methodology and algorithm for resolving the undefined plan-space frames is presented in this article. They are part of a comprehensive study of stresses in a knife bucket of an excavator.

The computational results from the external load on a specific frame will be described in future studies.

A description of the decision is forthcoming, by forces, lying in the plane and moments perpendicular to it.

References

Вълков М. Съпротивление на материалите – част 1 - еластостатика , Изд. Къща „Св. Ив. Рилски", 2011, 300с. (Valkov M., Saprotivlenie na materialite – chast 1- elastostatika, Izd. Kashta "Sv. Iv. Rilski", 2011, 300s.)

Вълков М. Теоретична механика – част 1 -Статика , Изд. Къща „Св. Ив. Рилски", 2004, 204s. (Valkov M., Teoretichna mehanika – chast 1- Statika, Izd. Kashta "Sv. Iv. Rilski", 2004, 204s.)

Вълков М., Ст.Пулев Ръководството за решаване на задачи по теоретична механика. Част I. Статика, Изд. къща „Св. Ив. Рилски", С., 2013, 133 с. (Valkov M., St. Pulev, Rakovodstvo za reshavane na zadachi po teoretichna mehanika. Chast I. Statika, Izd. kashta "Sv. Iv. Rilski", 2013, 133s.)

Динев Н., Р.Вучева, В.Трифонова-Генова, Изследване върху напрегнатото състояние на нож на кофа на роторен багер SRS 4000, *Годишник на МГУ „Св. Ив. Рилски"*, т. 59, св.I, 2016, 165 - 108. (Dinev N., R. Vucheva, V. Trifonova-Genova, Izsledvane varhu napregnatoto sastoyanie na nozh na kofa na rotoren bager SRS 4000, *Godishnik na MGU "Sv. Iv. Rilski"*, t.59, sv. I, 2016, 165 – 108.)

Кисьов И., Съпротивление на материалите, Д. И. "Техника", С., 1978, 594с. (Kisyov I., Saprotivlenie na materialite, D. I. "Tehnika", S., 1978, 594s.)

Трифонова-Генова В., М. Вълков, А. Стоянов, С. Сезонов, Съпротивление на материалите, Сборник от задачи и методични указания, Изд. Къща „Св. Ив. Рилски", 2017. (Trifonova-Genova V., M. Vulkov, A. Stoyanov, S. Sezonov, Saprotivlenie na materialite, Sbornik ot zadachi i metodichni ukazania, Izd. Kashta "Sv. Iv. Rilski", 2017.)

AN APPROACH FOR DETERMINING THE NATURAL FREQUENCY OF A STEPPED SHAFT

Violeta Trifonova – Genova[1], Gergana Tonkova[2]

[1]University of Mining and Geology "St. Ivan Rilski", 1700 Sofia, violeta.trifonova@yahoo.com
[2] University of Mining and Geology "St. Ivan Rilski", 1700 Sofia, g._pis @abv.bg

ABSTRACT. The article discusses the question of the natural vibration in a stepped shaft with a transition segment. The test shaft consists of three segments. The second segment of the shaft is the transition between the first and the third, with a rounded radius. In the process of operation, the shaft acts by its natural vibration. For their determination, the approximate Reilly method is applied. According to the method a computational scheme is selected and then the load is calculated. A suitable method for determining displacements in points of the shaft axis is chosen and finally the frequency of the natural vibrations is calculated. According to the approximate method used, the shaft is modeled as a free beam loaded with vertical forces. Their values are equal to the weights of the individual portions to which each segment of the shaft is divided. These forces are applied across the widths of the portions selected by the package engineer. To determine the displacements from the computation scheme, the differential equation of the elastic line is used. The presence of many forces requires application of the method of numerical integration of the equation. For the transition segment of the stepped shaft, mathematical forms for determining the radii and weights of portions are derived. Accordingly, an algorithm for calculating their stiffness has been developed. Also, the mathematical forms that define the reaction forces and the bending moments in the origin of forces of the computational scheme are presented. The expressions for the displacement and the oscillations frequency are given. The presented solution supplements other existing solutions and helps to calculate more accurately the vibration of the shaft.

Key words: natural vibration, a stepped shaft, oscillation frequency, approximate method, differential equation of the elastic line

ЕДИН ПОДХОД ЗА ОПРЕДЕЛЯНЕ НА ЧЕСТОТАТА НА СОБСТВЕНИТЕ ТРЕПТЕНИЯ НА СТЪПАЛЕН ВАЛ
Виолета Трифонова – Генова[1], Гергана Тонкова[2]
[1] Минно-геоложки университет "Св. Иван Рилски ", 1700 София, violeta.trifonova@yahoo.com
[2] Минно-геоложки университет "Св. Иван Рилски", 1700 София, g._pis @abv.bg

РЕЗЮМЕ. В статията се разглежда въпросът за собствените трептения, възникващи в стъпален вал с преходен участък. Изследваният вал се състои от три участъка. Вторият участък от вала се явява преход между първия и третия, като е изпълнен със закръгление с определен радиус. В процеса на работа, върху вала действат собствени трептения. За тяхното определяне е приложен приблизителният метод на Рейли. Съгласно него е избрана изчислителна схема и след това е изчислено натоварването. Избран е подходящ метод за определяне на премествания в точки от оста на вала и накрая е извършено изчисляване на честотата на собствените трептения. Съгласно използвания приблизителен метод, валът се моделира като проста греда, натоварена с вертикални сили. Стойностите им са равни на теглата на отделните сегменти, на които е разделен всеки участък от вала. Тези сили са приложени в средите на избраните от конструктора ширини на сегментите. За определяне на преместванията от изчислителната схема се използва диференциалното уравнение на еластичната линия. Наличието на много сили изисква прилагане на метода на числено интегриране на това уравнение. За преходния участък на стъпалния вал са изведени аналитични изрази за определянето на радиусите и теглата на сегментите. Съобразно тях е разработен алгоритъм за изчисляване на коравините им. Изведени са и аналитичните изрази, с които са определени опорните реакции и огъващите моменти в приложните точки на силите от изчислителната схема. Дадени са изразите за преместванията и честотата на собствените трептения. Представеното решение допълва съществуващите решения и спомага за по-точното изчисляване на трептенията на вала.

Ключови думи: собствени трептения, стъпален вал, честота на собствени трептения, приблизителен метод, диференциално уравнение на еластична линия

Introduction

Most of the shafts used in the industry are stepped. In order to determine their reliability and continuous duty in field application, it is important to choose a method for their dimensioning under static and dynamic loads. That is why the improvement of the theoretical and numerical methods is a constant object of the authorities in this field.

Classical methods are also applied to the stepped shafts. To determine the frequency of its natural vibrations on a stepped shaft, an approximate method based on the method of Reilly is known (Feodosiev, 1965). A full study of this method in a shaft with a curved section is of interest. After a study, a solution has been found in the present work to determine the frequency of the natural vibrations, occurring in a stepped shaft with a transition section. It should be borne in mind that this area is of small size.

Exposition

The main objective of the article is to develop an approximate method and describe the approach road for its application to the stepped shaft with a transitional curvilinear segment.

1. Formulation of the problem

A stepped cylindrical shaft with step and geometric parameters according to Figure 1 (Anchev, 2011) is investigated. Here l_1, l_2 and l_3 are the lengths of the three sections, r is the radius of the transition zone, D and d are the diameters of the first and third segment of the relevant shaft respectively.
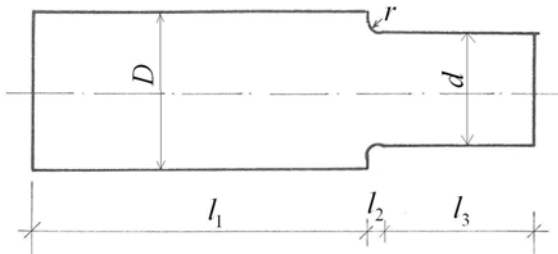

Fig. 1. Stepped shaft with a curved segment

2. Method for determination of internal forces
a) Weights of the portions in the individual segments of the shaft

In order to solve the problem a method is applied (Kisyov, 1965) according to which the shaft is divided into portions of sized widths $\Delta x_i, (i = 1, 2, 3)$ as shown in Figure 2. For each portion weights P_i are determined, as in the first and third segment are equal:

$$P_1 = V_1\gamma = S_1\Delta x_1\gamma = \pi R_1^2 \Delta x_1\gamma ,$$
$$P_3 = V_3\gamma = S_3\Delta x_3\gamma = \pi R_3^2 \Delta x_3\gamma , \tag{1}$$

where V_1 and V_3 are the volumes of portions in the first and third segments, S_1 and S_3 are the areas of their cross sections, expressed by the radii R_1 and R_3, and γ is the volumetric weight of the material of the shaft.
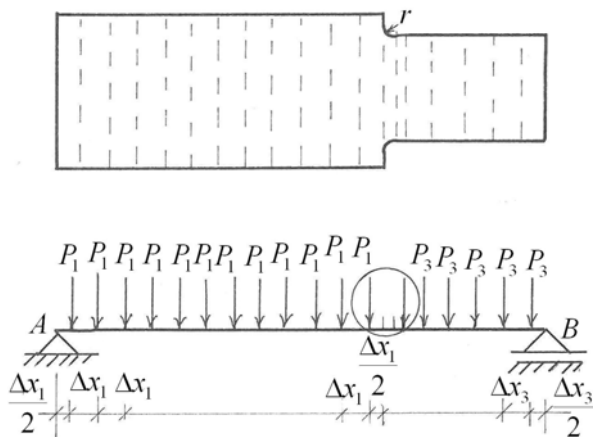

Fig. 2. Computational scheme

For the second curvilinear segment the weights of the portions are variables:

$$P_{2,i} = V_{2,i}\gamma = S_{2,i}\Delta x_2\gamma = \pi R_{2,i}^2 \Delta x_2\gamma , \tag{2}$$

where: $V_{2,i}$ are the volumes of the portions in the second segment; $S_{2,i}$ are the areas of the cross portions of the segments expressed by the radii $R_{2,i}$.

b) Current radius $R_{2,i}$ in second segment

The initial value of the radius in the second segment $R_{2,o}$ is the sum of the radius of the third segment and the bending radii (Fig. 3):

$$R_{2,o} = R_3 + r . \tag{3}$$

For a certain value of the arrow f_i dimensions central angle is determined, in degrees (Tsikunov, 1970):

$$\frac{n_i^o}{4} = \arcsin\sqrt{\frac{f_i}{2r}} . \tag{4}$$

On the other hand, the chord is expressed by the arrow of:

$$a_i = 2f_i \cot g\left(\frac{n_i^o}{4}\right) . \tag{5}$$

The current radius is expressed by the difference between the initial radius and the current chord:
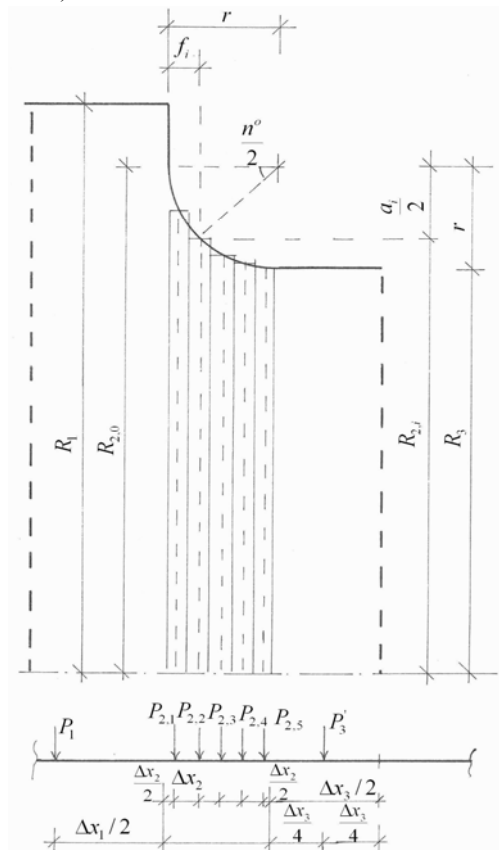
$$R_{2,i} = R_{2,o} - a_i . \tag{6}$$

Fig. 3. Computational scheme for a second segment

The diameters and moments of inertia are calculated according to the expressions:

$$D_{2,i} = 2R_{2,i}; \qquad J_{C2,i} = \frac{\pi D_{2,i}^2}{32}, \qquad (7)$$

and then the stiffness $EJ_{C_2 i}$.

In the next portion, the arrow accrues with the width:

$$f_i = f_{i-1} + \Delta x_2. \qquad (8)$$

Formulas (3), (4), (5), (6), (7) and (8) are used to calculate the stiffness of the second segment.

c) Algorithm for determining the stiffness of individual portions in a second segment

The algorithm for determining the stiffness of individual portions in the second segment consists of the following eleven steps:

Step 1 – Enter the values of f_1, r, R_3 and Δx_2.

Step 2 – A counter value is set i ($i = 1$).

Step 3 – Calculated $R_{2,o}$ from equation (3).

Step 4 – Calculated n_i^o from equation (4).

Step 5 – Calculated a_i from equation (5).

Step 6 – The current radius $R_{2,i}$ is calculated from equation (6).

Step 7 – Check that the current radius is smaller than the radius in the third section R_3 and if this is the case, go out of the cycle. Otherwise, move to the next step.

Step 8 – Calculate the diameter and the moment of inertia of (7), and then the stiffness $EJ_{C_2 i}$.

Step 9 – The counter is incremented by one.

Step 10 – The new arrow is calculated f_i from (8).

Step 11 – Check that the current arrow is larger than the bending radii. If this is the case, it goes out of the cycle. Otherwise, go to step 4.

An algorithm description is illustrated with a block diagram (Figure 4).

d) Determination of the supporting reactions

Consider the partial load computational scheme (Figure 5). The reaction forces are calculated (Valkov, 2004; Valkov et al., 2013):

$$A = \frac{1}{l}\left[P_1 \sum_{i=1}^{n_1} a_{i1} + \sum_{i=1}^{n_2} P_{2i} a_{i2} + P_3 \sum_{i=1}^{n_3} a_{i3} \right];$$

$$B = \frac{1}{l}\left[P_1 \sum_{i=1}^{n_1} a_{i4} + \sum_{i=1}^{n_2} P_{2i} a_{i5} + P_3 \sum_{i=1}^{n_3} a_{i6} \right]. \qquad (9)$$
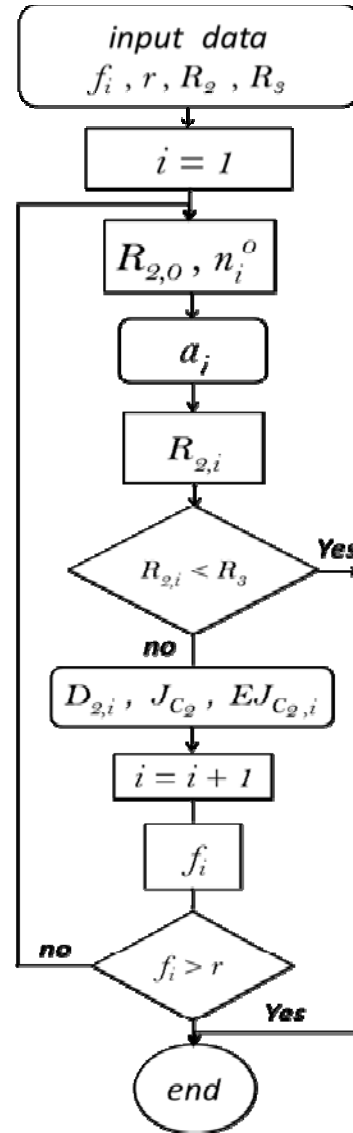

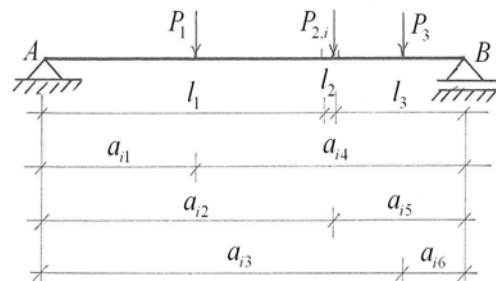Fig. 4. Block diagram of the algorithm for determining the radius $R_{2,i}$

Fig. 5. Computational scheme with partial load

In expressions (9) the arms of the forces a_{i1}, a_{i2}, a_{i3}, a_{i4}, a_{i5} and a_{i6} are determined by the expressions:

$$a_{i1} = \frac{\Delta x_1}{2} + \Delta x_1(i-1); \quad 0 \leq i \leq n_1;$$

$$a_{i2} = a_I + \frac{\Delta x_2}{2} + \Delta x_2(i-1); \quad 0 \leq i \leq n_2;$$

$$a_{i3} = a_I + a_{II} + \Delta x_3(i-1); \quad 0 \leq i \leq n_3; \quad (10)$$

$$a_{i4} = a_{III} + a_{II} + \frac{\Delta x_1}{2} + \Delta x_3(i-1); \quad 0 \leq i \leq n_1;$$

$$a_{i5} = a_{II} + \frac{\Delta x_2}{2} + \Delta x_2(i-1); \quad 0 \leq i \leq n_2;$$

$$a_{i6} = \Delta x_3(i-1); \quad 0 \leq i \leq n_3,$$

where

$$a_I = n_1 \Delta x_1; \ a_{II} = n_2 \Delta x_2; \ a_{III} = n_3 \Delta x_3.$$

e) Bending moment diagram

The moments in the individual points are determined with the following expressions (Kisyov, 1978; Valkov, 2011):

$$M_i = -A\overline{b}_{1i} + P_1 \Delta x_1 S_1; \qquad 0 \leq i \leq n_1;$$

$$M_i = -B\overline{b}_{3i} + P_3 \Delta x_3 S_1; \qquad 0 \leq i \leq n_3; \quad (11)$$

$$M_i = -A\overline{b}_{2i} + \Delta x_2 S_2; \qquad 0 \leq i \leq n_2;$$

where

$$S_1 = \sum_{j=1}^{i-1}(i-j); \ S_2 = \sum_{j=1}^{i-1} P_{2,j}(i-j),$$

$$b_k = \frac{\Delta x_k}{2}; \qquad b_{jk} = b_k + \Delta x_k(i-1); \quad (12)$$

$$j = 1,2,3; \qquad k = 1,2,3.$$

3. Natural vibrations

The slope of the elastic line is determined by integration, expressed by the sum of (Feodosiev, 1965):

$$\theta_i^* = \sum_{k=1}^{i} \frac{M_k}{EJ_k} \Delta x_k + C_1; i = 1,..n. \quad (13)$$

After integrating the expression (13) the displacement to point i is determined:

$$w_i = \sum_{k=1}^{i} \theta_i^* \Delta x_k + C_1 x_i + C_2 \quad (14)$$

In expression (14) C_1 and C_2 are coefficients which are determined by the boundary conditions $w_1(0) = 0$ and $w_n(l) = 0$, such as:

$$C_2 = 0 \text{ or } C_1 = -\frac{\sum_{k=1}^{n} \theta_k^* \Delta x_k}{l}. \quad (15)$$

The frequency of natural vibration has the form (Kisyov, 1978):

$$\left(\omega^I\right)^2 = \frac{\sum_{k=1}^{n} P_k^I w_k}{\sum_{k=1}^{n} P_k^I w_k^2}. \quad (16)$$

This determines the frequency of the first iteration of the approximate method. The forces are calculated according to:

$$P_i^{II} = P_i^I \frac{w_i\left(\omega^I\right)^2}{g}. \quad (17)$$

Here P_i^I is the value of the force, and w_i is the displacement from the first iteration.

Proceed with calculating the other parameters of the first iteration. The resulting solution is compared with that of the first iteration. The process continues until the results of two consecutive solutions differ with a predefined error.

4. Key findings

An approach for the application of the approximate method for a stepped shaft with curved transition segment is described in the article.

Analytical expressions for the radii and weights of the portions in the studied transition segment in the stepped shaft are obtained. According to them an algorithm for calculating the stiffness of the portions is developed. Typical of this is the choice of portion width. At a small width, a more accurate solution is reached. The derived expressions are the displacements and frequency of the natural vibrations.

The resulting solution is a summary described in (Feodosiev, 1965) approach to the natural frequency of the shaft.

Conclusion

The main advantage of the proposed algorithm is that it gives an accurate solution to the problem of determining the frequency of the natural vibrations of a stepped shaft with a curvilinear segment.

The disadvantage of the method under consideration is the possibility of a slight influence of the curvilinear segment on the value of the natural vibrations. This should be checked and tested on a real shaft, which is the subject of the next team work.

References

Анчев А, М. Ичкова, Определяне на коефициента на концентрация на напреженията при опън - натиск по МКЕ - известия на ТУ Габрово, том 42, 2011, 22-24с. (Anchev A., M. Ichkova, Opredelyane na koefitsienta na kontsentratsiya na naprezheniyata pri opan – natisk po МКЕ – Izvestiya na TU Gabrovo, tom 42, 2011, 22-24s.)

Вълков М. Съпротивление на материалите – част 1 - еластостатика , Изд. Къща „Св. Ив. Рилски", 2011, 300с. (Valkov M., Saprotivlenie na materialite – chast 1 - elastostatika, Izd. Kashta "Sv. Iv. Rilski", 2011, 300s.)

Вълков М. Теоретична механика – част 1 - Статика , Изд. Къща „Св. Ив. Рилски", 2004, 204с. (Valkov M., Teoretichna mehanika – chast 1- Statika, Izd. Kashta "Sv. Iv. Rilski", 2004, 204s.)

Вълков М., Ст.Пулев Ръководството за решаване на задачи по теоретична механика. Част I. Статика, Изд.

къща „Св. Ив. Рилски", С., 2013, 133 с. (Valkov M., S. Pulev, Rakovodstvo za reshavane na zadachi po teoretichna mehanika. Chast I. Statika, Izd. kashta "Sv. Iv. Rilski", 2013, 133s.)

Кисьов И., Съпротивление на материалите, Д. И. "Техника", С., 1978, 594с. (Kisyov I., Saprotivlenie na materialite, D. I. "Tehnika", S., 1978, 594s.)

Феодосиев В. И., Съпротивление на материалите, "Техника", София, 1965, 547с. (Feodosiev V. I., Saprotivlenie na materialite, "Tehnika", S., 1965, 547s.)

Цикунов А. Е. Сборник математических формул, Изд. „Вышэйшая школа", Минск, 1970, 203с. (Tsikunov A. E., Sbornik matematicheskih formul, Izd. "Vaishaya shkola" Minsk, 1970, 203s.)

DIGITAL CONTROL SYSTEM SYNTHESIS FOR THE OWI-535 ROBOTIC ARM EDGE MANIPULATOR

Yassen Gorbounov[1], Stefan Petrov[2], Tihomir Dzhikov[3]

[1] *University of Mining and Geology "St. Ivan Rilski", E-mail   y.gorbounov@mgu.bg*
[2] *University of Mining and Geology "St. Ivan Rilski", E-mail   stivannet@gmail.com*
[3] *University of Mining and Geology "St. Ivan Rilski", E-mail   itihomir.dzhikov@gmail.com*

ABSTRACT. An upgrade of the OWI-535 ROBOTIC ARM EDGE manipulator is discussed in the paper. It is done by building a multichannel PWM modulator to control the power circuits of the DC motors of the five coordinates of the manipulator. The modulator is built on a programmable logic device that allows easy configuration and scaling of the controller. Running parallel algorithms is inherent to this type of devices, which offers a significant advantage over conventional processors. A proposal is made to control the manipulator wirelessly over a mobile platform (smart phone or tablet) by using the Arduino open source platform as an intermediate controller that links the Bluetooth serial channel and the multichannel PWM modulator.

Keywords: Robotic manipulator, Arduino, Pulse Width Modulation (PWM), Programmable Logic Device (PLD)

СИНТЕЗ НА ЦИФРОВА СИСТЕМА ЗА УПРАВЛЕНИЕ НА МАНИПУЛАТОР OWI-535 ROBOTIC ARM EDGE
Ясен Горбунов[1], Стефан Петров[2], Тихомир Джиков[3]
[1] *Минно-геоложки университет "Св. Иван Рилски", 1700 София, E-mail   y.gorbounov@mgu.bg*
[2] *Минно-геоложки университет "Св. Иван Рилски", 1700 София, E-mail   stivannet@gmail.com*
[3] *Минно-геоложки университет "Св. Иван Рилски", 1700 София, E-mail   tihomir.dzhikov@gmail.com*

РЕЗЮМЕ. В статията е разгледана модернизация на манипулатора OWI-535 ROBOTIC ARM EDGE. Това е направено чрез изграждане на многоканален ШИМ модулатор за управление на силовите схеми на постояннотоковите двигатели на петте координати на манипулатора. Модулаторът е изграден на базата на програмируема логическа схема, която дава възможност за лесно конфигуриране и мащабиране на управлението. За тези схеми е присъща възможността за паралелно изпълнение на алгоритми, което е съществено предимство спрямо конвенционалните процесори. Предложена е възможност за създаване на безжично управление през мобилна платформа (смартфон или таблет) чрез използване на платформата с отворен код Arduino в качеството на междинен контролер, осъществяващ връзка между Bluetooth сериен канал и многоканалния ШИМ модулатор.

Ключови думи: Манипулатор, Ардуино, Широчинно-импулсна модулация (ШИМ), Програмируеми логически схеми

Introduction

The OWI-535 ROBOTIC ARM EDGE (OWI Inc., 2017) is a robotic hand with 5 degrees of freedom suitable for educational and training purposes (see in Fig. 1). The drive system for all coordinates is comprised of DC motors with gearboxes for which mechanical overload protection is provided. The control is carried out remotely on a wired connection, with the possibility of simply switching on or off the respective motor without changing the speed. The original schematic of the manipulator is depicted in Fig. 2. As is seen from the figure, the direction reversal is done with two-way switches. This limits the control options to merely manual control with no possibilities for any algorithmic control implementation or future extensibility. Furthermore, the motors exercise no torque at zero speed which means that one must rely on the capabilities of the mechanics alone.
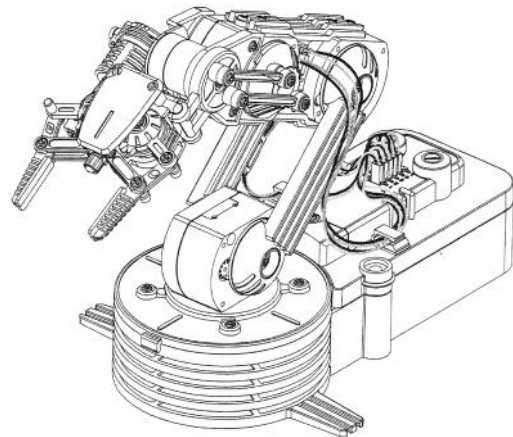

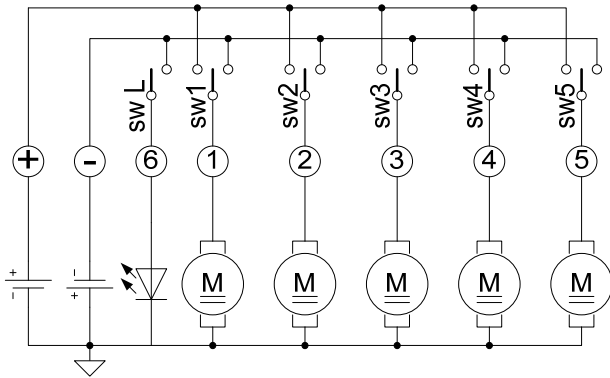**Fig. 1. OWI-535 Robotic Arm Edge Wired Controlled Arm Kit**

Fig. 2. OWI-535 Robotic Arm Edge original schematic

This paper discusses an upgrade of the drive system by implementing a PWM controller with dead time that is suitable for controlling full H-bridge power stages. This allows implementing both soft-chopping and hard-chopping switching strategies. This approach provides several advantages:

-   Smooth control over a wide speed range;
-   Achievement of a significant holding torque at zero speed;
-   High efficiency coefficient with full protection of the power transistors with no shoot-through.

The PWM module works at the lowest control level. The fact that it is embedded in a programmable logic device allows for all the axes to be driven simultaneously, which means that it can be easily expanded over industrial grade manipulators that run real-time algorithms.

After introducing the H-bridge driver and the PWM module, a proposal is made in the paper for using the open-source Arduino platform acting as an intermediate controller that links a remote mobile device, such as a mobile phone or a tablet PC, with the low-level control logic via a wireless Bluetooth serial connection. This allows the user higher-level interface to be designed on such a platform as Android OS or similar. The final objective, however, is to enable the OWI-535 manipulator to interface with scientific products such as Matlab or its free equivalent – Scilab. This will make it possible to study various algorithms for trajectory control, interpolation, etc.

H-bridge motor drive
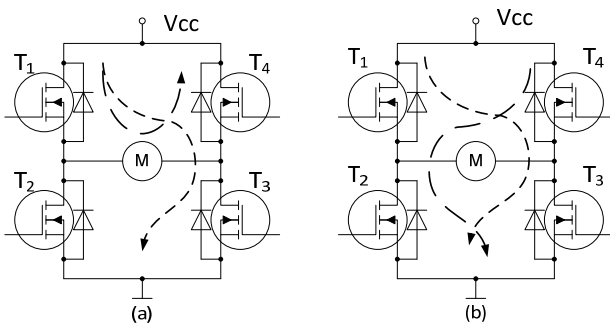
In Fig. 3 below, a full H-bridge is presented.

Fig. 3. Full H-bridge power stage built with N-channel MOSFETs

N-channel MOSFET transistors are used as power switches. They are controlled by voltage pulses and typically have internal resistance in the order of few milliohms when in on-state. This leads to very low active power dissipation. Since the motor windings are inductive in nature, a flyback diode is connected in parallel to the gate and source terminals. Two basic control strategies can be implemented with this circuit, namely: soft-chopping mode (Fig. 3, a) and hard-chopping mode (Fig. 3, b).

In soft-chopping (or non-symmetrical) mode, the transistor T1 is turned on for the entire phase excitation period while T2 and T4 are cut off. The diametrically opposed transistor T3 is controlled by the PWM pulses. When T3 is cutoff, a voltage with reverse polarity is created that attempts to maintain the value of the current flowing through the winding. There are two options: the current loop closes through T1 and the flyback diode of T4, or transistor T4 must be switched on to dissipate the stored energy. This method is not suitable for control at high speeds as the phase current diminishes relatively slowly and in some machines this can lead to a negative torque. In soft-chopping mode, the switching losses are lower and, hence, the energy efficiency is higher. This is good for the load in regards to the temperature.

In hard-chopping (or symmetrical) mode, all the transistors in the circuit are actively switching. In this mode, the switching losses are significant, which results in efficiency reduction. The increase in the operating frequency is limited as the switches have certain heat dissipation capabilities. This is a heavy operating mode in terms of temperature. On the other hand, this is the only way to achieve a static torque at zero speed. In this mode, both the speed and the direction depend on the PWM duty cycle, which is the same for each pair of transistors, T1-T3 or T2-T4. In this mode, the motor will rotate in the positive direction when the duty cycle is more that 50% and it will rotate in the negative direction when it is less than 50%. With a duty cycle of 50%, the motor is stopped despite the fact that it is fully loaded electrically. The latter guarantees the presence of a static torque at zero speed. One main peculiarity of this circuit is that a shoot-through can emerge if the transistors T1 and T2 or T3 and T4 remain switched on at the same time. Such a situation can occur if T2 is turned on before T1 cuts off and this can happen because of the recovery time of each transistor which prevents it to be cut off instantaneously. To ensure proper operation, the bridge shoot through should be avoided. This necessitates the introduction of the so called "interlock delay time" or "dead time" into the control scheme which represents a short period that ensures some time for the corresponding power switch to be fully turned off. The dead time calculation will not be discussed here but it should be mentioned that it is typically in the order of 0.3 to 5us (Selva, 2014; Infineon Technologies AG, 2007).

Pulse width modulator

The Pulse Width Modulation (PWM) is a technique for obtaining analog voltages by digital means. It is commonly used in power switching circuits like switched power supplies or motor inverters. For producing PWM, digital control is used to create a square wave which is a signal switched between on

and off. This is usually done using a triangle-shaped voltage and a comparator. Unfortunately, this very simple setup is not suitable for driving H-bridge topologies. Such circuits need the introduction of some current-less time period, known as the dead time. A two-way PWM module with configurable dead time is discussed below. It is written in Verilog HDL and implemented in a programmable logic device of the CPLD type. The block diagram of the module is given in Fig. 4.
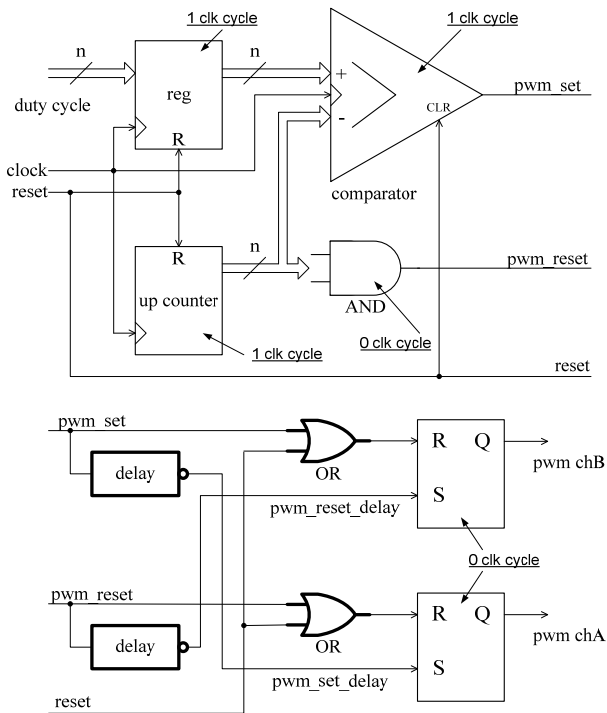

Fig. 4. Block diagram of the PWM module with dead time control capabilities

The operating principle of the circuit is based on the use of a counter and a comparator. When the reset signal is low (log. 0), the input register "reg", the counter, the comparator, and finally the two RS flip-flops at the output are all zeroed. If the reset goes high (log. 1), then at the first rising edge of the clock, the duty cycle assignment is stored in the input register "reg" and the up-counter increases by one. When the counter value reaches the duty cycle value, the comparator sets its output to log. 1 (rises the "pwm_set") thus resetting the output of channel B (see Fig. 5). At the same time, this signal starts up a monostable multivibrator (the upper "delay" block in the figure) which outputs a pulse with predefined length. Its output is negated and serves to set the output of channel A (see Fig. 5). The counter counts up and when it reaches the maximum value (all bits in log. 1 state; it saturates), the output of the AND gate ("pwm_reset") resets the output of channel A. At the same time, this pulse starts up a monostable multivibrator (the lower "delay" block in the figure) whose output serves to set the output of channel B. On the next rising edge of the clock, the counter overflows and starts counting again from 0. Then the whole algorithm repeats.

Fig. 4 shows the clock cycles that are consumed by each element. As is seen, all clocked modules consume 1 clock cycle, i.e. their output becomes valid after 1 clock period. All the asynchronous modules switch their outputs immediately.

The bold blocks in the figure represent the logic for implementing the dead time delay. The length of the delay pulse can be configured by setting a parameter in the "delay" block which technically leads to adding serially a flip-flop inside this block. That means that each delay unit corresponds to one clock cycle. The introduction of such a delay module allows for a precise setting of the dead time up to the resolution of the clock. Naturally, it can be assumed that the duty cycle of this PWM device is limited at both ends by the duration of the dead time. Therefore, the duty cycle should not be less than the dead time. If this condition is violated, the two channels will overlap and will be active at the same time, which is a prerequisite for a shoot-through and must be avoided. It is obvious that the higher the frequency and the resolution of the PWM are, the less the impact of this drawback is. In practice, this limitation is negligible as it falls outside of the useful operating mode.
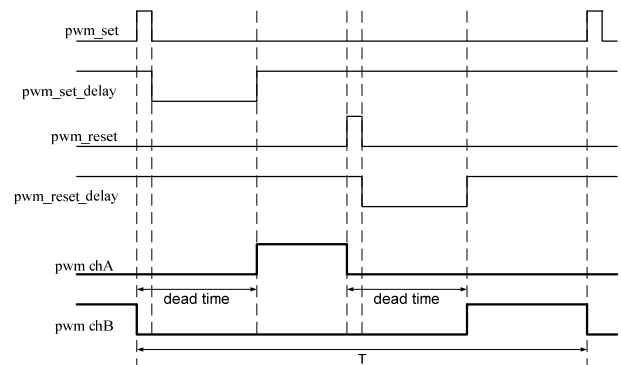
Fig. 5. Waveform that clarifies the principle of operation of the PWM

Fig. 6 and Fig. 7 show the experimentally obtained waveforms of an 8-bit PWM with clock frequency of 100 kHz. That means that the time resolution is 10us and the frequency of the PWM is about 390Hz. The usage of a CPLD permits the resolution to be configured to almost any value such as 9, 13 or 24 bits if needed. Also, the clock frequency can be augmented in the order of tens to thousands MHz. In the figures, the dead time, which is 30us for the sake of the experiment, can easily be seen.

Fig. 6. Output of channels A and B for an 8-bit PWM with duty cycle of 0xD0 at 100 kHz clock

Fig. 7. Output of channels A and B for an 8-bit PWM with duty cycle of 0x02 at 100 kHz clock

The elaborated PWM module can be easily modified to support multiple parallel running channels. The setup is depicted in Fig. 8. As is seen, the up-counter and the AND gate are common to all channels, so they are instantiated once for the entire device. The duty cycle register, the comparator, and the delay logic are rep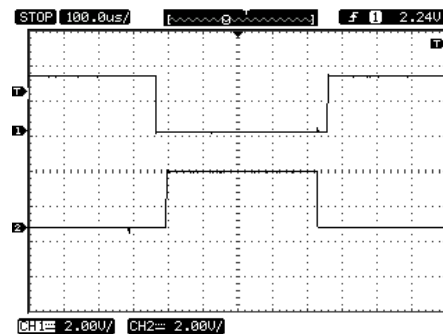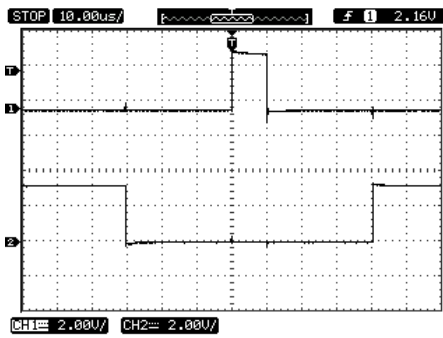eated for every channel. The number of channels depends on the available resources on the selected chip and does not affect the performance of the module as the CPLD makes them running in parallel. For the OWI-535, the PWM consists of 5 channels – one channel per coordinate. The usage of CPLD device resources increments linearly with the increase of the channel count and this makes the design flow quite predictable.
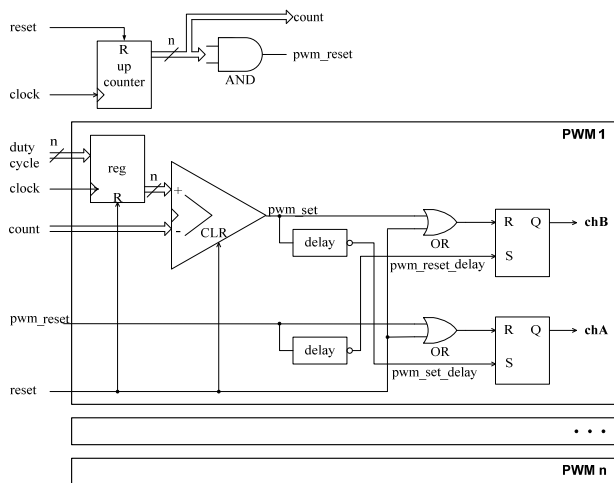

Fig. 8. Multichannel PWM configuration

Arduino intermediate controller

The PWM module discussed so far serves as a low-level controller for driving the motor. For the OWI-535 manipulator to be controlled, a higher-level device is required. The proposal here is to use the Arduino open source platform as an intermediate controller that makes a bridge between the PWM module and the user interface, or to use it as a standalone controller that generates the assignments for each axis. A block diagram of such a configuration is depicted in Fig. 9.
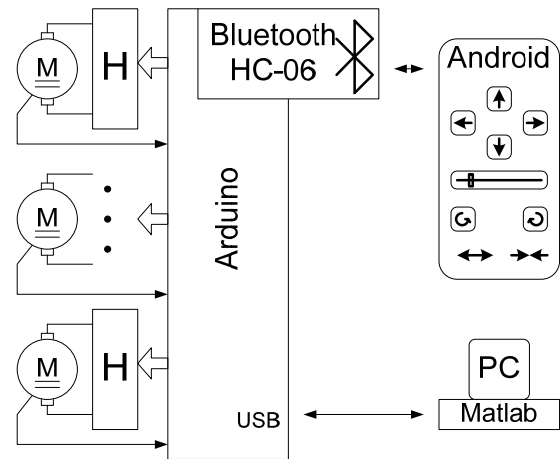

Fig. 9. Remote control of the OWI-535

Two options are shown. First, it is the Bluetooth serial connection. The main function of the Arduino is to translate the serially received commands to duty cycle assignments for each axis of the manipulator. Besides, the Arduino will check for boundary conditions for the assignments. This configuration will permit the manipulator to be controlled remotely. Second, it can be the interface between the OWI-535 ROBOTIC ARM EDGE manipulator and the commercial Matlab or the open source Scilab mathematical tool. This will give opportunity for studying algorithms and applying them to a real robot. And this is the final goal of this project.

The precise control of any device requires feedback information, so this is another function of the Arduino. A quadrature encoder can be used to obtain positional feedback. Another option is to build a sensorless control system by using a current sensor such as a Hall-effect sensor or a current transformer. It is convenient to implement maximum current control for limiting the force and protecting the motors. Furthermore, building a current feedback will provide information about the loading on each axis.

Future work

The results reported in this paper open possibilities for future work. This includes interfacing the OWI-535 ROBOTIC ARM EDGE manipulator with the Matlab scientific software. If a bigger programmable logic device (FPGA) is to be used, then an embedded microprocessor, such as Microblaze Soft Processor Core (Xilinx Inc., 2017) or Nios II (Intel Corp., 2017), can be implemented into the chip making the whole controller a standalone intelligent module. Also, SoC devices exist which incorporate FPGA fabric together with a single or dual core ARM MCU in a single chip.

Conclusions

An upgrade of the OWI-535 ROBOTIC ARM EDGE manipulator has been discussed in the paper. As a core component, a pulse width modulator module with embedded dead time control was described. The functioning of this module has been verified in practice on a XC2C256

CoolRunner CPLD from Xilinx. Two switching strategies have been evaluated: the soft-chopping and hard-chopping modes. Although being unfavorable for the motor because of the greater power losses, the hard-chopping mode proved to be more suitable for precision control of positioning devices since it guarantees significant static torque at zero speed and smooth control over a wider speed range.

The authors hope that the synthesized digital control system can be applied in several course units in the Department of Automation of Mining Production at the University of Mining and Geology "St. Ivan Rilski" in Sofia.

References

Gorbounov, Y. Fundamentals of digital design (in Bulgarian), University of Mining and Geology "St. Ivan Rilski", Sofia, 2016, ISBN 978-954-353-307-7

Gorbounov, Y. Application of programmable logic devices in electric drives (in Bulgarian), University of Mining and Geology "St. Ivan Rilski", Sofia, 2016, ISBN 978-954-353-306-0

Infineon Technologies AG, How to calculate and minimize the dead time requirement for IGBTs properly, AN2007-04, Application Note, V1.0, 2007

Intel Corp., Nios II Processor, USA, 2017, https://www.altera.com/products/processors/overview.html (Accessed July, 2017)

OWI Inc. dba: RobotiKits Direct, 17141 Kingsview Avenue, Carson, CA 90746, USA, http://www.owirobot.com/robotic-arm-edge-1/ (Accessed July, 2017)

Pavlitov, K. Programmable logic in electromechanics (in Bulgarian), Technical University of Sofia, ISBN 978-954-438-645-0, 2007

Selva R., V. Karthick, D. Arun. A Review on Dead-Time Effects in PWM Inverters and Various Elimination Techniques, School of Electrical and Electronics Engineering, SASTRA University, Thanjavur, Tamil Nadu, International Journal of Emerging Technology and Advanced Engineering, ISSN 2250-2459, ISO 9001:2008 Certified Journal, Volume 4, Issue 1, January 2014

Xilinx Inc., MicroBlaze Soft Processor Core, USA, 2017, https://www.xilinx.com/products/design-tools/microblaze.html (Accessed July, 2017)

The article is reviewed by Assoc. Prof. Dr. Diana Decheva and Assoc. Prof. Dr. Zdravko Iliev.

CHARGE ACCUMULATION IN THE PROCESS OF FILLING OF ELECTRIFIED LIQUID INSIDE A RESERVOIR

Stefan Stefanov[1], Ivan Prodanov[2]

[1] *University of Mining and Geology "St. Ivan Rilski", 1700 Sofia*

[2] *University of Mining and Geology "St. Ivan Rilski", 1700 Sofia, e-mail: enemko@mail.bg*

ABSTRACT. This study observes the problem with charge accumulation in the process of filling of electrified liquid inside a reservoir, to which Ohm's law applies.

Keywords: static electricity, electrification

НАТРУПВАНЕ НА ЗАРЯДИ В ПРОЦЕСА НА ЗАПЪЛВАНЕ НА НАЕЛЕКТРИЗИРАЩА СЕ ТЕЧНОСТ В РЕЗЕРВОАР
Стефан Стефанов[1], Иван Проданов[2]

[1] *Минно-геоложки университет "Св. Иван Рилски", 1700 София,*

[2] *Минно-геоложки университет "Св. Иван Рилски", 1700 София, E-mail: enemko@mail.bg*

РЕЗЮМЕ. Разглежда се проблемът за натрупване на заряди в процеса на запълване на резервоар с наелектризиращи се течности, за които е справедлива теорията на Ом за електризацията.

Ключови думи: статично електричество, електризация

Introduction

In the process of pumping of oil products along pipelines through pumps and filters, electrical charges are generated within the liquid. The filling of reservoirs is accompanied by the accumulation of electrical charges within the tanks' volumes. An electrical field with high voltage is generated in the gas space of the tank. The voltage of the electrical field is often sufficiently high to cause electrical discharges.

The risk of static electricity in oil industry, along with its effect on technical progress in the field of transport and storage of oil and oil products calls for the development of methods for prevention. This article studies the problems associated with static electricity during oil basic operations in the sequence that is determined by the technological production: charge generation and electrical leak in the pipelines; calculation of the electrical field in the reservoirs; methods for preventing static electricity risk.

To determine the static electricity risk in reservoirs, the electrical field energy should be regarded concurrently with the change of the concentration of oil product vapours within the vapour volume of the reservoirs during the forcing of electrified oil products [1].

This report focuses on the issue of charge accumulation during the filling of a reservoir with electrified liquid for which Ohm's law applies.

Exposition

1. Non-sectional tank

The input equation for charging in time is of the following type [2, 3]

$$\frac{dQ}{dt} = \left(\frac{dQ}{dt}\right)_{in} + \left(\frac{dQ}{dt}\right)_{rel}, \qquad (1)$$

where: $\frac{dQ}{dt}$ is the variation of charge Q, $[C]$, in the tank per unit of time t, $[s]$; $\left(\frac{dQ}{dt}\right)_{in}$ is the variation of charge in the tank per unit of time corresponding to the input current I_{in}, $[A]$ transferred by the stream of the tank incoming liquid; $\left(\frac{dQ}{dt}\right)_{rel} = I_{rel}$ is the variation of charge per unit of time determined by the charge relaxation.

For any moment of time t, equation (1) is valid where the phenomenon of relaxation is described. Employing this equation, we can put down

$$\left(\frac{dQ}{dt}\right)_{rel} = -\frac{Q}{\tau}, \tag{2}$$

where τ is the time-constant of the liquid relaxation, $\left[s\right]$.

Using the new notation, equation (1) is changed into

$$\frac{dQ}{dt} = I_{in} - \frac{Q}{\tau}, \tag{3}$$

The solution to equation (3) is

$$Q(t) = Q_{est}.(1 - e^{-\frac{t}{\tau}}), \tag{4}$$

where $Q_{est} = I_{in}.\tau$

The charge density is $\rho_V(t)$ established by dividing equation (4) by the liquid volume

$$\rho_V(t) = \frac{\tau.\left(1 - e^{-\frac{t}{\tau}}\right)}{t}.\rho_{in.V}. \tag{5}$$

For $t \gg \tau$ we have

$$\rho_V(t) = \rho_{in.V}.\frac{t}{\tau}. \tag{6}$$

2. Sectional tank

We discuss the common case of a partition of the tank into two sections by means of a barrier.

The liquid enters the first section and flows into the second section through an opening in the barrier. The liquid level in the two sections is equal.

The input equation for section one is of the type

$$\frac{dQ_1}{dt} = I_{in} - I_{rel.1} - I_{tr.1,2}, \tag{7}$$

where $\frac{dQ_1}{dt}$ is the charge variation per unit of time in the first section; $I_{rel.1}$ is the relaxation current in section one; $I_{tr.1,2}$ is the current transferred by the liquid and entering section two.

We write equation (7) using a new notation

$$\frac{dQ_1}{dt} = I_{in.} - \frac{Q}{\tau} - \frac{Q_1.(V_0 - V_1)}{V_1.t}, \tag{8}$$

where $V_0 - V_1$ is the total filling capacity of the first tank..

We introduce the notations $Q_1^* = \dfrac{Q_1}{I_{in.}.\tau}$ and

$f = \dfrac{V_0 - V_1}{V_1}$ and obtain

$$\frac{dQ_1^*}{dt} + \left(\frac{1}{\tau} + \frac{f}{t}\right).Q_1^* - \frac{1}{\tau} = 0. \tag{9}$$

The solution to equation (9) is as follows:

$$Q_1^* = \frac{\int_0^t e^{-\frac{t}{\tau}}.e^{\frac{1}{f}}.dt}{\tau.e^{-\frac{t}{\tau}}.e^{\frac{1}{f}}}. \tag{10}$$

The graphical dependence of $Q_1^* = \dfrac{Q_1}{I_{in.}.\tau.} = f.\left(\dfrac{t}{\tau}\right)$ is

such that Q_1^* increases proportionally to the rise of $f.\left(\dfrac{t}{\tau}\right)$.

After a given value of $f.\left(\dfrac{t}{\tau}\right)$, this proportion is disturbed and

a steeper rise of $f.\left(\dfrac{t}{\tau}\right)$ corresponds to a minor increase of

Q_1^*. The graph runs almost parallel to the $\dfrac{t}{\tau}$ axis.

The charge Q_2^* in the second section of the tank is determined by way of the charge variation in this section.

$$\frac{dQ_2}{dt} = I_{tr.1,2} - I_{rel.1,2} = I_{tr1,2} - \frac{Q}{\tau}, \tag{11}$$

where $I_{rel.1,2}$ is the relaxation charge in the second section.

Upon dividing equation (11) into $I_{in.}.\tau$, we get

$$\frac{dQ_2^*}{dt} = \frac{I_{tr.1,2}^* - Q_2^*}{\tau}. \tag{12}$$

To solve equation (12) with respect to Q_2^*, we need to have the numerical dependence of $I_{tr.1,2}$, determined by equation (7).

3. Approximate equation for determining the volume of a relaxation vessel

The variation in the amount of charge Q in the oil product that is forced into an earthed relaxation vessel is described by the following equation:

$$-\frac{dQ}{dt} = \frac{Q}{\tau} - i,\qquad(13)$$

where i is the current determined by the motion of the charged dielectric liquid in the pipeline; $\tau = \frac{\varepsilon_r.\varepsilon_0}{\gamma}$ (where ε_0 is the absolute dielectric permeability of the void: $8,86.10^{-12}\ \frac{F}{m}$, ε_r is the relative dielectric permeability of the liquid, and γ is the electrical conductivity of the liquid, $[\Omega^{-1}.m^{-1}]$).

Bearing in mind that there is no charge in the relaxation vessel at the initial moment of forcing the liquid, i.e. at $t = 0$ and with $Q = 0$, we get the following equation:

$$Q = i.\tau.(1 - e^{-\frac{t}{\tau}}),\qquad(14)$$

Since the stay period of the liquid in the relaxation vessel $t \gg \tau$, for the established mode, equation (13) changes into:

$$Q \approx i.\tau,\qquad(15)$$

In this manner, the amount of charge that is contained in the whole volume of the pumped oil product to be found in the relaxation vessel is approximately equal to the current i multiplied by the time for the product relaxation τ. The velocity of the flow in such a vessel is low; therefore, the charge generated in the vessel can be disregarded.

If V is the volume of the relaxation vessel, the average volume density of the liquid charge ρ_V is determined by the equation:

$$\rho_V = \frac{Q}{V} = \frac{i.\tau}{V},\qquad(16)$$

The value of the current induced by the flow of liquid that passes into the vessel at the forcing speed of $G\ \left[\frac{m^3}{s}\right]$ is

$$i_{res} = \rho_V.G = \frac{\tau.G}{V}.i,\qquad(17)$$

Deriving from expression (17), we can approximately determine the necessary volume of the relaxation vessel that provides the leak of a given amount of charge during continuous forcing of the oil product in the tank:

$$V = \frac{\tau.G}{k_0}.100,\ \left[m^3\right],\qquad(18)$$

where $k_0 = \frac{i_{res}}{i}.100$ is the amount of residual charge in the flow of the oil product from its initial value, $[\%]$.

It is worth noting that in formulating equation (18), the charge leak in the relaxation vessel is presumably due to the conductivity of the oil product and the convectional and diffusion current in the vessel itself which can both affect the charge leak in the vessel are not taken into consideration. Consequently, the actual necessary volume of the relaxation vessel might differ slightly from the calculated one. This is particularly valid for the dielectric liquid with specific volume resistance within the range of $10^{12}\ [\Omega.m]$ and higher.

Conclusion

A relaxation vessel should be used for removing hazardous accumulation of electrostatic charges during the forcing into tanks of combustible dielectric liquids with specific volume electrical conductivity of $10^{-9} \div 10^{-13}\ [\Omega^{-1}.m^{-1}]$. It necessarily has to be employed in cases when, with the aid of pumps and filters that are themselves sources of mass generation of electrical charges, the liquid is loaded into tanks with gas and vapour spaces by means of short pipelines or by means of a pipeline filled with an insulation material (e.g. polyvinylchloride).

References

Стефанов, С., И. Проданов. Статично електричество – теория и практика. С., Авангард Прима, 2013. (Stefanov, S., I. Prodanov. Statichno elektrichestvo – teoria i praktika. Sofia, Avangard Prima, 2013.)

Максимов, Б. К, А. А. Обух. Статическое электричество в промьшлености и защита от него. М., Энергия, 1978. (Maksimov, B. K., A. A. Obuh. Staticheskoe elektrichestvo v promaishlenosti I zashtita ot nego. M., Energiya, 1978.)

Попов, Б.Г, В.Н. Верьовкин, В. А. Бондарь, В. И. Горшков. Статическое электричество в химической промьшлености. Л., Химия, 1971. (Popoov, B. G., V. N. Veryovkin, V. A. Bondary, V. I. Gorshkov. Staticheskoe elektrichestvo v himicheskoi promaishlenosti. L., Himiya, 1971.)

CHARGE RELAXATION IN A RESERVOIR FILLED WITH ELECTRIFIED LIQUID

Stefan Stefanov[1], Ivan Prodanov[2]

[1] *University of Mining and Geology "St. Ivan Rilski", 1700 Sofia,*

[2] *University of Mining and Geology "St. Ivan Rilski", 1700 Sofia, e-mail: enemko@mail.bg*

ABSTRACT. This study observes the process of charge relaxation in a reservoir filled with electrified liquid, containing positively and negatively charged particles with volume density, as a function of the state of the liquid inside the reservoir, and of time.

Keywords: static electricity, charge relaxation

РЕЛАКСАЦИЯ НА ЗАРЯД В РЕЗЕРВОАР, ЗАПЪЛНЕН С НАЕЛЕКТРИЗИРАНА ТЕЧНОСТ
Стефан Стефанов[1], Иван Проданов[2]
[1] *Минно-геоложки университет "Св. Иван Рилски", 1700 София,*

[2] *Минно-геоложки университет "Св. Иван Рилски", 1700 София, e-mail: enemko@mail.bg*

РЕЗЮМЕ. Разглежда се процесът на релаксация на заряд в резервоар, запълнен с наелектризирана течност, съдържаща положително и отрицателно заредени частици с обемна плътност, явяваща се функция на положението на течността в резервоара и на времето.

Ключови думи: статично електричество, релаксация на заряд

Introduction

Contemporary multi-tonnage production requires high efficiency of the pipeline transport; therefore, limiting transportation speed to the safe values of between 0.7 and 1.4 $\left[\dfrac{m}{s}\right]$ presupposes the use of costly wide-diameter pipes.

Loading the apparata and tanks through a vertical pipe that has been lowered almost to the bottom ensures the safe liquid feed at a considerably high rate (permissible outflow rate). First, however, this type of feed is not always possible to ensure, and second, the permissible feed rates for liquids with high density charges are not that high. In both cases, it is necessary to use special gadgets that reduce electrification of the liquid flow along the pipeline and create more favourable conditions for discharging of the charge resulting from the free jet which moves below the liquid layer and the surface liquid in the tank.

Relaxation vessels of various structures are the most common means of reducing the value of the charge that is transferred to the tank from the jet outgoing from the pipeline [1]. The relaxation vessel of a relatively small size is placed on the feed pipe at the very inlet of the tank or apparatus. While residing in the relaxation vessel, the liquid gives off to the walls a larger part of the charge that has been transferred by the pipeline, exits the pipeline, and moves to the major tank or apparatus already relatively weakly charged. To avoid a possible inside blast, the relaxation vessel must all be filled up with liquid. The relaxation vessel must have such volume which ensures that the liquid residence time in it considerably exceed the relaxation period of the charge.

This report examines the process of charge relaxation in a reservoir filled with electrified liquid containing positively and negatively charged particles with volume density as a function of the position of the liquid in the tank, and of time.

Exposition

A random shape volume V with a surface area equal to S is studied. The volume is filled with electrified liquid containing positively and negatively charged particles with volume density ρ_+ and ρ_-, $\left[\dfrac{C}{m^3}\right]$ that are the function of the position of the liquid in the reservoir, and of time. The liquid charge is

$$\int_V (\rho_+ - \rho_-).dV \,. \tag{1}$$

The charge current in V is equal to

$$-\frac{\partial}{\partial t}(\rho_+ - \rho_-).dV = \int_S \vec{\delta}.d\,\vec{S}\,, \tag{2}$$

where $\vec{\delta}$ is the current density through surface S, $\left[\dfrac{A}{m^2}\right]$.

Employing the vector equation

$$\int_S \delta.dS = \int_V div\ \delta.dV, \tag{3}$$

We can put down

$$-\frac{\partial}{\partial t}(\rho_+ - \rho_-).dV = \int_V div\ \delta\, dV. \tag{4}$$

As far as the discussed volume V is random, integration can be omitted

$$-\frac{\partial}{\partial t}(\rho_+ - \rho_-).dV = div\ \vec{\delta}. \tag{5}$$

Let's establish the relation between current and intensity of the electrical field that generates the liquid charge

$$\vec{\delta} = k.(\rho_+ - \rho_-).\vec{E}, \tag{6}$$

where k is the ion mobility factor in the liquid, $\left[\dfrac{m^3}{V.s}\right]$, and

$\vec{E}$, $\left[\dfrac{V}{m}\right]$, is the vector of the intensity for the electrical field that generates the liquid charge.

In conformity with Poisson's equation

$$div\ E = \frac{\rho_+ - \rho_-}{\varepsilon_r.\varepsilon_0} = \frac{\rho_V}{\varepsilon_r.\varepsilon_0}, \tag{7}$$

where ε_0 is the absolute dielectric permeability of the void: $8,86.10^{-12}\ \dfrac{F}{m}$ and ε_r is the relative dielectric permeability of the liquid.

Combining equations (5) and (6) we get

$$-\frac{\partial}{\partial t}(\rho_+ - \rho_-) = div\left[k.(\rho_+ - \rho_-).\vec{E}\right] =$$
$$= k.(\rho_+ - \rho_-).div\ \vec{E} + \vec{E}.grad\left[k.(\rho_+ - \rho_-)\right] \tag{8}$$

Equation (8) is the output for determining the law of liquid charge relaxation.

It is generally considered [2, 3] that with liquids with specific electrical resistance of $10^{12}\ [\Omega.m]$ and less the degree of electrification does not influence electrical conductivity, i.e. under various conditions and with different liquids we have a sufficient amount of charge carriers from the two polarities, in other words $(\rho_+ - \rho_-) = const.$

In this case

$$k.(\rho_+ - \rho_-) = \gamma = const. \tag{9}$$

where γ is the electrical conductivity of the liquid, $[\Omega^{-1}.m^{-1}]$.

Upon substitution of equation (7) in equation (8), and taking into account equation (9), we obtain the differential equation

$$-\frac{\partial \rho_V}{\partial t} = \frac{\gamma.\rho_V}{\varepsilon_r.\varepsilon_0} = \frac{\rho_V}{\tau}, \tag{10}$$

where τ is the time-constant of the liquid relaxation, $[s]$.

The solution to equation (10) is of the type

$$\rho_V(t) = \rho_0.e^{-\frac{t}{\tau}}, \tag{11}$$

Multiplying equation (11) by volume V, we get the total liquid charge

$$Q(t) = Q_0.e^{-\frac{t}{\tau}}, \tag{12}$$

Where Q_0 and $Q(t)$ are respectively the total liquid charge, $[C]$, in the beginning $(t = 0)$ and at a random point of time.

Equation (12) is the law of liquid relaxation.

As long as $\tau = \dfrac{\varepsilon_r.\varepsilon_0}{\gamma}$, the charge relaxation rate is entirely determined by its specific electrical resistance $\dfrac{1}{\gamma}$, $[\Omega.m]$, since $\varepsilon_r.\varepsilon_0$ does not actually change in dielectric liquids with the change of electrical conductivity.

In conformity with equation (12), charge relaxation is commonly called Ohm's relaxation or Ohm's law.

For liquids with a rather high specific electrical resistance ($\rho \geq 10^{13}\Omega.m$), where the number of charge carriers determining their electrical conductivity is small, it would be

incorrect to assume that the complete number of carriers during the process of liquid excitation is constant. In this case it is assumed that the charging liquid contains carriers of only one polarity since the charges of one polarity are removed during excitation and charges of the opposite polarity are added. As a rule, electrical conductivity of such a liquid may exceed the initial conductivity due to excitation. Bearing in mind the above assumption, and considering the charge distribution as uniform throughout the whole volume, equation (8) is transformed into

$$\frac{\partial \rho_V}{\partial t} = \frac{k.\rho_V^2}{\varepsilon_r.\varepsilon_0} \,, \qquad (13)$$

In this case, ρ_V is the charge density with one plus or minus sign, depending on what the sign of the electrifying liquid is.

The solution to equation (13) is

$$\rho_V(t) = \frac{\rho_V}{1 + k.\rho_{V0}.\dfrac{t}{\varepsilon_r.\varepsilon_0}} = \frac{\rho_{V0}}{1 + \dfrac{t.\gamma_0}{\varepsilon_r.\varepsilon_0}} \,, \qquad (14)$$

where γ_0 is the electrical conductivity of the electrified liquid and ρ_{V0} is the charge density of the liquid at point $t = 0$.

Multiplying the left- and the right-hand sides of equation (14) by the volume of the liquid, we obtain Ohm's law of the relaxation of the liquid volume charge

$$Q(t) = -\frac{Q_0}{1 + \dfrac{t.\gamma_0}{\varepsilon_r.\varepsilon_0}} \,, \qquad (15)$$

Conclusion

As follows from equation (15), the value of the charge decreases in time according to a law that is similar to the hyperbolic law. In relation to this theory, the relaxation of a liquid whose electrical conductivity is less than $10^{-13} \ [\Omega^{-1}.m^{-1}]$ is generally referred to as hyperbolic.

According to equation (14), relaxation depends only on the initial charge density ρ_{V0} and on the ion mobility k.

In the intermediate range of liquid electrical conductivity, $10^{-9} \div 10^{-13} \ [\Omega^{-1}.m^{-1}]$, the process of charge relaxation is described as a combination of Ohm's law and the hyperbolic theory. In this case, the conductivity of the uncharged liquid γ_∞ is reported.

References

Стефанов, С., И. Проданов. Статично електричество – теория и практика. С., Авангард Прима, 2013. (Stefanov, S., I. Prodanov. Statichno elektrichestvo – teoria i praktika. Sofia, Avangard Prima, 2013).

Захарченко, В.В, Н.И. Крячко, Е.Ф. Мажара, В.В. Севриков, Н. Д. Гавриленко. Электризация жидкостей и ее предотвращение. М., Химия, 1975. (Zaharchenko, V. V., N. I. Kryachko, E. F. Mazhara, V. V. Sevrikov, N. D. Gavrilenko. Elektrizatsiya zhidkostey I ee predotvrashtenie. M.,Himiya, 1975).

Бобровский, С.А, Е.И. Яковлев. Защита от статического электричество в нефтяной промышлености. М., Недра, 1983. (Borovskiy, S. A., E. I. Yakovlev. Zashtita ot staticheskogo elektrichestvo v neftyanoi promaishlenosti. M., Nedra, 1983).

The article is reviewed by Prof. Dr. K. Trichkov and Assoc. Prof. Dr. Romeo Alexandrov.

DEFINING THE SPECIFIC LOSSES OF ACTIVE POWER IN SYNCHRONOUS ELECTRIC MOTORS FOR THE GENERATION OF REACTIVE POWER

Kiril Dzhustrov[1], Ivan Stoilov[2]

[1]*University of Mining and Geoology, 1700 Sofia, E-mail: justrov@mgu.bg*
[2]*University of Mining and Geoology, 1700 Sofia, E-mail: ivan.stoilov@mgu.bg*

ABSTRACT. The paper presents a methodology for the experimental defining of the specific losses of active power in the synchronous electric motors for the generation of reactive power. Experimental tests in the operation of powerful synchronous electric motors, driving mill units, disintegrators and pumps are made. The specific losses of active power for the generation of reactive power are defined in the synchronous electric motors in big mining and mineral processing enterprises in the country.

Keywords: specific losses, compensation of reactive loads

ОПРЕДЕЛЯНЕ СПЕЦИФИЧНИТЕ ЗАГУБИ НА АКТИВНА МОЩНОСТ НА СИНХРОННИ ЕЛЕКТРОДВИГАТЕЛИ ЗА ГЕНЕРИРАНЕ НА РЕАКТИВНА МОЩНОСТ

Кирил Джустров[1], Иван Стоилов[2]
[1]*Минно геоложки университет, 1700 София, E-mail: justrov@mgu.bg*
[2]*Минно геоложки университет, 1700 София, E-mail: ivan.stoilov@mgu.bg*

РЕЗЮМЕ. Дадена е методика за експериментално определяне на специфичните загуби на активна мощност в синхронни електродвигатели за генериране на реактивна мощност. Проведени са експериментални изследвания в практиката на мощни синхронни електродвигатели, задвижващи мелнични агрегати, дезинтегратори и помпи. Определени са специфичните загуби на активна мощност за генериране на реактивна мощност в синхронните електродвигатели на големи минно-обогатителни предприятия в страната.

Ключови думи: специфични загуби, компенсиране на реактивни товари

Introduction

The powerful synchronous electric motors have a wide application in our mining industry. They are used for driving of mill units, pumps, ventilation units and compressors. For instance, the overall installed power of the synchronous electric motors in the mineral processing plant in Asarel Medet JSC is 54.2 MW, of which 41.7 MW are operational. 13 synchronous electric motors with an overall installed power of 28.2 MW are in constant operation in the flotation mill in Elatsite Med JSC. The synchronous electrical motors operate in a regime for generation of reactive power with capacitive character which facilitates ensuring the balance of the reactive power for the overall enterprise. This is of particular importance for enterprises that do not have to achieve an average power factor below the neutral (cosφ = 0.9) for a 15 minute interval.

In order to compensate the reactive loads in the mining enterprises in our country capacitor batteries, operating mainly at a medium voltage of 6 kV, are also used. The elimination of the cost of consumed excess or reactive energy returned to the system, in accordance with the current electricity tariff and the maximum unloading of the reactive power grids, should be considered as a condition for optimal operation of compensating devices. The solution of the complex problem for optimum combined compensation of reactive loads in big enterprises requires assessment of the losses of active power for the generation of reactive power by the compensating devices.

The specific losses of active power for the generation of 1kVAr reactive power by the modern medium voltage capacitors are unambiguously accepted in the literature and are about 0.003 kW/kVAr. However, there is a different problem with the loss of active power by synchronous electric motors. There is insufficient data, often in a wide range of the specific losses during the reactive power generation, in the literature. For example, in (Dankov, 1991) are quoted values of specific losses of 0.009-0.05 kW/kVAr. Significantly higher values are given in (Fedorov, Kamneva, 1984): synchronous electric motors with power up to 5000 kW – 0.05-0.1 kW/kVAr; for low-speed motors - 0.1-0.15 kW/kVAr. The conducted experimental studies of synchronous electric motors of 2.5 MW and 1.6MW in (Chobanov, Menteshev, 2007) show an average value of the specific losses of 0.03 kW/kVAr. Apart from the large differences in the quoted values, it is not explained in what operating conditions the specific losses are obtained and whether they reflect the losses in all the units of the synchronous motor - coordinating transformer, rectifier, rotor coil and stator coil.

The lack of accurate data on the values of specific losses of the active power for reactive power generation is a significant obstacle for conducting a proper technical and economic analysis to optimize the allocation of reactive capacities within the plant. The purpose of this study is to develop the actual specific losses of active power to generate reactive power (α) of the main synchronous electric motors in our mining and mineral processing plants. During the production process, experimental tests of different types of synchronous machines were performed under normal operating modes and the values of α were determined.

Measuring equipment

All experimental studies were carried out with modern digital network analyzers FLUKE 437-II, FLUKE 435-II и FLUKE-43B. Accuracy class of the instruments during measurement:
- of the voltage ± 0.1% of nominal (1000V);
- of the current for the corresponding clamp-on ammeter ±0.5%;
- of the power ±1.0%.

Methods for conducting the experiment

The objective is to selectively determine the specific losses of active power in the stator coil, in the rotor coil and in the transformer-rectifier coordinating unit. For this purpose, a three-phase network analyzer is connected to measure current and power in the stator coil of the motor. A second three-phase network analyzer is connected to measure the current and the input power of a matching transformer. A single-phase FLUKE-43 network analyzer is used to measure the power, current and voltage for determining the losses only in the synchronous

motor. The experiment aims at capturing how the specific losses α are changed at different values of the generated reactive power, stepwise changing the magnitude of the field current, and recording all measured quantities.

Experimental tests

The described methodology will be illustrated with the results from the measurements of a synchronous electric motor type SDS 19-56-40 u4, driving mill unit type MSHTS 4.5 x 6.0, indicated in the text with MA1.

Fig. 1 shows the change of the active and reactive power as well as the current in the stator and the rotor captured by the experimental tests of mill unit M1. From the dependencies shown, it can be seen that the change of the field current (Irotor) significantly changes the reactive power (Q) and the stator current (Ist), but the active power (P) remains almost constant. Therefore, the determination of the active losses in the stator coil of the electric motor does not have to be done by reading the drawn active power at change of the field current. The losses are calculated by considering the change of the current in the stator coil for certain values of the field current and the active losses are calculated by the formula:

$$\Delta P = 3.I_{st}^2.R_{st}.10^3, kW \qquad (1)$$

where: I_{st}, - current in the stator coil of the synchronous electric motor, A;

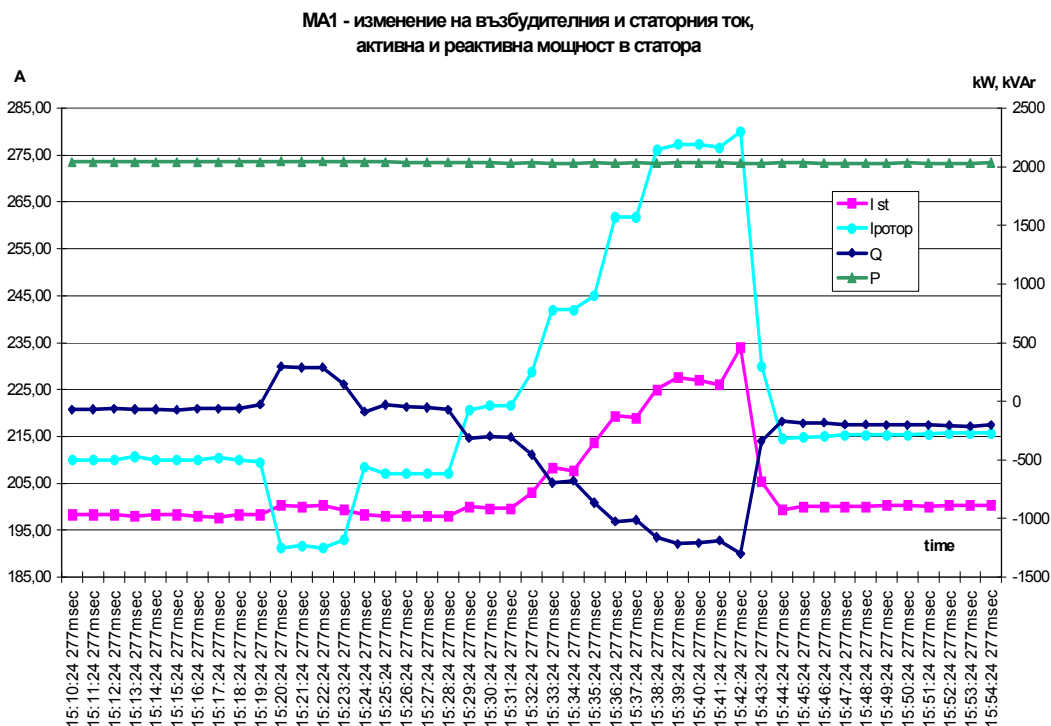R_{st} - active resistance of the stator coil of the synchronous electric motor, Ω.

Fig. 1. MA1 – change in the field and stator current, acive and reactive power in the stator

To determine the losses in the excitation circuit, the three-phase active power on the ~ 380V side of the transformer supplying the thyristor exciter TE-8E for different field current values is measured. Thus, the losses in the power transformer, the losses in the rectifier itself and the losses in the rotor coil are taken into account. The constant current losses in the rotor coil are reported by the single-phase network analyzer

Table 2 gives the results of the measurements of mill unit M1. For each value of the field current Ic, the current in the stator Ist, the active power P and the reactive Q in the stator of the synchronous electric motor are registered. The "-" sign before the reactive power means that the synchronous machine generates reactive power of capacitive character, and the positive values of Q mean reactive power consumption with inductive character.

Table 2. *Specific losses of active power for the generation of reactive power in a synchronous motor type SDS 19-56-40 u4 (M1).*

I rotor, A	I st, A	P rotor, kW	P ~380, kW	P st, kW	Q st, kVAr	Losses for excitation, kW/kVAr	Losses in the rotor, kW/kVAr	Losses in the stator, kW/kVAr	Overall losses, kW/kVAr
191.2	200.0	18.3	23.3	2046	288				
207.1	198.0	20.6	27.3	2039	-37				
210.0	198.3	21.0	27.5	2040	-92				
215.3	199.1	21.8	28.6	2034	-183	0.0092	0.0085	0.0012	0.0104
221.6	**200.6**	**22.8**	**30.8**	**2036**	**-298**	**0.0134**	**0.0086**	**0.0016**	**0.0150**
242.0	208.0	26.5	36.6	2033	-677	0.0145	0.0092	0.0026	0.0171
261.8	219.0	30.2	42.8	2033	-1025	0.0157	0.0098	0.0036	0.0193
277.3	227.0	33.3	46.8	2034	-1210	0.0166	0.0108	0.0042	0.0208

The three-phase active power (P ~ 380) of the coordinating transformer (TC3B 100) to the thyristor exciter TE-8E is also registered. The table also shows the power change in the DC rotor circuit (P rotor). The table also shows the power change in the DC circuit in the rotor (P rotor).

The specific losses of active power for generating reactive (kW / kVAr) total for the excitation circuits, stator coil and total specific losses are determined. For example, at an operating field current of 221.6 A, the stator current is 200.6 A, the rotor coil power is 22.8 kW, and the power output from the 380V side of the matching transformer is 30.8 kW. The synchronous motor is loaded with an active power of 2036 kW and generates a capacitive output of 298 kVAr. Under these conditions, the overall specific active losses for reactive power generation are 0.015 kW/kVAr, distributed as follows: in stator coil - 0.0016 kW/kVAr, in the excitation - 0.0134 kW/kVAr. Of these, the specific losses in the rotor coil are 0.0086 kW/kVAr and the remaining 0.00726 kW/kVAr are in the matching transformer and rectifier.

The percentage ratio of losses in the individual units of the synchronous electric motor in normal operating mode is: in the stator coil – 10.66%; in the rotor coil - 57.33%; and overall in the transformer and rectifier - 48.4%. With the increase of the field current, the specific losses also increase and with excitation of 277.3 A - the total specific losses are 0,0208 kW/kVAr. The percentage of losses in individual units also changes. Compared to the normal operating mode, the percentage of losses in the stator coil (20.19%) is almost doubled, at the expense of reducing the percentage of transformer and rectifier (27.88%).

The results obtained show in that the specific loss estimate for the specific losses in the rotor coil alone leads to significant errors of about 40-50%. For accurate estimation of the specific losses of active power for reactive power generation, it is necessary to simultaneously measure the values in the stator coil of the electric motor, the field current and the active power at the input of the matching transformer.

Table 2. *Specific losses kW/kVAR*

Type of motor	Driven machine	Coefficient of loading	Specific losses kW/kVAR
SDS-19-56-40 UHL-4 P = 2500kW, U_H = 6kV, I_H = 281A, n = 150min^{-1}, $\cos_ц$ = 0.9, U_{exc} = 162V, I_{exc} = 225A, Efficiency = 95.0	Ball mills, type MSHTS 4.5 x 6.0.	0.8	0.0138
SDS 19-56-40 y4 P=2500 kW, U_H.=6 kV, I_H.=281 A, n=150 min^{-1}, $\cos_ц$=0.9, U_{exc}.=145 V, I_{exc}.=278 A, Efficiency=94.8	Ball mills, type MSHTS 4.5 x 6.0	0.82	0.0150
SDM-32-22-34 UHP-4 P = 1600kW, U_H.= 6kV, I_{stat} = 185A, n = 100min^{-1}, $\cos_ц$ = 0.9, I_{exc} = 290A	Mills for wet self-grinding MMS 7.0 x 2.3.	0.3	0.0323
SDN -2-16-74 6UZ P = 2000kW, U_H.= 6kV, I_{stat}.= 221A, U_{exc} = 46V, n = 1000min^{-1}, $\cos_ц$ = 0.9, I_{exc}.=295 A, Efficiency = 96,6	Pump	0.9	0.00717
SDS 3 I 5 -64-6UZ P = 2500kW, U_H = 6kV, I_{stat} = 278A, U_{exc}.= 72 V, $\cos_ц$ = 0.9	Pump	0.72	0.00728

According to the presented methodology, the specific losses of active power for generating reactive power from the main electric drives with synchronous electric motors in the mineral processing plants of Assarel-Medet JSC and Elatsite Med JSC have been experimentally determined. The results have been summarized in a Table 2. The well-known fact that higher-speed synchronous motors have lower specific losses has been quantitatively confirmed. For example, the low speed motor SDS-19-56-40 (n = 150 min^{-1}) has values of α = 0.0138 kW / kVAr, whereas the electric motor with the same power SDS 3 I 5-64-6Э3 (n = 1000 min^{-1}) has specific losses α = 0,00728 kW /kVAr.

Conclusion

The results obtained for the specific losses α during the conducted studies and the conducted technical and economic analyzes for optimum compensation of the reactive loads of large mining and mineral processing enterprises have led to the following:

1. A methodology for selectively determining the specific losses of active power in the individual units of the synchronous electric motor when generating reactive power is proposed.

2. According to the proposed methodology, data on the specific losses of the main synchronous electric motors in the mineral processing plants at Asarel-Medet JSC and Elatsite Med JSC have been obtained.

3. On the basis of the actual data on specific losses of active power for reactive power generation, a feasibility study was carried out to optimize the distribution of the reactive capacities in the processing plants at Asarel-Medet JSC and Elatzite Med JSC.

4. Asarel-Medet JSC has implemented the proposals in practice and has compensated the combined reactive loads - with synchronous electric motors and with capacitor batteries, which has led to a significant economic effect.

References

Данков, Е.Е., Електроснабдяване на минните предприятия. С. Техника, 1991. (Dankov, E.E., Elektrosnabdyavane na minnite predpriyatia. S. Tehnika, 1991)

Чобанов, С., М. Ментешев, Ефективна компенсация на реактивните товари със синхронни двигатели, Годишник на МГУ „Св. Иван Рилски", Том 50, св.III, 2007г. стр. 107-110. (Chobanov, S., M. Menteshev, Efektivna kompensatsia na reaktivnite tovari sas sinhronni dvigateli, Godishnik na MGU "Sv. Ivan Rilski", Tom 50, sv. III, 2007, 107-110 p.)

Гойхман, В.М., Ю.П. Миновский, Регулировани еэлектропотребления и экономия электроэнергии на угольных шахтах.М., Недра, 1988. (Goihman, V.M., U.P. Minovskii, Regulirovani elektropotreblenia i ikonomiya elektroenergii na ugolnih shahtah. M., Nedra, 1988)

RESULTS FROM AN EXPERIMENTAL STUDY AT *"STOMANA INDUSTRY"* SA OF THE POWER QUALITY AT THE LEVEL OF 220 kV WHEN OPERATING ELECTRIC ARC FURNACES

Todor Nikolov

"Stomana Industry" S.A.

ABSTRACT. The report presents the results from the experimental studies of the impact of the electric arc furnaces operation on the electric power quality indicators at the 220 kV side. The voltage deviation and the higher harmonics in the voltage curve under different operating modes of the electric arc furnaces and of the ladle furnaces have been studied. The results of the registered current loads of the 220/35 kV transformers, the active and reactive power, and the values of the power factor have also been given. Conclusions have been made on the influence of the operating modes of the furnace transformers upon the "pollution" (deterioration) of the 220 kV system voltage.

Keywords: electric power quality indicators, electric arc furnaces

ЕКСПЕРИМЕНТАЛНИ ИЗСЛЕДВАНИЯ НА КАЧЕСТВОТО НА НАПРЕЖЕНИЕТО НА НИВО 220 kV ПРИ РАБОТА НА ЕЛЕКТРОДЪГОВИ ПЕЩИ В „СТОМАНА ИНДЪСТРИ" АД

Тодор Николов
„Стомана Индъстри" АД

РЕЗЮМЕ: В доклада са представени резултатите от експериментални изследвания на влиянието на работата на електродъговите пещи върху показателите на качеството на електрическата енергия на страна 220kV. Изследвани са отклонението на напрежението и висшите хармоници в кривата на напрежението при различни работни режими на електродъговите пещи и кофъчно-пещните инсталации. Дадени са и резултатите от регистрираните токови натоварвания на трансформаторите 220/35 kV, активната и реактивната мощност и стойностите на фактора на мощността. Направени са изводи относно влиянието на работните режими на пещните трансформатори върху „замърсяването" на системното напрежение 220 kV.

Ключови думи: показатели за качеството на електрическата енергия, електродъгови пещи.

Introduction

By its very nature, the electric power is a commercial product that should possess an inherent adequate quality. The widely used concept "Power Quality" (PQ) means uninterrupted power delivery to the consumers, and the parameters of the supply-line (mains) voltage shall be within a specified range, allowing for the normal functioning of the net-connected power loads. A perfect power supply implies that the mains voltage should never be interrupted, its value and the frequency shall be within the allowable range specified by the applicable standards and have a perfectly/pure sinusoidal (wave) form without superimposed noises. The meaning of PQ has always been seriously paid attention to since the very creation of the power grids, but today, it is much more important due to two basic reasons. The latter can be said to be closely related to the existence of a great number of state-of-the-art types of loads, which, on one hand, need a high/good PQ, but on the other - they deteriorate it because of their inherent action. As an example, it will be enough to mention the electric arc furnaces in the metallurgical plants. There are plenty of human activities where the deterioration of the PQ is related to considerable financial losses, mainly, in the uninterrupted production processes. Another example is the short-time interruptions of the network voltage that can bring about substantial losses in glass-making and steel-making industries, as well as in telecommunications.

It is well known, each non-sinusoidal current is a sum of sinusoidal current with a mains frequency f (basic harmonic), as well as sinusoidal currents with frequencies nf, where n is a random positive integer (n-th harmonic). The flow of the harmonic currents in the network creates voltages with their frequency, i.e., the mains voltage also stops being sinusoidal. According to the studies cited in (Chobanov S., 2015), the harmful consequences caused by the presence of higher harmonics in the electrical networks are as follows:
- The existence of harmonics in the mains voltage leads to additional energy losses in the furnace transformers and to overheating of their windings (due to the impedance increase) and of the core (due to Foucault currents). The losses are roughly proportional to the square of the harmonics frequency and may be up to ten times greater than is the case with a mains voltage with a purely sinusoidal shape. The harmonics cause additional heating of the power cables too, but apart from this, they create unwanted vibrations that cause faster wear, resulting in cable breakdowns and reduced insulation resistance of the wires themselves.

- There are also changes that may set in in the cosø correction devices (17% probability). Because of the harmonics, the performance of the furnace transformers is deteriorated, and the correction is not effective enough. Damage to the coils can also occur when the harmonics frequency coincides with its resonant frequency.
- Switching on and off of heavy loads linked to the electric arc furnaces is associated with large pulse currents that generate significant voltage jumps up and down, especially for long connecting wires. The probability of disturbing the normal operation of the grid is 12.3%, while the reduction of this phenomenon needs resizing of the wires.
- If there are harmonics, the sum of their amplitudes may reach an order of magnitude equal to that of the fundamental harmonic/component and accidentally trigger protective relays or switches (probability 7.5%).
- The probability for the harmonics to interfere with the optimal use of the current-carrying networks is 3.6%, and a harmonics control should also be established on top of that of the reactive energy.

The voltage and current higher harmonics cause specific losses that, according to Kirov and Iliev (2017), can be examined from the following points of view:
- Additional power and electricity losses in case of higher harmonics;
- Additional cost of increased electrical equipment failure as a result of the accelerated aging of the insulation;
- Additional costs of disturbing the operation of the relay protections by reverse sequence currents and unbalanced capacitive currents in earth connections;
- Additional costs due to the negative influence of the higher harmonics on the operation of the communication and automation media.

In the metallurgical plant of *"Stomana Industry" SA*, there are currently two electric arc furnaces (EAF) and two ladle-furnace installations (LF). The electric capacity of the furnaces is respectively: EAF1 - 120 MW, EAF3 - 75 MW, and that of LF No. 1 – 18 MW and LF No.2 – 18 MW. The furnace transformers are supplied by a voltage of 35 kV from two power transformers 220/35 kV with power respectively 200 MVA and 180 MVA.

The main purpose of the experimental research carried out was to determine how the operation of the EAF and the LF influences the electric power quality parameters of the power transformers on the 35 kV and the 220 kV side. The results from the 35 kV network research are given in (Stoilov Iv., K. Dzhustrov, T. Nikolov, 2015). The results from the experimental studies on the 220 kV side are examined here.

Experimental Studies

1. All experimental research has been performed with modern digital network analyzers FLUKE 437-II and FLUKE 435-II. The devices are connected to the secondary circuits of the measuring transformers.

Measurement accuracy class of the instruments:
- in terms of voltage - 0.1% of the nominal (1000V);
- in terms of current for the corresponding ammeter jaws - 2.0%
- voltage harmonics - 0.1% ± n. 0.1%, where n is the number of the respective harmonic;
- voltage THD (the voltage curve sinusoidality distortion factor) - ± 2.5%.

2. The measurements have been carried out simultaneously on the 220 kV and 35 kV side in the following technological modes:
- idle operation of the transformer 220/35 kV;- simultaneous operation of EAF No. 1 and LF-1.

All measurements of the electricity quality indicators have been performed according to the methodology formulated in IEC 61000-4-30:2008.

3. Cumulative results of the 220 kV side measurements under the simultaneous operation of EAF No. 1 and LF-1 for one heat processing period.

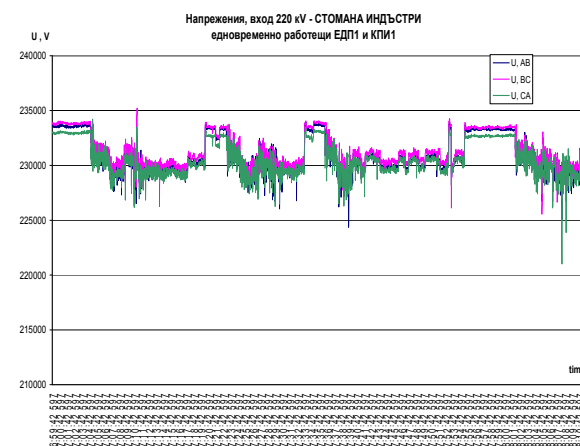*3.1. Voltages in the three phases (Fig.1).*

Fig.1. Voltages, 220kV input – STOMANA INDUSTRY, EAF1 and LF1 operating in parallel

The registered idle voltage of the transformer in the individual phases is in the range of 233 to 234 kV, the difference not exceeding 0.5%. During the operation of the electric arc furnaces, the voltage is relatively constant and with a value of about 230 kV. There have been registered short-term voltage peaks only at the moments of a sharp drop in current. The maximum registered value is 235.2 kV. The minimum recorded instantaneous voltage value during the heat process has been 221 kV. When both the electric arc furnace EAF No. 1 and LF-1 are in operation, the voltage quality indicators defined in EN 50160:2010 are not disturbed.

3.2. Current loading (Figure 2)

The records attached herein show the transformer current load on the 220kV side.

During the electric-arc melting, peak currents are recorded in one of the phases exceeding 350 A. Most of the time, the current ranges from 200 to 250 A.
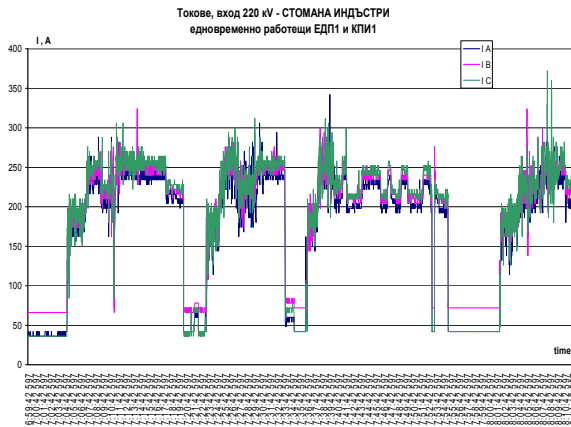

Fig. 2. Currents, 220 kV input – STOMANA INDUSTRY, EAF1 and LF1 operating in parallel
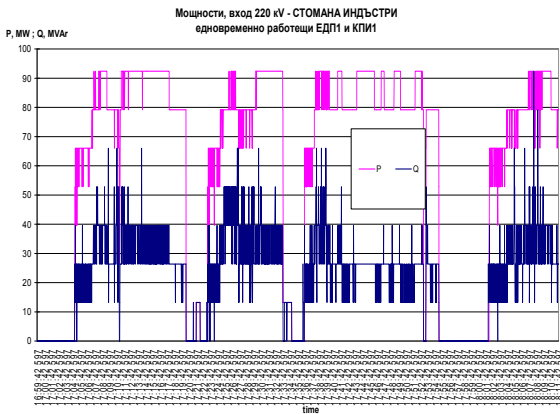
3.3. Active and reactive power (Fig. 3).

Fig. 3. **Power values, 220 kV input – STOMANA INDUSTRY, EAF1 and LF1 operating in parallel**

The change in the active and reactive power during the liquid bath smelting characterizes the variable power loads of the production facilities during the process. The maximum active power values do not exceed 93 MW.
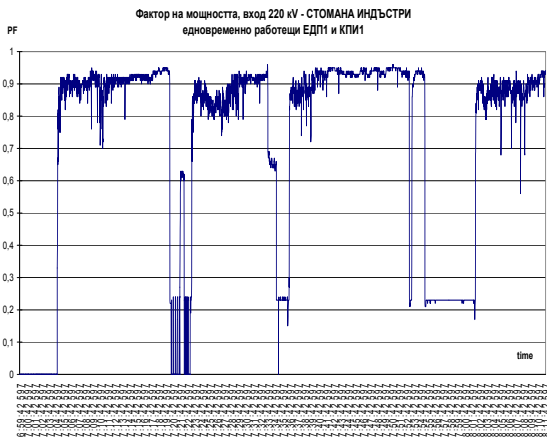
3.4. Power factor (Fig. 4).

Fig. 4. Power factor, 220 kV input – STOMANA INDUSTRY, EAF1 and LF1 operating in parallel

The figure shows the operation of the compensating devices. There are time intervals in which the power factor is below the standard (normative) value of 0.9.

3.5. Total factor of non-sinusoidality – THD (total harmonic distortion factor in %) (Fig. 5).
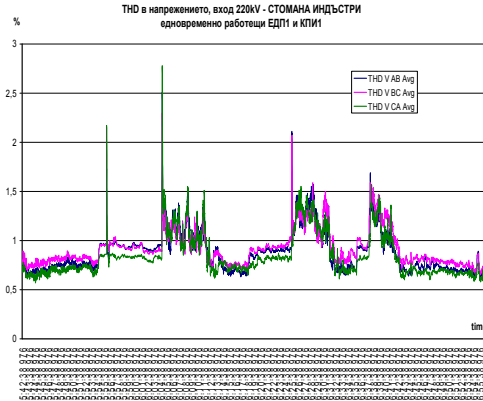

Fig. 5. **Voltage THD, 220 kV input – STOMANA INDUSTRY, EAF1 and LF1 operating in parallel.**

According to the requirements of standard EN 50160:2010, the total harmonic distortion factor (THD) in the 220 kV voltage supply networks shall not exceed 2,0%. From the recordings carried out, it can be seen that during the smelting process the THD ranges from 0.6% to 1.5%. Three cases were registered during the recording, in which short-term (about 5 s) THD values exceeded the normative ones: 2.77%, 2.17% and 2.11%. Since the standard EN 50160:2010 specifies the THD values as average within a 10-minute interval, one can positively claim that the parallel operation of EAF No. 1 and LF-1 does not disturb the 220 kV system voltage with higher harmonics.

3.6. Mean values of the harmonics up to No. 50 for the entire period of the heat process (Fig.6).

Fig. 6. **Bar chart of the mean value of the voltage harmonics - 220 kV input – STOMANA INDUSTRY, EAF1 and LF1 operating in parallel**

From the histogram (bar graph) attached herein, the values of the higher harmonics are recorded as averaged for each single phase of the heat-processing period. The total harmonic distortion factor THD (also called the voltage waveform distortion factor) for the three phases has values of 0.88, 0.92,

and 0.84. The highest values belong to the 5th harmonic - 0.66%, followed by the 11th - with 0.36%, the 3rd - with 0.33%, the 7th - with 0.19% and the 2nd - with 0.17%. All registered values of the higher harmonics are significantly lower than those specified as acceptable in the EN 50160:2010 standard.

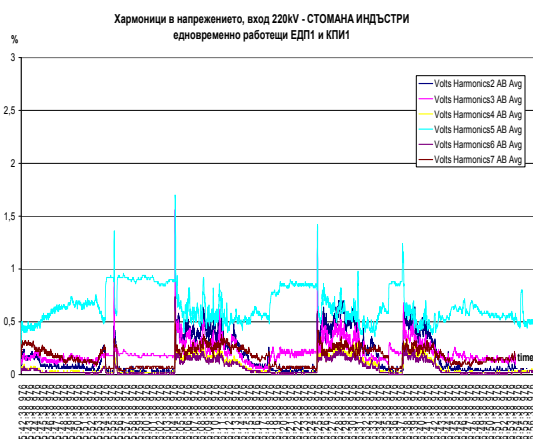*3.7. Phase A harmonics from the second to the seventh for the entire measurement period (Figure 7).*

Fig. 7. **Voltage harmonics - 220 kV input – STOMANA INDUSTRY, EAF1 and LF1 operating in parallel**

It is evident from the record attached herein, that, for the heat-processing period, the momentary values of the quoted harmonics do not exceed the individual coefficients specified in EN 50160:2010. There are two moments recorded, in which the 3rd and 5th harmonic exceed the factor of 1.5% as allowed by the standard above. These unit values have a duration of less than 6 seconds and reach: the 5th - 1.7% and the 3rd - 1.56%. Since the standard specifies the individual coefficients of non-sinusoidality as mean values within a 10-minute interval, apparently, the individual harmonic factors can also be deemed as not infringing the normative requirements.

Conclusion

1. Experimental data have been obtained for the voltage quality indicators at the level of 220 kV during the heat processes conducted in the electric arc furnaces (EAF) and the ladle-furnace installations (LF) at *"Stomana Industry" SA*, involving different modes of operation of the furnace transformers;
2. The nature of the current load in the three phases during the smelting process of one heat has been determined;
3. The loading diagram has been registered in terms of active and reactive power at 220kV for a single smelting process.

The main conclusion from the research conducted is that the simultaneous operation of the electric arc furnace (EAF) and the ladle furnaces (LF) in *"Stomana Industry" SA* does not generate unacceptable values in the quality parameters of the electrical energy in the system voltage of 220 kV. On the basis of these results, the entity *"Stomana Industry" SA* has been designated for the so-called "tertiary" production facilities control in the electric power system of the country.

References

EN 50 160:2010 Voltage characteristics of electricity supplied by public distribution systems.

IEC 61000-4-30:2008 Electromagnetic compatibility (EMC) - Part 4: Testing and measurement techniques – Power Quality Measurement Methods (MOD)

Stoilov, Iv., K. Dzhustrov, T. Nikolov, Study of the harmonic composition of the voltage and current in the operation of electric arc furnaces. The International Energy Forum, Varna 2015.

Chobanov, S. Losses in medium and low voltage power lines containing higher harmonics, S., St. Ivan Rilski, 2016.

Kirov R., Il. Iliev, Electricity Efficiency, ENA Ltd., Varna, 2017.

DISPLAY MEASURING SYSTEM

Krasimir Velinov

University of Mining and Geology "St. Ivan Rilski", 1700 Sofia, candela@mail.bg, http://light-bg.eu/

ABSTRACT. The development of modern technologies has allowed the creation of increasingly sophisticated systems for visualizing information. The evolution of the technology in this area has taken place in the following sequence: CRT, LCD, LED, OLED, AMOLED. Within the existing LCD, LED, OLED, AMOLED technologies, 2D, 3D and holographic displays can be developed. A team of engineers from the European Union are engaged in the development of elements of this technology. For this purpose, the Optintegral project has been activated with the idea of developing better and more modern LED display displays using the use of pressurized injection molding. Optintegral's goal is to demonstrate the feasibility of technology, flexibility, resilience and cost savings in this revolutionary manufacturing process. This will enable the competitive production of a wide range of LED displays within the European labor market. The consortium includes nine European partners from 5 European countries, including Fundació Privada Ascamm (ASCAMM), Simulacions Optiques SL (SNELL) and Spain's Spanish Association for Standardization and Certification (AENOR), VTT Technical Research Center of Finland (VTT) Neonelektro Oy (NEO) from Finland, LumyComp Design Ltd. (LUMY) and Megatex Commerce Ltd (MEGATEX) from Bulgaria, Holografika Hologramelőállító Fejlesztő és Forgalmazó Kft. (HOLOGRAFIKA) from Hungary and UBATH from the United Kingdom. In order to evaluate the qualities of the constructed modules and displays, a system to measure their parameters has been developed at the NIL "Lighting Engineering" at the University of Mining and Geology "St. Ivan Rilski". The system is a set of optical measuring equipment and a specially designed and manufactured coordinate table with a JETI specbos 1201 spectrometer mounted. The coordinate table has dimensions of 1300x1400 mm and allows measurement of displays up to 1200x1200 mm. The shifting of both axes X and Y is accomplished by two stepping motors. For testing, a measurement methodology has been compiled in accordance with current regulatory documents. With the measurement system so constructed, control measurements of a LED module.

Keywords: display, measuring system

СИСТЕМА ЗА ИЗМЕРВАНЕ НА ДИСПЛЕИ
Красимир Велинов
Минно-геоложки университет "Св. Иван Рилски", 1700 София, candela@mail.bg, http://light-bg.eu/

РЕЗЮМЕ. Развитието на съвременните технологии позволява създаване на все по-съвършени с540 ситеми за визуализиране на информацията. Еволюцията на технологиите в тази област протича в следната последователност: CRT, LCD, LED, OLED, AMOLED. В рамките на съществуващите технологии LCD, LED, OLED, AMOLED могат да се разработят 2D, 3D и холографски дисплеи. Екип инженери от Европейския съюз са се заели с разработката на елементи от тази технология. За целта е активиран проектът Optintegral с идеята да се разработят по-добри и модерни рекламни LED дисплеи, като се използва технологията на хибридно интегриране чрез шприцване под налягане. Целта на Optintegral е да се докаже приложимостта на технологията, да се демонстрира гъвкавостта, устойчивостта и намаляването на разходите при този революционен производствен процес. Това ще даде възможност за конкурентноспособно производство на широк кръг от разнообразни LED дисплеи в рамките на европейския трудов пазар. Консорциумът включва девет европейски партньори от 5 европейски страни, в това число Fundació Privada Ascamm (ASCAMM), Simulacions Optiques S.L.(SNELL) и Испанската асоциация по стандартизация и сертификация (AENOR), Центъра за технически проучвания (VTT) и Neonelektro Oy (NEO) от Финландия, LumyComp Design Ltd. (LUMY) и Megatex Commerce Ltd.(MEGATEX) от България, Holografika Hologramelőállító Fejlesztő és Forgalmazó Kft.(HOLOGRAFIKA) от Унгария и Университета в Бат (UBATH) от Обединеното Кралство (UK). За да се направи оценка на качествата на конструираните модули и дисплеи, в НИЛ "Осветителна техника" при Минно-геоложкия университет "Св. Иван Рилски" беше създадена система за измерване на параметрите им. Системата представлява набор от апаратура за оптични измервания и специално конструирана и изработена координатна маса с монтиран спектрорадиометър JETI specbos 1201. Координатната маса е с размери 1300x1400 мм и позволява измерване на дисплеи до размер 1200x1200 мм. Преместването по двете оси X и Y се осъществява от два стъпкови двигателя. За провеждане на изпитанията е съставена методика за измерване в съответствие с действащите в момента нормативни документи. С така създадената измервателна система са извършени контролни измервания на светодиоден модул, предназначен за изработка на дисплеи. Създадената измервателна система е тествана, като са извършени контролни измервания на светодиоден модул, предназначен за изработка на дисплеи. Тестовете са показали нейната работоспособност. Направени са препоръки за бъдеща работа.

Ключови думи: дисплей, измервателни системи

Introduction

For a relatively short period of time, I have witnessed how technical devices for visual information have changed. Initially, these were CRT displays for displaying textual information, but it quickly came to the idea that a picture was more powerful than the text, and the first PCs had the ability to display graphical images. The quality was cryptic - a screen resolution of 320x240 dots and a monochrome image. Things changed, however, as in 1986, the most common computer had a standard display with a resolution of 640x480 tp. The most common screen resolution currently is from 1280x1024 t to 1920x1200 t.

The development of state-of-the-art technologies has allowed us to create increasingly sophisticated systems for visualizing information. The evolution of the technology in this area was performed in the following sequence: CRT, LCD, LED, OLED, AMOLED. The last three technologies have enabled an even higher resolution - full-color 4K - 4096 x 3112 dots, with low energy costs.

In August 2016, Japan's national television company, NHK, launched the world's first regular 8K satellite broadcasting. The Super Hi-Vision Test Channel ran on Aug. 2 with a picture resolution of 7,680 to 4,320 pixels. Last September, Sharp presented a 85-inch receiver with a resolution of $ 133,000. [1]

The processing of such an image requires large computational power. At the SIGGRAPH 2016 event, the AMD Radeon Pro graphics card has demonstrated an equivalent monitor resolution of 16K - 15,360 x 8640 (132 megapixels) [2].

Within the existing LCD, LED, OLED, AMOLED technologies, 2D, 3D and holographic displays can be developed. A team of engineers from the European Union are engaged in the development of elements of this technology. For this purpose, the Optintegral project has been activated with the idea of developing better and more modern LED displays using the use of pressurized injection molding.

Optintegral's goal is to demonstrate the feasibility of technology, demonstrate flexibility, sustainability and cost savings in this revolutionary manufacturing process. This will enable the competitive production of a wide range of LED displays within the European labor market. OptIntegral will initially develop three different prototypes of large-scale displays - 3D glasses-free, lightpipe Displays and LED direct-illuminated displays - designed for the store network, for transport and hotels. These prototypes of displays will be produced and demonstrated by three European SMEs and an effective impact on observers will be tested and evaluated through the use of state-of-the-art medical computerized imaging technologies with EEG enrollment. OptIntegral: This is a three-year project, launched on 01.02.2015 with funding provided by the European Union amounting to 5,675,337 Euros. The consortium includes nine European partners from 5 countries, including Fundació Privada Ascamm (ASCAMM), Simulacions Optiques SL (SNELL) and Spain's Spanish Association for Standardization and Certification (AENOR), VTT Technical Research Center of Finland (VTT) Neonelektro Oy (NEO) from Finland, LumyComp Design Ltd. (LUMY) and Megatex Commerce Ltd. (MEGATEX) from Bulgaria, Holografika Hologramelőállító Fejlesztő és Forgalmazó Kft. (HOLOGRAFIKA) from Hungary and the UBATH University of the United Kingdom (UK).
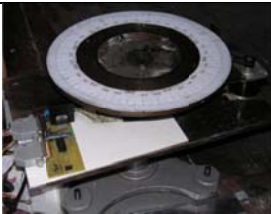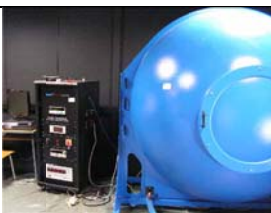
In order to evaluate the qualities of the constructed modules and displays a system has been developed to measure their parameters in the Lab "Lighting Engineering" at the University of Mining and Geology "St. Ivan Rilski".

The work was done in the following sequence:
1. Buying standards describing the testing methodology of 2D, 3D and holographic displays.
2. Creating a test methodology
3. Construction of an apparatus and a system of measuring instruments to perform the tests.
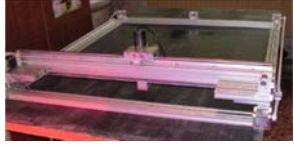
Description of a display measurement system

To carry out the measurements a complete system was used with the following equipment:

Equipment	
LMT Photometer B520, ID 04B4021	
luminance-meter L 1003 of angular field 1°, producer "LMT" Germany, ID 0686191	
Automated goniophotometer	
Power Meter HM8115-2 ID 015447345	
Stabilized power supply ZAFV1.5/270;	
Digital multimeter DMM4050;	
Ulbricht photometer with diameter 2m	
Laser rangefinder DLE-40	

spectroradiometer JETI specbos 1201;	
Pulse light meter	
Automated display measuring table	
Spreadsheet generator	

In order to carry out the measurements, a coordinate table was constructed, on which spectrometer JETI specbos 1201 (Figure 1) was mounted. The coordinate table has a size of 1300x1400 mm and allows measurement of displays up to 1200x1200 mm. The displacement on both axes X and Y is accomplished by two stepping motors.

Fig. 1. Coordinate table for measuring displays

A suitable software was developed for coordinate table management and reading of the spectroradiometer data.

With the system so constructed, the following tests can be carried out:

- Measuring the viewing angle and distribution of brightness in the space;

- Measuring the pulsation coefficient of light;

- Measurement of white light chromaticity and its uniformity in liquid crystal display and devices with built-in backlighting system;

- Reproduction of colors;

The test methodology has been compiled in accordance with the documents [3 - 13]. In Fig. 2 and Fig. 3. the conditions under which the measurements are made are shown.
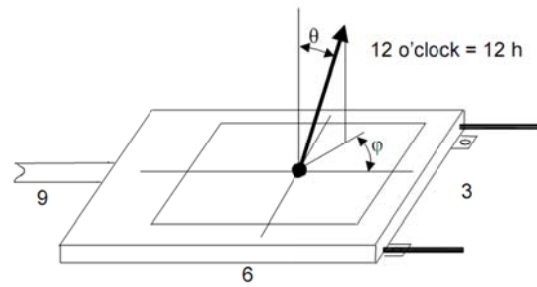
Fig. 2. Definition of polar coordinates θ φ
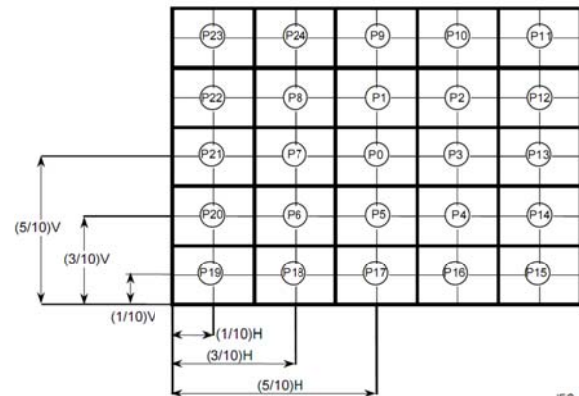
Fig. 3. Standard measurement positions in the centers of all rectangles P0-P24

Results

With the measurement system so constructed, control measurements of a LED module designed for display were made. The photo of the module is shown in Fig. 4.

Luminous flux emitted from the 37 lm module.

Distribution of brightness on the red color display, cd/sqm

66.4	68.5	75.1
47.0	73.0	64.0

Minimum value = 47.0 cd/sqm
Average value = 65.7 cd/sqm
Uniformity – Uo = 0.72

275	289	289
185	252	186

Minimum value = 185 cd/sqm
Average value = 246 cd/sqm
Uniformity – Uo = 0.75
Brightness distribution on blue color display, cd/sqm

49.7	50.2	49.9
36.7	47.5	29.4

Minimum value = 29.4 cd/sqm
Average value = 43.9 cd/sqm
Uniformity – Uo = 0.67
Brightness distribution on white, cd/sqm

352	372	363
234	406	235

Minimum value = 234 cd/sqm
Average value = 327 cd/sqm
Uniformity – Uo = 0.72
Brightness in the middle of the bright segment = 220 cd/sqm
Brightness in the middle of the dark segment = 0.75 cd/sqm
Brightness at the end of the bright segment = 137 cd/sqm
Brightness at the end of the dark segment = 20.3 cd/sqm
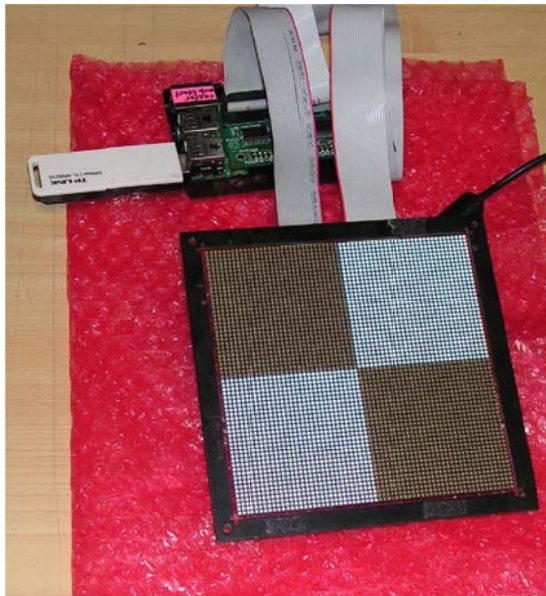
Fig. 4. LED display module
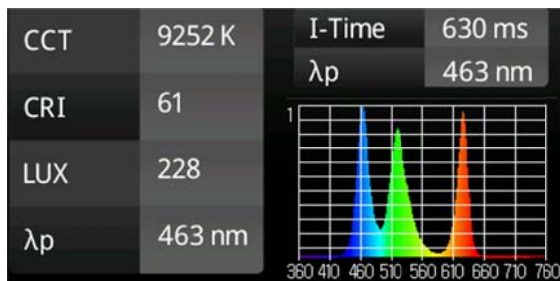
Fig. 5. Spectral characteristics
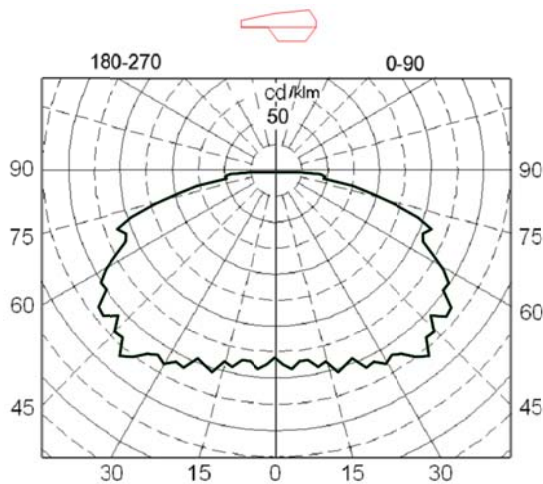
Fig. 6. Light distribution of the display module

Conclusion

The established measurement system has been tested by performing a control measurement of a LED module designed to produce a display. Tests have shown its efficiency.

Guidelines for future system upgrading - mounting an extra camera to capture portions of the display. From the captured images, defective pixels, spacing pixels and nonlinearities are determined directly.

References

1. https://fakti.bg/technozone/196546-v-aponia-pusnaha-8k-televizia
2. http://news.desktop.bg/novini/amd-radeon-pro-uspya-da-se-spravi-i-s-16k-rezolyutsiya-15-360-x-8640/
3. БДС EN 61747-4 Liquid crystal display devices - Part 4: Liquid crystal display modules and cells - Essential ratings and characteristics (IEC 61747-4:2012)
4. БДС EN 61747-4-1, Liquid crystal display devices - Part 4-1: Matrix colour LCD modules - Essential ratings and characteristics
5. БДС EN 61747-5, Liquid crystal and solid-state display devices, Part 5: Environmental, end1лance and mechanical test methods (IEC 61747-5:1998)
6. БДС EN 61747-5-2, Liquid crystal display devices -- Part 5-2: Environmental, endurance and mechanical test methods - Visual inspection of active matrix colour liquid crystal display modules
7. БДС EN 61747-6, Liquid crystal and solid-state display devices Part 6: Measuring methods for liquid crystal modules – Transmissive type
8. БДС EN 61747-6-2, Liquid crystal display devices -- Part 6-2: Measuring methods for liquid crystal display modules - Reflective type
9. БДС EN 61747-6-3, Liquid crystal display devices -- Part 6-3: Measuring methods for liquid crystal display modules - Motion artifact measurement of active matrix liquid crystal display modules
10. БДС EN 61747-10-1, Liquid crystal display devices - Part 10-1: Environmental, endurance and mechanical test methods - Mechanical
11. БДС EN 61747-30-1, Liquid crystal display devices -- Part 30-1: Measuring methods for liquid crystal display modules - Transmissive type
12. EN 62629-1-2 August 2013, 3D Display devices - Part 1-2: Generic -Terminology and letter symbols (IEC 62629-1-2:2013)
13. БДС EN 62629-22-1, May 2013,3D display devices -Part 22-1: Measuring methods for autostereoscopic displays - Optical (IEC 62629-22-1:2013)

POSSIBILITIES FOR INCREASING THE RELIABILITIY OF THE INSULATION MONITORING DEVICES

Radi Tenev

Kardzhali Branch of the University of Mining and Geology "St. Ivan Rilski" - Sofia, 6600 Kardzhali, raditenev@abv.bg

ABSTRACT. Because of the specific conditions in the mining industry (increased humidity, high temperature, dustiness), of the three possible grounding systems TN, TT and IT, the IT system has been used because of its undisputed advantages. It provides safety to the service staff and minimum risk of fire. In fact, the system retains its qualities only in case of robust insulation. In case of damaged insulation and presence of leakage currents, the IT system becomes more dangerous than the TN system. That is why insulation quality is constantly monitored by insulation monitoring devices. This article deals with the possibilities for increasing the reliability of the insulation monitoring devices. The insulation monitoring devices that are most commonly used in Bulgaria are explored, the UACI. The reasons for their failure are examined. The main principles of reliability are explained: self-control of the elements, and the Reservation principle. The operation of insulation monitoring devices with increased reliability that are used in the mining industry is described.

Keywords: IT systems, principle of self-control, insulation resistance, reliability, element control.

ВЪЗМОЖНОСТИ ЗА ПОВИШАВАНЕ НА НАДЕЖДНОСТТА ПРИ АПАРАТИТЕ ЗА КОНТРОЛ НА ИЗОЛАЦИЯТА
Ради Тенев
Филиал - Кърджали на Минно-геоложки университет „Св. Иван Рилски" – София, 6600 Кърджали, raditenev@abv.bg

РЕЗЮМЕ. Поради специфичните условия в миннодобивните предприятия (повишена влажност, висока температура, запрашеност), от трите възможни схеми за заземяване - TN, TT и IT, IT системата се е наложила поради безспорните си предимства пред останалите, като безопасност на обслужващия персонал и минимална вероятност за възникване на пожари. Реално IT системата запазва своите качества единствено при изправна изолация. При повредена изолация и наличие на утечни токове тя става значително по-опасна от TN системата. Ето защо е необходимо постоянно да се следи състоянието на изолацията. Това се прави от апарати за контрол на изолацията. Настоящата статия е посветена на възможностите за повишаване на надеждността при апаратите за контрол на изолацията. Разгледани са най-често използваните апарати в България – УАКИ. Посочени са причините, които водят до техния отказ. Обяснени са основните принципи на надеждността: самоконтрол на елементите и принцип на резервиране. Описана е работата на апаратурата за контрол на изолацията с повишена надеждност, която намира приложение в минната промишленост.

Ключови думи: мрежа с изолирана неутрала, принцип на самоконтрол, съпротивление на изолацията, надеждност, контрол на елементите

Introduction

In general, reliability is associated with an unacceptable refusal of the device, i.e. the property's ability to maintain its working capacity over a long period without forced interruptions or, in other words, this is the absence of unforeseen changes in its performance during the operation (Druzhinin, 1977).

According to the analysis of electric trauma and fires, no lethal exits or fires have been recorded as a consequence of leakage currents in case of defensive protection, but in case of failure the cases of lesions are present. This is explained first with deficiencies of operation, and secondly with insufficient reliability of the means for protective shut-down of the leakage relay and the disconnection devices. According to the normative documents adopted, the file-save operation of the isolation control devices (refusal processing) is 20 000 hours.

In order to increase the safety of the exploited network, it is necessary to increase the reliability of the leakage relay.

The automatic circuit breaker is the leakage protection device. If it fails with a leaked relay, the voltage is not switched off, the relay remains under voltage for a long time, its contacts run through high currents, and as a result it goes out of action.

According to statistics, about 30% of the failures of the automatic switches lead to failures of leakage protection (Kolosyuk, 1980).

Other studies have shown that this percentage has increased, about 60% of failures of automatic switches lead to failures of leakage protection.

The estimated theoretical time for faultless operation of UACI-660 leakage relay is 12000 hours, and of UAKI-380 – 13000 hours. In standby tests, the same relays displayed 10460 hours - UAKI-380, and 9200 hours - UAKI-660.

The operational reliability of serial UAKI leakage relays varies greatly. In real conditions, the following data were obtained: UAKI-660 Leakage Relay Fault Reset, not more than 4750 hours and no more than 7820 hours for UACI-380.

Causes for failure of the insulation monitoring devices

The leakage relay fails mainly for the following reasons: fault on the choke and resistors, windings, diode failure, burner on the mounting wires, short circuit in the relay.

The faulty leakage relay not only results in material losses, but also disturbs the safe operation of the grid. An isolated neutral electric network is safe only when it is insulated, and when a relay fails, such a network becomes more dangerous than a network with grounded neutral.

In order to increase the reliability of the whole system, it is necessary to increase the reliability of both the leakage relay and the automatic circuit breaker.

If the leakage relay and the slot machine are considered as elements joined in series, assuming that their failures are independent events subject to the exponential law, we can write down the reliability parameters of the leakage protection system:

$$P_c = P_p . P_a \tag{1}$$

$$\lambda_c = \lambda_p + \lambda_a \tag{2}$$

$$T_c = \frac{1}{\lambda_c} = \frac{1}{\lambda_p + \lambda_a} \tag{3}$$

where P is the possibility for safe operation of the relay and the automatic machine;

λ is the intensity of failures;

T_c is the processing of failure of the protection system.

The parameters read by the above formulas are given in Table 1.

Conditionally, the reliability can be divided into total reliability or technologically (that depends on the reliability of all elements in the apparatus) and functional (which is determined by the reliability of those elements whose failure results in a violation of the protective functions).

Many components of the fail-over leakage relay do not affect the security features, such as the scale light, the check button, etc. Therefore, the overall reliability of the leakage relay may be lower than the functional leakage relay.

The required reliability can be achieved through constructive actions and proper prevention and replacement of the necessary elements.

The increasing requirements for the leakage relay determine a larger number of elements in the circuit which, in turn, leads to a decrease in design reliability. That is why the structures that are designed most often do not provide the necessary functional reliability even with the highest reliability of the individual elements. Because of the total rejection, intensity is equal to the sum of the intensities of the failures of all the elements.

In order to provide the necessary functional reliability of the protection devices, the principle of self-control and reservation of the elements, principles used in automation, can be used.

Table 1. *Apparatus reliability requirements*

Security device	Network voltage, Volts	Probability of faultless operation per 1000 hours	Intensity of failures 1/h	Refusal process, hours
UACI	380	0.907	0.096×10^{-3}	10460
UACI	660	0.897	0.109×10^{-3}	9200
Feeding machine	380	0.874	0.136×10^{-3}	7350
Feeding machine	660	0.864	0.174×10^{-3}	6800
Leakage protection system	380	0.791	0.232×10^{-3}	4310
Leakage protection system	660	0.774	0.256×10^{-3}	3910

Self-control of the elements

The principle of self-control is realized in such a way that the complete or partial failures of the elements which provide functional reliability lead to the disconnection of the protected network or to rising sensitivity. This measure does not reduce the failure of the power supply with sufficient reliability. The principle of self-control provides a high, close to one-time, probability of faultless performance of the protections

functions. Under these conditions, the principle of self-control is considered necessary.

Increasing reliability at the expense of element self-control is shown in the scheme proposed by Assoc. Prof. H.M. Zhelihovski (Figure 1).

Self-control is achieved by the fact that the relay K works when the anchor is released and any damage to the elements in the circuit causes the current flowing through the winding to

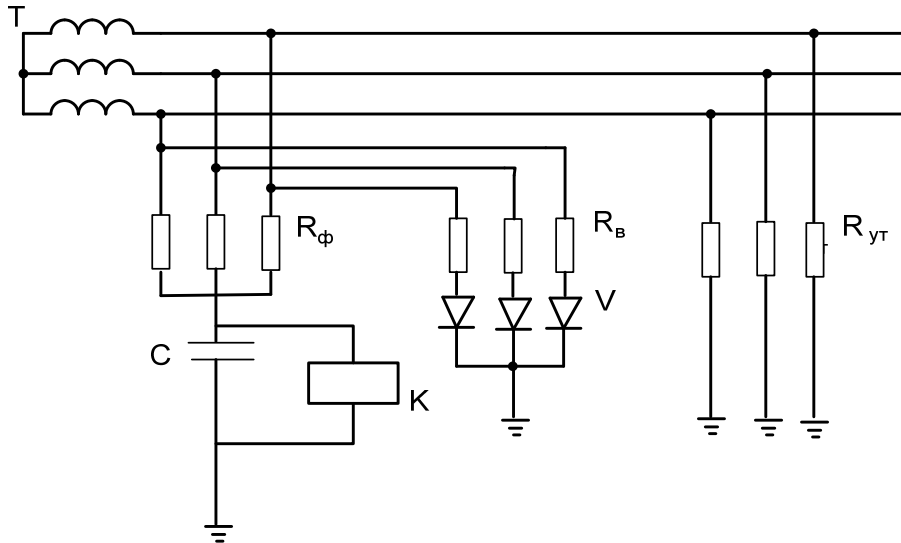cease or reduce the relay releasing its anchor or becoming   more sensitive.

Fig. 1. Self-contained protection device based on the use of constant operating current

The relay contact is in the circuit of the shut-off coil which disconnects the voltage both in the presence of leakage and in the case of a damaged element.

In the circuits where control of the elements is introduced, the elements not provided with element control affect only the overall technological reliability and do not affect the functional reliability of the leakage relay. Theoretically, these schemes reach 100% of reliability, which is virtually impossible because there are elements for which self-control is impossible.

The functional reliability of such protection devices is determined only by the reliability of non-secured elements, such as the execution relay, for example, because the failure of the other elements does not lead to a loss of protection functions. In most cases, the relays used have a failure response T= 10^5 hours. If such a relay is placed in the above scheme, higher functional reliability can be expected.

The above equations clearly show that for the complete leakage protection system, reliability is mainly determined by the reliability of the automatic circuit breaker. This is why particular attention is paid to it. It is necessary to increase the reliability of the exclusion coil and the separation mechanism.

The principle of self-control may be applied to the shut-off coil, eventual failure to trigger the machine.

The principle of the reserve

It is not possible to execute such self-control to the separation mechanism. The reserve principle is then applied. A spare machine or high voltage cell is used to feed the mobile station or transformer.

Such a scheme has been developed by V. Kolosyuk and N. A. Kissimov (Kolosyuk, V., 1980) and implemented to UACI leakage relay (Figure 2).

The circuit is equipped with a back-up switch and switches off even when the sensing relay of the leakage relay has failed.

For the purpose, a sensing element is included between the zero point of the rectilinear bridge and the ground via a closing contact block of the automatic circuit breaker. The sensing element is connected in parallel to the main relay. Thus, the additional sensing element is energized simultaneously with the main relay 4 by the same operating voltage. Two additional elements, resistor 6 and capacitor 5, are connected to relay 3, which determine the relay triggering time within the standard.

Contact 7 of relay 3 triggers the second automatic circuit breaker or the high voltage cell. In the first case, a normally open contact is used, and in the second, a normally closed one.

If a leak arises and if 0,2 s does not work on the first vending machine, a relay 3 is triggered which triggers the back-up shut-off.

The principle of booking as a method of increasing reliability is that the backup switch is turned off when the first one fails.

The probability of faultless operation of the reserved system is determined by the formula:

$$P_0 = 1 - (1 - P_a)(1 - P_c)$$
(4)

where: P_a and P_c are the probabilities of faultless operation of the exclusion system and of the high-voltage cell.

We assume that $P_a = P_c$ and we get:

$$P_0 = 1 - (1 - P_a)^2$$
(5)

For the entire system with reserved shutdown:

$$P_s = P_0 \cdot P_r$$
(6)

$$P_s = P_r[1 - (1 - P_a)^2] \tag{7}$$

The calculations show that at P_a>0,82 the probability is P_s> 0,964. In this way, the leakage protection system using a self-controlling leakage relay and a reserved grid disconnection device have high reliability parameters with the existing automatic switches.

In the absence of a reservation, the required reliability of the leakage protection system may reach P_A>0,965 which is difficult to realize in practice.
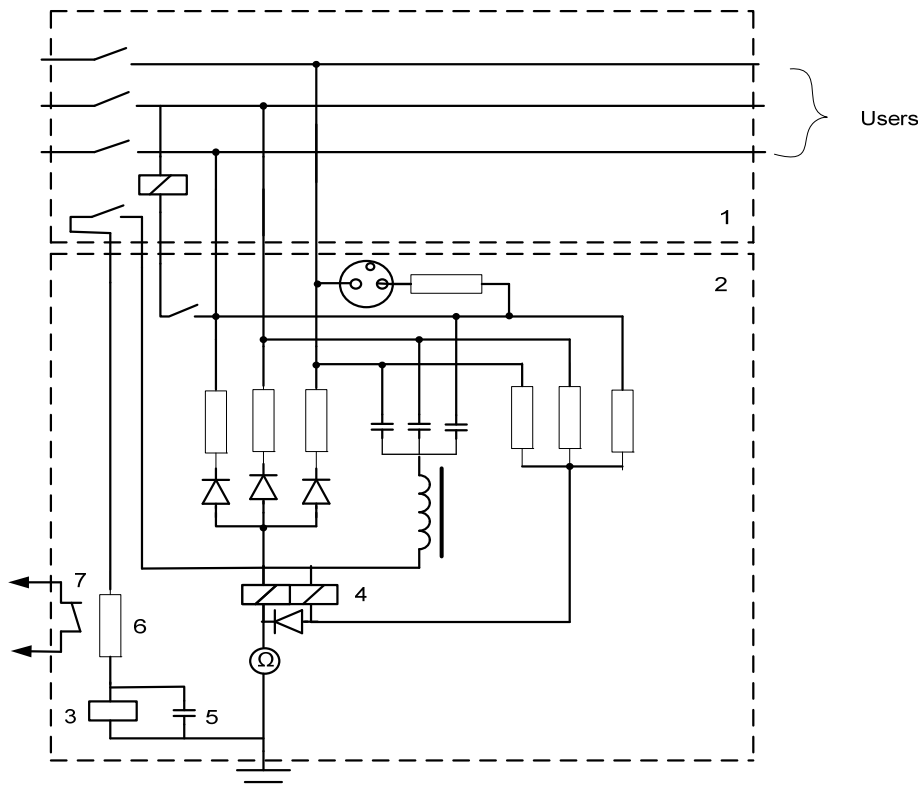

Fig. 2. Scheme using the Reserve Principle

Figure 3 shows a general flow diagram of a leakage relay at a voltage of 1140V.

The capacity C1 in parallel to the relay K1 smooths the current and prevents false activation caused by transient processes. The circuit uses a three-phase transformer that provides high resistance for the alternating current and low impedance for the DC operating current. The primary and secondary coils are star connected. The primary coil is supplied with 1140 volts, the secondary coil delivers 380 volts in and feeds a three-phase rectifier. After the rectifier we get 255 volts.

$$U_{op} = 0,675\,U_c = 0,675 \cdot 380 = 255\;V \qquad (8)$$

where: U_c is the linear voltage.

A sensible relay is included between the zero point of the primary winding of the transformer and the ground terminal through R4 and R3 and the KΩ meter.

The reserve sensing element (relay K2) is switched between the zero points of the primary and the secondary windings of the transformer ТДР. Through R6, K2 threshold is set, the capacitor C3 serves to increase the switching time of K2, V5

and C4 to stabilize the operating voltage. The K1 circuit is triggered by V4 and C2.

The relay contacts K1 are connected in the circuit breaker circuit or the high voltage cell. The device is also equipped with a CCU (capacity compensation unit).

The leakage relay works as follows:

In case of leakage, part of the operation current flows through the leakage, grid, primary transformer coil, KΩmeter, relay K2, resistor R6 and "-" of the rectifier, as a result of which the current through relay K1 decreases and K2 increases.

If the leakage resistance is equal to the threshold relay K1 triggers and activates the switch that shuts off the leakage. Relay K1 starts earlier than relay K2 .

If the circuit breaker does not shut off for any reason, it operates K2 and shuts off the high voltage cell.

To reactivate of relay K1, it is necessary to briefly press the button S. The circuit of the operating current is interrupted. On the release of the S button, the diver V4 is drained and the capacitors are discharged through the relay coils K1 and the relay is energized. C2 is intended to be triggered and in normal operation is off with a relay contact.

In the case of failure of functional circuit elements, e.g. diode break down, relay failure etc., the operating current through relay K1 decreases (the gain resistance threshold is increased) or is terminated altogether, resulting in the actuator being triggered.

In more recent developments, relay K1 has been replaced with a transistor key scheme.
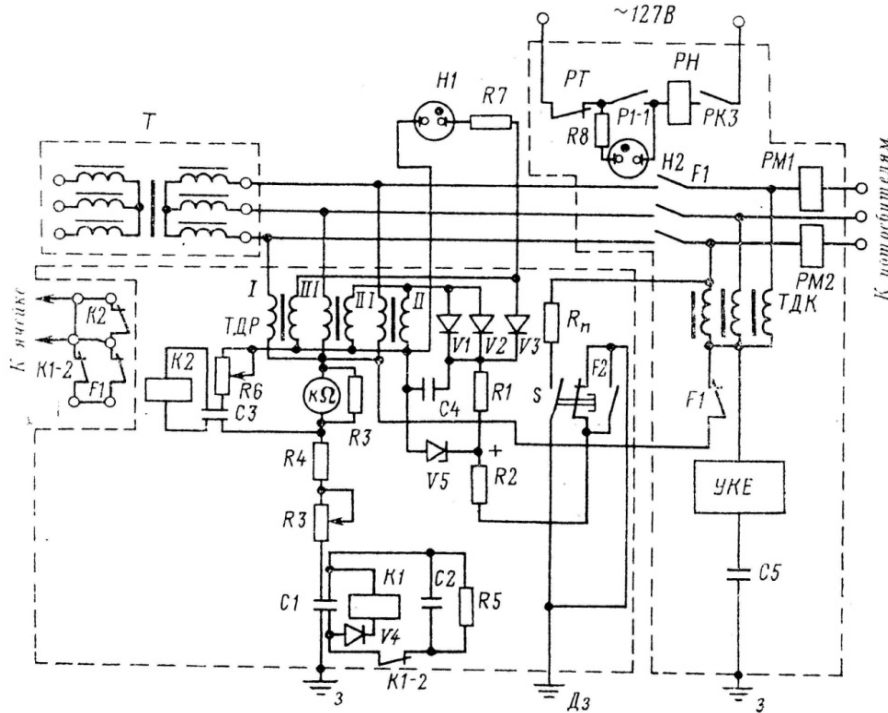
Fug. 3. Insulation monitoring device for 1140 V

References

БДС 10880-83. Съоръжения електрически руднични. Апарати за защита от токовете на утечка за мрежи с напрежение до 1200V с изолиран звезден център. Технически изисквания и методи за изпитване. С., 1983. (BDS 10880-83 Saorazhenia elektricheski rudnichni. Aparati za zashtita ot tokovete na utechka za mrezhi s naprezhenie do 1200V s izoliran zvezden tsentar. Tehnicheski iziskvania i metodi za izpitvane. Sofia, 1983.)

Дружинин, Г. В. Надеждность автоматизированных систем. М., Энергия, 1977. (Druzhinin, G. V. Nadezhdnosty avtomatizirovannaih system. M., Energiya, 1977.)

Колосюк, В. П. Защитное отключение рудничных электроустановок. М., Недра, 1980. - 137-143, - 167-170. (Kolosyuk, V. P. Zashtitnoe otklyuchenie rudnichnaih elektroustanovok. M. Nedra, 1980. - 137-143, - 167-170.)

INFORMATION MODEL OF A UNIVERSAL AGENT FOR DISTRIBUTED POWER GENERATION MANAGEMENT

Mila Ilieva-Obretenova

University of Mining and Geology "St. Ivan Rilski", 1700 Sofia, milailieva@abv.bg

ABSTRACT. Smart Grid is an electrical grid which includes a variety of operational and energy measures including smart meters, smart appliances, renewable energy sources, and energy efficient resources. Electronic power conditioning and control of the production and distribution of electricity are important aspects of Smart Grid. The roll-out of Smart Grid technology also implies fundamental re-engineering of the electricity services industry, although the typical usage of the term is focused on the technical infrastructure. The paper aims to propose information model of a universal agent for power supply management. The model is designed for user interface developers and operating officers. The hypothesis is as follows: the description of the nodes through which the agent runs should contain software definitions. The software of each node is sufficient to be detailed with elements up to level Manager and Program. The model should possess the following features: The nodes through which the agent runs should be represented as physical points. For each point software is represented as a set of functions. Functions are grouped according to open systems interconnection (OSI) areas: security, maintenance, configuration, accounting, and performance. We focus on the configuration area because it contains the agent's routing data. The software components in the configuration area are detailed to the functional element access manager, which directs the agent to the next element on his way.
Design methodology for this information model includes defining of managed object classes for the nodes through which the agent runs. Definitions are represented verbally and by UML (Unified Modeling Language) diagrams. UML diagrams are classified in two types: behavior diagrams and structure diagrams. Class diagrams, a type of structure diagrams, are suitable for describing nodes in Smart Grid. Class diagrams describe objects types in the system and different types of static relationships among them. These diagrams also show "Part-of" relationships, associations, attributes, class operations, and limits in the way the objects are connected. The models are influenced by similar management models in telecommunications. The result is a management model design for Smart Grid: a model for the management of a network and its elements through which a universal agent runs. The object oriented method is used. The objects classes that are managed are defined in compliance with the managed units. Guidelines for the definition of managed objects (GDMO) from the network management standards are observed. UML is used for the model description. At this stage, objects are represented only with names, "Part-of" relationships, and associations. At the next stage, attributes and operations will be added to the managed objects. With this defining level, the model is a good basis for user interface development.

Keywords: Information model, universal agent, distributed energy resources (DER), distributed power generation

ИНФОРМАЦИОНЕН МОДЕЛ НА УНИВЕРСАЛЕН АГЕНТ ЗА УПРАВЛЕНИЕ НА РАЗПРЕДЕЛЕНО ГЕНЕРИРАНЕ НА МОЩНОСТ

Мила Илиева-Обретенова

Минно-геоложки университет "Св. Иван Рилски", 1700 София, milailieva@abv.bg

РЕЗЮМЕ. Smart Grid е електромрежа с разнообразие от оперативни и енергийни измервания, включващи умни електромери, умни приложения, възобновяеми енергийни източници и енергоефективни ресурси. Обуславяне на електронна мощност и контрол на производството и разпределението на електричество са важни аспекти на Smart Grid. Разгръщането на технологията за Smart Grid изисква препроектиране на индустрията за електроуслуги, въпреки че типичното използване на термина се фокусира върху техническата инфраструктура. Статията цели да предложи информационен модел на универсален агент за управление на електроснабдяването. Моделът е предвиден за разработчици на потребителски интерфейс и служители по експлоатация. Хипотезата е следната: Описанието на възлите, през които преминава агентът, трябва да съдържа дефиниции на софтуер. Софтуерът на всеки възел е достатъчно да се детайлизира с елементи до ниво мениджър и програма. Моделът трябва да притежава следните качества: Местата, през които минава агентът, се представят като физически възли. За всеки възел софтуерът е като множество от функции. Функциите се групират в съответствие с областите за взаимодействие на отворени системи (OSI): защита, поддържане, конфигурация, таксуване и технически характеристики. Фокусираме върху област конфигурация, защото тя съдържа данни за маршрутизиране на агента. Софтуерните компоненти в област конфигурация се детайлизират до мениджър Достъп до елемент, който насочва агента към следващия елемент по неговия път. Методологията за проектиране на този информационен модел включва дефиниране на класове управявани обекти за възлите, през които преминава агентът. Дефинициите са представени словесно и чрез диаграми на UML (Унифициран език за моделиране). UML диаграмите се класифицират в два вида: диаграми на поведение и диаграми на структура. Диаграмите на класове, вид диаграми на структура, са подходящи за описване на възлите в Smart Grid. Диаграмите на класове описват типовете обекти в системата и различните видове статични взаимоотношения между тях. Тези диаграми показват също отношение „Част от", асоциации, свойства, операции на класовете и ограничения в начина, по който са свързани обектите. Моделите имат влияние от аналогични модели за управление на телекомуникациите. Резултатът е проект на модел за управление в Smart Grid: модел за управление на мрежа и нейните елементи, през които преминава универсален агент. Използван е обектно ориентиран метод. Класовете управявани обекти са дефинирани в съответствие с управляваните единици. Следвани са Препоръки за дефиниране на управявани обекти (GDMO) от стандартите за управление на мрежи. За описание на модела е използван UML. На този етап обектите са представени само чрез имена, отношения „Част от" и асоциации. На следващия етап ще се добавят атрибути и операции към управляваните обекти. С това ниво на дефиниране моделът представлява добра основа за разработване на потребителски интерфейс.

Ключови думи: информационен модел, универсален агент, разпределени енергийни ресурси, разпределено генериране на мощност

Introduction

Modern power supply includes the intensive introduction of renewable energy sources. This leads to the accumulation of large energy quantities in the network and causes disbalance. One of the solutions to the problem is energy distribution automation. The concept is called Smart Grid (IEC, 2012). Smart Grid is an electro grid which includes a variety of operating end energy measurements and uses smart meters, smart applications, renewable energy sources, and energy efficient resources. Electronic power conditioning and energy manufacturing and distribution control are important network aspects. Smart Grid deployment also includes fundamental redesign of electro services industry, although the typical term usage focuses on the technical infrastructure.

In contrast to the traditional network, Smart Gird enables each node to produce and store energy all over the network. This means that the energy is not bound to the source where it was originally produced. The energy could run through the network and could be stored where it is most needed. This potentially guarantees faster supply. Recently, big producers have been paying a lot of money for energy supply networks. With Smart Grid, the whole network could act as a supply network. Each node with a capacity, not just the producers, could demonstrate the presence of energy. There are special security mechanisms embedded in Smart Grid basic levels, which guarantee the secure uploading and storage of energy.

The information model of agent and nodes should use the block chain technology (https://www.hyperledger.org/projects/fabric 2017). It creates an architecture based on the storage and usage of energy and not on the location in the network. There are two types of flows in a block chain: energy and agent (request). The user sends an agent to the network to find energy and to provide it back. The agent has a label – a string of bits. The label is named Uniform Resource Identificator (URI). URI uses the hierarchical naming system and has three basic parts:

- Prefix, which nodes use to find the general direction for energy;
- Date and time when the agent was created;
- Source number which should be checked together with the whole number of sources in this direction.

For instance, an agent could be named so: Direction/020617/1633/source=1:5/.

In this case, Direction is the routable prefix for energy, 020617 is the date 2nd of June 2017, 1633 is the time 16:33, it begins to check source 1 in this direction, the possible sources are 5.

New way of routing

For the energy of "Direction" to be distributed in Smart Grid, a node (Smart Meter) issues an energy request labeled with routable Direction. The nearest node sends the request while it finds energy. Then the node sends the energy back to the user by following the same way and using the same interface or gateway through which the request has entered the system.

However, if the node does not contain energy in its storage, the forwarding-machine writes the request in Pending Interest Table, or PIT (a log which consists of the running copy of all requests that have recently passed through the node and have not found energy). Also, the gateway, through which every request enters, is remarked, as well as the gateway, through which it runs forward. When a new request comes and it is written in the PIT, the forwarding-machine sees all unsatisfied requests and sends the new one along exactly the same route. The idea is that the entries in the PIT create a trail for every request to trace its route through the network, while it finds the searched energy. Then this trail consults the PIT in every node to follow the reverse way to the original user and notes that the request has been satisfied. However, if a request enters the node and the forwarding-machine finds neither uploaded energy, nor any entry for a previous request in the PIT, the node calls the Forwarding Information Base (FIB). FIB is a table with all URI-prefixes (the routable prefixes for the whole network). When a new source is installed, it is entered in FIB and a new entry is added in PIT for future calling. When the next request comes and the last source could not satisfy it, the forwarding-machine checks FIB. Then it sends the request through a gateway which moves it nearer to this location. Figure 1 shows the new way of routing. Figure 2 shows Elements of Node.
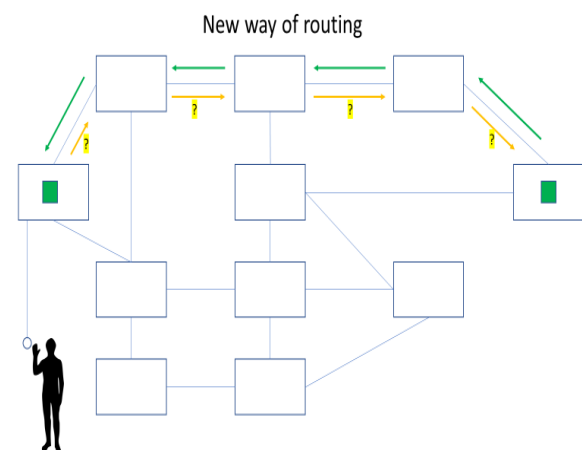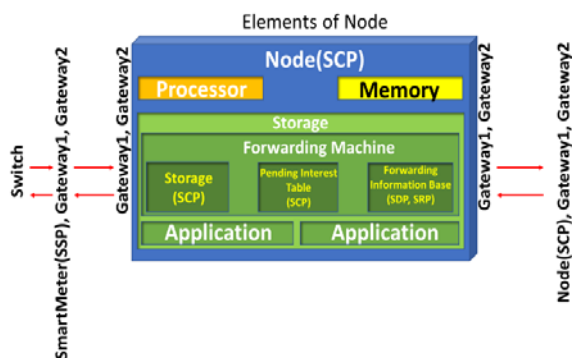

Fig. 1. New way of routing

Fig. 2. Elements of Node

Scope

This paper aims to offer an information model of a universal agent for power supply management. The model is designed for user interface developers and operating officers.

Thesis

The model should include description of nodes through which the agent runs.

Hypothesis

The description of nodes should include software definitions. It is sufficient for the software of each node to be detailed with elements up to level Manager and Program. The model should possess the following features: the places through which the agent runs are represented as physical points; software as a set of functions is represented for each node; functions are grouped according to OSI areas: security, maintenance, configuration, accounting, and performance; the focus is on the configuration area because in contains agent routing data; software components in the Configuration area are detailed up to Element access manager which directs the agent to the next element on his way.

Methodology

The mmethodology for the information model design of an agent for distributed power generation includes a definition of the managed object classes for the nodes through which the agent runs. Definitions are represented verbally and by UML (Unified Modeling Language) diagrams (Gentleware, 2017; Fowler, 2004). UML diagrams are classified in two types: behavior diagrams and structure diagrams. Class diagrams, a type of structure diagrams, are appropriate for the Smart Grid node description. A class diagram describes the types of objects in the system and the different kind of static relationships between them. Diagrams also show "Part of"-relationships, features, and operations of classes, and the limits of the way in which the objects are connected. The "Part of"-relationship is shown with a rhombus and a line. The features are one term but they are represented with two quite different notations: attributes and associations. The notation for an attribute describes a distinct feature like text (second row) in a rectangle envisaged for a class. The association is a directed line between two classes and its direction is from class-source to class-aim. The name of a feature is set on the aimed end of the association with its majority. The end-aim of the association is connected to the class which is the feature type. The majority of a feature is a note for how many objects could complete the feature. Operations are actions which a class could realize. Obviously, they correspond to the methods of a class. Although there is a distinction between Operation and Method, Operation is the term for a method – declaration of procedure. The method is a code from which the procedure consists. Operation and Method are differentiated by polymorphism. The models have the impact of similar models for telecommunications management (Magedanz, 1994).

Results

In this section are represented designed models for management in Smart Grid: the model for the management of a network and its elements through which a universal agent runs. Object oriented method is used. The classes of managed objects are defined according to the managed units. The Guidelines for definitions of managed objects (GDMO) (ISO/IEC/IS, 1989) from the network management standards are followed. UML is used for Model description. At this stage, objects are represented with names, "Part of"-relationships, and associations.

A. Managed Objects Classes for node SSP (Service Switching Point – Smart Meter)

A Managed object (MO) Switch represents the information for a switch in the user's premises. MO SSP represents the management information for a node SSP. MO SSF (Service Switching Function) represents the management information for SSP functionality. MO SSFConfiguration represents the configuration of SSF functionality. MO SSFMaintenance represents the duties for maintenance of SSF functionality. MO SSFSecurity represents the rules for security of SSF functionality. MO SSFPerformance represents parameters for the performance of SSF functionality and their management. MO SSFAccounting represents the management information for the accounting of the used energy. MO TriggerTable represents service trigger information in Smart Grid. MO TriggerInfo represents the trigger description needed for request (agent) direction to service execution. MO FeatureSupplyManager represents the mechanism for competitive realizations support of service in Smart Grid and of service out of Smart Grid in a request. MO SGSwitchingManager represents the mechanism which interacts with SCF (Service Control Function) for service provision. SCF detects events which should be reported to active service realization and it manages SSF resources which should support service realizations. MO FEAccess Manager represents the mechanism for information exchange with functional elements by notifications. MO SCF will be represented in the next paragraph. MO BasicSupplyManager represents the mechanism for basic service return, after search execution. MO NonSGFeatureManager represents the mechanism for feature calling out of Smart Grid (for instance, the usage of own solar source). MO SSFUsageLog represents collected entries for energy usage. MO SSFAccountingLog represents the collected entries for energy accounting during service execution. Figure 3 shows UML diagram of Managed Objects Classes for SSP (Smart Meter).
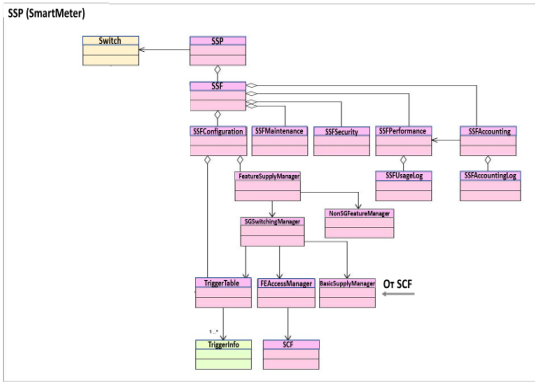
Fig. 3. UML diagram of Managed Objects Classes for SSP-SmartMeter

B. Managed Objects Classes for node SCP (Service Control Point – Storage, PIT)

MO SCP represents the information for node SCP. MO SCF (Service Control Function) represents the management information for a SCP. MO SCFMaintenance represents the rules for the maintenance of SCF. MO SCFSecurity represents the rules for the security of SCF. MO SCFConfiguration represents the configuration of SCF. MO SCFPerformance represents the parameters of performance for SCF and their management. MO SCFAccounting represents the information for accounting management in SCF.MO SCFPreventiveFunction represents testing programs in SCF by normal work conditions. MO LogicExecutionEnvironment represents the environment for logic execution with all the participating managers, programs and data. MO LogicExecutionManager represents the information for the functionality which processes and controls the whole service execution. MO ProgramLibrary represents the resource for different programs storage in SCF. MO Program represents the description of a service logic program. MO DataAccessManager represents the information for the storage, management, and access to SCF shared information and for the access to remote information in other functional elements by MO FEAccessManager. MO FEAccessManager and MO SSF are represented in paragraph A. Managed Objects Classes for node SSP. MO SCF is represented above. MO SDF will be represented in the next paragraph. MO SCFUsageLog represents the collected entries for the usage of SCF. MO SCFAccountingLog represents the collected entries for the accounting of SCF during service execution. Figure 4 shows the UML diagram of the managed objects classes for node SCP.
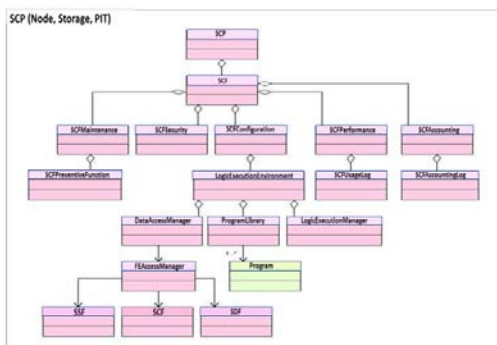

Fig. 4. UML diagram of Managed Objects Classes for node SCP

C. Managed Objects Classes for node SDP (Service Data Point – FIB)

MO SDP (Service Data Point) represents the information for a node SDP. MO SDF (Service Data Function) represents the management information for a SDP. MO SDFConfiguration represents the configuration of SDF. MO SDFPerformnce represents the quantity parameters of SDF and their management. MO SDFAccounting represents management information for the accounting of SDF. MO SDFMaintenance represents the rules for maintenance of SDF. MO SDFDataManager represents the information for the storage, management, and access to data in SDF. MO SDFDataBase represents the information for the Data Base in SDF. MO FEAccessManager is represented in paragraph A. Managed Objects Classes for node SSP. MO SDFData represents an entry in functional element SDF for a service request. MO Template represents the description of an entry format for each request in Smart Grid. MO SCF was explained in the previous paragraph. MO SRF will be represented in the next paragraph. Figure 5 shows the UML diagram of Managed Objects Classes for node SDP.
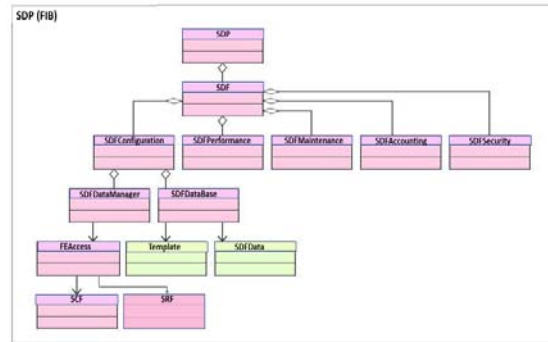

Fig. 5. UML diagram of Managed Objects Classes for node SDP

D. Managed Objects Classes for node SRP (Service Resource Point – FIB)

MO SRP (Service Resource Point) represents the information for the distributed power sources. MO SRF (Service Resource Function) represents management information for a SRP. MO SRFPerformance represents the parameters for the performance of SRF and their management. MO SRFAccounting represents the management information for accounting in SRF. MO SRFMaintenance represents the rules for the maintenance of SRF. MO SRFSecurity represents the rules for the security of SRF. MO FEAccessManager is represented in the previous paragraph. MO ResourceManager represents the information for the resources managed from SRF. MO SRFDataBase represents the information for Data Base in SRF. MO SRFUsageLog represents the collected entries for the usage of SRF. MO Resource represents the description of the resources used as energy sources. MO AtomicPowerSt describes the data for the atomic power stations used. MO CoalPowerSt describes the data for the coal power stations used. MO WaterPowerSt describes data for used water power stations. MO SolarPowerSt describes the data for the used solar power stations. MO WindPowerSt describes the data for the used wind power stations. MO SDF was represented in paragraph C. Managed Objects Classes for node SDP. Figure 6 shows

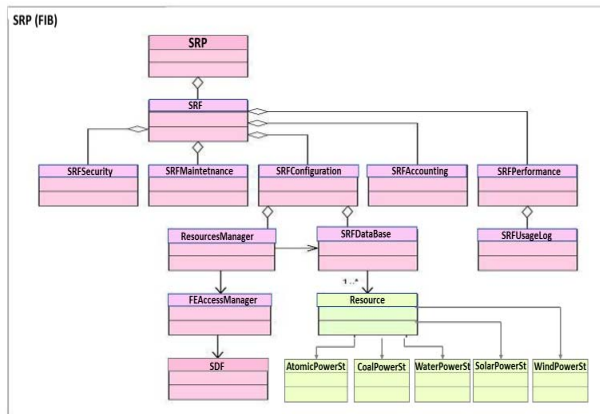the UML diagram of the Managed Objects Classes for node SRP.

Fig. 6. UML diagram of Managed Objects Classes for node SRP

The chosen granularity degree by node description gives an idea about the work volume which should be completed in the development phase. The comparison of the proposed model and those of other researchers is difficult because they are business secrets. The differences could be found in the managed objects names and in the organization of the structures. The disadvantages could be found in the limited number of details.

Conclusion

This paper represents the design of an information model for a universal agent for power generation and supply management in Smart Grid. The model corresponds to the responsibilities of actor Network operator. Managed objects classes are defined that represent managed resources for network elements following the object oriented method. Managed Objects Classes are organized in a hierarchy which shows the correlation between them and relates to their easier realization. At this stage, the software for the management of each node is detailed with elements up to level Manager and Program. The managed objects are defined only with name, "Part of" relationships, and associations. Attributes and operations will be added at the next stage. Nevertheless, the model is a good basis for user interface development.

References

Fowler, M. UML Distilled: A Brief Guide to the Standard Object Modeling Language. 3rd ed. Addison-Wesley Professional, 2004

Gentleware AG, Posseidon For UML CE 8.0, www.gentleware.com, (accessed 2017)

International electrotechnical commission, Smart Grid Standards Map, IEC 61968-1: 2012; http://smartgridstandardsmap.com/ (accessed 2017)

ISO/IEC/IS 7498 – 4 CCITT Recommendation X 700: Information Processing – Open Systems Interconnection – Basic Reference Model - Part 4: Management Framework, 1989, pp. 19-30

Magedanz, T., An integrated management model for intelligent networks, Munchen, Wien: Oldenburg, 1994

https://www.hyperledger.org/projects/fabric (accessed 2017)

THE EQUILIBRIUM OF A BODY LOADED WITH A SPATIAL SYSTEM OF FORCES

Asen Stoyanov

University of Mining and Geology "St. Ivan Rilski", 1700 Sofia

ABSTRACT. A comparative research has been carried out on the equilibrium of a body loaded with a spatial system of forces from which one of the distributed loads has an intensity which is changed after a non-linear law. For the purposes of this article, two analytical solutions to a specific task have been compared. The manual solution is classic. In it, the resultant forces and resultant moment from the distributed loads are determined. After that, the concentrated forces are decomposed into components, and the equations for equilibrium are composed. Finally, the unknown values are determined and the solution is checked.

The second solution is performed by means of MathCAD 15. The graph of the non-linear function $q_2(y)$ is automatically depicted in the figure. The equations for the equilibrium are represented in the $A.X = B$ matrix form, and its solution is the solution to the problem.

Keywords: three-dimensional system of forces, inverse matrix, MathCAD

РАВНОВЕСИЕ НА ТЯЛО, НАТОВАРЕНО С ПРОСТРАНСТВЕНА СИСТЕМА ОТ СИЛИ
Асен Стоянов
Минно-геоложки университет "Св. Иван Рилски", 1700 София

РЕЗЮМЕ. Проведено е сравнително изследване на равновесието на тяло, натоварено с пространствена система от сили, от която едно от разпределените натоварвания има интензивност, която се променя по нелинеен закон. В статията за конкретна задача са сравнени две аналитични решения. Ръчното решение е класическо. В него се определят равнодействащите сили и резултантният момент от разпределените натоварвания. След това концентрираните сили се разлагат на компоненти и се съставят уравненията за равновесие. Накрая се определят неизвестните и се проверява решението.

Второто решение се изпълнява с MathCAD 15. Графиката на нелинейната функция се изобразява автоматично на дадената фигура. Уравненията за равновесие са представени в матрична форма $A.X = B$, и нейното решение е решение на задачата.

Ключови думи: пространствена система от сили, обратна матрица, Маткад

Introduction

The article studies the equilibrium of a beam with a broken axis loaded with a spatial system of forces. One of the two distributed loads is with variable intensity. The function that describes the change of this intensity is square.

Determining the resultant force $\vec{R}_2$ and the resultant moment $\vec{M}_{2x}$ requires integration within the boundaries of the section loaded with $q_2(y)$. The resulting algebraic projection M_2x is directly involved in the equilibrium equation (for this specific example, in equation $\sum Mx_i = 0;$).

Difficulties that arise when solving problems in theoretical mechanics, and in particular in statics, are mathematical. In the example under consideration, integrating a square function is not a problem. However, if the intensity is expressed by a function other than a polynomial, the difficulties become very prominent.

Such problems in engineering practice are not uncommon. Their solution is easy when using any of the mathematical packages, such as MATLAB, Maple, MathCAD, and the like.

The beam is studied classically, "by hand", and with the help of the MathCAD package. The analysis of the two types of solution makes it easy to assess their efficiency.

A similar problem has been solved by Doev and Dronin (2016). The authors cited have chosen a positive function for the intensity in the loaded section.

In the current article, the solution to similar a problem has been improved. The author has chosen the law for the change of intensity in such a manner that the distributed load changes its direction of action over part of the loaded section - see fig. 1.

The equilibrium of $3D$ systems of forces is examined also by Bertyaev (2005) and Stoyanov (2014, 2016).

The system of forces acting on a free moving body is successfully studied in a dynamical setting and by means of the MATLAB programme (Ivanov, A., 2014, Ivanov, I., Y. Yavorova, 2017).

Solution "by hand"

The beam is stationary in the thee-dimensional space within the reading system $Oxyz$ (see fig. 1).

The support devices at points A and B have been replaced by the corresponding reaction forces (see fig.1).

The assignment is to find analytically all the reaction forces, if the geometry and load on the beam are known:

$$a = 3\,m;\ b = 4\,m;\ c = 3\,m;\ d = 2,5\,m;\ \alpha = \frac{\pi}{3};$$

$$\beta = \frac{\pi}{4};\ P_1 = 35\,kN;\ P_2 = 32\,kN;$$

$$q_1 = 33\,kN/m;$$

$$q_2(y) = -50.y^2 + 50.y + 287,5\,kN/m.$$

Solution:

1) **Decomposition of the forces $\vec{P_1}$ and $\vec{P_2}$ into components**

$$\vec{P_1}\begin{vmatrix} P_{1y} = P_1.\sin\alpha = 30,311\,kN; \\ P_{1z} = P_1.\cos\alpha = 17,5\,kN; \end{vmatrix}$$

$$\vec{P_2}\begin{vmatrix} P_{2x} = P_2.\sin\beta = 22,63\,kN; \\ P_{2y} = P_2.\cos\beta = 22,63\,kN. \end{vmatrix}$$
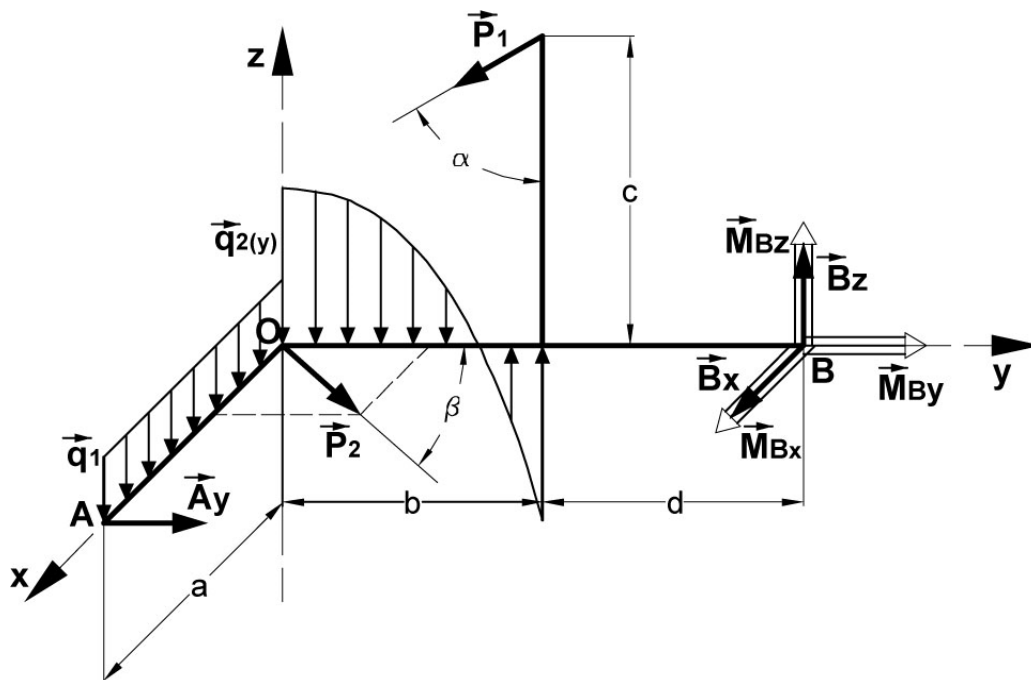
Fig. 1. Calculation scheme

2) **Determining the sizes of the resultants $\vec{R_1}$ and $\vec{R_2}$**

$$R_1 = q_1.a = 33.3 = 99\,kN;$$

$$R_2 = \int_0^b q_2(y).dy = \int_0^b (-50.y^2 + 50.y + 287,5).dy;$$

$$R_2 = -16,67.y^3\Big|_0^4 + 25.y^2\Big|_0^4 + 287,5.y\Big|_0^4$$

$$R_2 = 483,333\,kN.$$

3) **Determining the sizes of the resultant moment $\vec{M}_{2x}$**

$$M_{2x} = \int_0^b y.q_2(y).dy;$$

$$M_{2x} = -12,5.y^4\Big|_0^4 + 16,667.y^3\Big|_0^4 + 143,75.y^2\Big|_0^4;$$

$$M_{2x} = 166,667\,kN.m.$$

4) **Determining the coordinate of the resultant force $\vec{R_2}$**

$$y_2 = \frac{M_{2x}}{R_2};\ \ y_2 \approx 0,345\,m.$$

5) Compiling a system of equations for the equilibrium of the beam

$$\sum X_i = 0; \quad B_x + P_{2x} = 0;$$

$$\sum Y_i = 0; \quad A_y + P_{2y} - P_{1y} = 0;$$

$$\sum Z_i = 0; \quad -R_1 - R_2 - P_{1z} + B_z = 0;$$
$$\sum Mx_i = 0;$$
$$P_{1y}.c - P_{1z}.b + M_{Bx} - M_{2x} + B_z.(b+d) = 0;$$

$$\sum M_{iy} = 0; \quad R_1.a.0,5 + M_{By} = 0;$$

$$\sum M_{iz} = 0; \quad A_y.a + M_{Bz} - B_x.(b+d) = 0.$$

6) Solving the equilibrium equations

The equilibrium equations in this case (p.5)) are independent with relation to the unknown values and can be solved separately.

$$B_x = -22,63\,kN;$$

$$A_y = -22,63 + 30,311 = 7,681\,kN;$$

$$B_z = 99 + 483,12 + 17,5 = 599,833\,kN;$$

$$M_{Bx} = -30,311.3 + 17,5.4 + 166,667 - 6,5.599,62$$
$$M_{Bx} = -3753,1805\,kN.m;$$

$$M_{By} = -99.3.0,5 = -148,5\,kN.m;$$

$$M_{Bz} = -7,681.3 - 22,63.6,5 = -170,138\,kN.m.$$

If it is necessary to solve a linear system of six equations with six unknown values "by hand", the system can be presented in the compact matrix form –

$$A.S = B \qquad\qquad (1)$$

Where:
- A is the matrix of coefficients in front of the unknowns with dimensionality NxN ($N = 6$);
- S is a vector whose elements are unknown reaction forces and reaction moments;
- B is a vector whose elements are known magnitudes (the free members of the system on p. 5) multiplied by (-1).

The solution to matrix equation (1) is searched in the species $S = A^{-1}.B$. In order to determine the reversibility of A (i.e. $|A| \neq 0$), it is necessary to use the Gauss-Jordan method.

7) Verification

The head moment of the forces (active and passive) that are applied to the beam relative to axis "S" with a single vector $\vec{e}_s = \dfrac{1}{\sqrt{3}}(\vec{i} + \vec{j} + \vec{k})$ must be equal to zero –

$$M_s = \frac{1}{\sqrt{3}}(R_1.0,5.a - R_2.0,345 + A_y.a -$$
$$- P_1.\cos\alpha.b + P_1.\sin\alpha.c + B_z.(b+d) -$$
$$- B_x.(b+d) + M_{Bx} + M_{By} + M_{Bz}) \overset{?}{=} 0;$$

$$Ms = \frac{1}{\sqrt{3}}(148,5 - 166,75 + 23,043 - 70 +$$
$$+ 90,933 + 3898,9145 + 147,095 -$$
$$- 3753,1805 - 148,5 - 170,138 =$$
$$= \frac{1}{\sqrt{3}}.(4308,4855 - 4308,5685) =$$
$$= -0,04792 \approx 0!$$

Solution to the problem with the MathCAD package

The algorithm of the solution is as follows:

- The output data are introduced – see fig.2;
- The resultant forces $\vec{R}_1$ and $\vec{R}_2$, the resultant moment $\vec{M}_{2x}$, and the "y_2" coordinate are determined – see fig.2.;
- The distributed load $q2(y)$ is graphically presented – see fig. 2;
- The vectors p_1, p_2, R_1, and R_2 are formed - see fig.2.;
- The square matrix is formed and its reversibility is verified, i.e. $\det A \neq 0$ – see fig.2;
- Vector B is formed with elements that are free members in the equations from p.5) and those are multiplied by (-1) – see fig. 2.
- The support reactions are determined – see fig. 2.

$P1 := 35 \quad P2 := 32 \quad q1 := 33 \quad q2(y) := -50 \cdot y^2 + 50 \cdot y + 287.5$

$a := 3 \quad b := 4 \quad c := 3 \quad d := 2.5 \quad \alpha := \dfrac{\pi}{3} \quad \beta := \dfrac{\pi}{4} \quad \text{ORIGIN} := 1$

$R2 := \displaystyle\int_0^b q2(y)\, dy \qquad M2x := \displaystyle\int_0^b y \cdot q2(y)\, dy \quad y2 := \dfrac{M2x}{R2} \quad R2 = 483.333$

$M2x = 166.667 \quad y2 = 0.345 \quad y := 0,.0001 .. 4 \quad p1 := (0 \;\; -P1 \cdot \sin(\alpha) \;\; -P1 \cdot \cos(\alpha))^T$

$R1 := (0 \;\; 0 \;\; -99)^T \qquad R2 := (0 \;\; 0 \;\; -483.333)^T \quad p2 := (P2 \cdot \sin(\beta) \;\; P2 \cdot \cos(\beta) \;\; 0)^T$
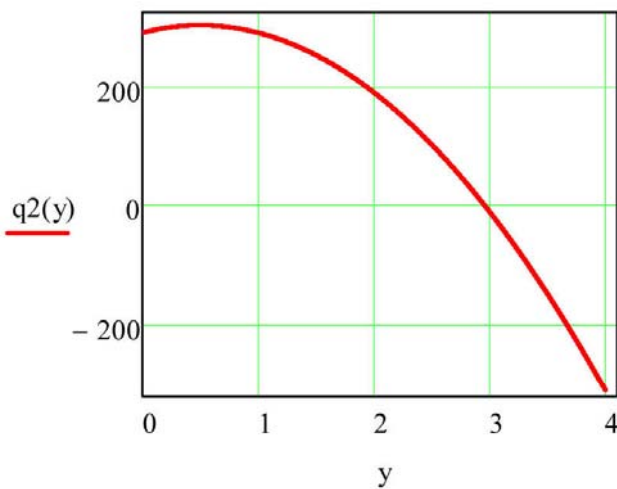
$$A := \begin{bmatrix} 0 & 1 & 0 & 0 & 0 & 0 \\ 1 & 0 & 0 & 0 & 0 & 0 \\ 0 & 0 & 1 & 0 & 0 & 0 \\ 0 & 0 & b+d & 1 & 0 & 0 \\ 0 & 0 & 0 & 0 & 1 & 0 \\ a & -(b+d) & 0 & 0 & 0 & 1 \end{bmatrix} \quad |A| = -1 \quad B := \begin{bmatrix} -p2_1 \\ -p2_2 - p1_2 \\ (-R1)_3 - R2_3 - p1_3 \\ -(-p1_2) \cdot c + (-p1_3) \cdot b + M2x \\ R1_3 \cdot .5 \cdot a \\ 0 \end{bmatrix}$$

$$S := (Ay \;\; Bx \;\; Bz \;\; Mx \;\; My \;\; Mz)^T \quad S := A^{-1} \cdot B \quad S = \begin{pmatrix} 7.683 \\ -22.627 \\ 599.833 \\ -3.753 \times 10^3 \\ -148.5 \\ -170.129 \end{pmatrix}$$

Fig. 2. Partially automated solution to the beam with the MathCAD package

Conclusion

The actual directions of reaction $\vec{B}_x$ and reactive moments $\vec{M}_x$, $\vec{M}_y$ and $\vec{M}_z$ are opposite to the displayed ones - see fig.1.

The study presented, in which the problem is solved both "by hand" and with the MathCAD package for mathematical research, gives a clear idea of the advantages of the MathCAD application compared to the solution "by hand".

The solution "by hand" is sometimes accompanied not only by the difficulties mentioned in the introduction, but also by errors. The latter are difficult to detect because the process of tracking the solution is longer than that with the MathCAD package. Furthermore, when the problem is solved correctly, it is possible for the routine error to be made in the course of the verification.

When it a linear system of six equations with six unknowns is solved "by hand", the Gauss-Jordan method must be applied correctly, i.e. $(A|E \rightarrow E|A^{-1})$. The plausible presentation of the distributed load $\vec{q}_2(y)$ on the diagram by hand (see fig.1.) requires the use of tools for drawing (the calculation scheme in the fig. 1. is drawn with AutoCAD).

The partially automated solution to the beam with the MathCAD package is quick and compact and it accurately represents the square function $q_2(y)$ – see fig. 2.

The solution to the problem with the MathCAD package cannot guarantee the lack of errors, but those can easily be found in the short and clear record – see fig. 2.

The use of the graphic editor in MathCAD package helps for establishing the connection between a geometric or a force parameter and reaction forces and reaction moments.

References

Бертяев, В. Теоретическая механика на базе MathCAD практикум, Санкт–Петербург, „БХВ–Петербург", 2005, 739 с. (Bertyaev, V. Teoreticheskaya mehanika na baze MathCAD praktikum, Sankt-Peterburg, "BHV-Peterburg", 2005, 739 p.)

Доев, В.С., Ф.А. Доронин. Сборник заданий по теоретической механике на базе MathCAD, Санкт Петербург, Москва, Краснодар, Лань, 2016, 585 с. (Doev, V.S., F.A. Doronin, Sbornik zadaniy po teoreticheskoy mehanike na baze MathCAD, Sankt-Peterburg, M., Krasnodar, Lany, 2016, 585p.)

Иванов А., Пространствено изследване летежа на тенис топка, сп. Механика на машините, том 2, год. XII, 2014, 34 ÷ 37 с. (Ivanov A., Prostranstveno izsledvane letezha na tenis topka, sp. Mehanika na mashinite, tom 2, god. XII, 2014, 34 ÷ 37p.)

Стоянов, А. Определяне равновесието на пространствена система сили посредством MathCAD, XIV Международна научна конференция ВСУ'2014, 2014г. 44–47 с. (Stoyanov, A., Opredelyane ravnovesieto na prostranstvena sistema sili posredstvom MathCAD, XIV Mezhdunarodna nauchna konferentsiya VSU'2014, 44–47)

Стоянов, А., Матрични операции с MathCAD в теоретичната механика Статика, Кинезиология БГ, София 2016, 165с. (Stoyanov, A. Matrichni operatsii s MathCAD v teoretichnata mehanika Statica, S. Kineziologiya BG, 2016, 165p.)

Ivanov A., Javorova J., Three dimensional golf ball flight, J. Tehnomus, P-ISNN-1224-029X, E-ISNN-2247-6016, 2017, 54 ÷ 61 p.

ALGORITHM FOR OPTIMIZING THE ROLL FORM IN CENTRAL BAR ROLL MILLS

Simeon Sezonov

University of Mining and Geology "St. Ivan Rilski", 1700 Sofia, sezonov_si@abv.bg

ABSTRACT: The article investigates the change of the roll shape of a centrifugal roller mill in its wear during the process of operation. An optimal shape is sought to compensate for the reduction in the roll mass by increasing its working area. A solution to the task is used as a result of the grinding theory with maintaining a constant grain size of the product, which determines the optimum change of the longitudinal profile of the roll resulting from the working process. In this connection, an algorithm has been developed to calculate the current height of the worn portion of the roller. It consists eight steps. It sets the starting center radius, the current radius of the weft pulley, and the minimum allowable radius. In addition, an algorithm has been developed to determine the co-ordinates of points from a curve that describes the worn portion. It is applied at a set height of the worn part and consists of six steps.
The first algorithm has been numerically tested using the Excel product. This solution complements the analytical expressions of the task of form modification. The proposed algorithms can be used by engineers to select optimum sizes for roll the from a cylindrical roller mill. A numerical example is attached.

Keywords: centrifugal roller mill, optimum roll profile, stresses.

АЛГОРИТЪМ ЗА ОПТИМИЗИРАНЕ ФОРМАТА НА РОЛКАТА В ЦЕНТРОБЕЖНО РОЛКОВИТЕ МЕЛНИЦИ
Симеон Сезонов
Минно-геоложки университет "Св. Иван Рилски ", 1700 София, sezonov_si@abv.bg

РЕЗЮМЕ: В статията се изследва промяната на формата на ролката в центробежно-ролкова мелница при износването й в процеса на работа.
Търси се оптимална форма, която да компенсира намаляването на масата на ролката чрез увеличаване на работната й площ. Използва се решение на задачата като резултат от теорията на смилането при поддържане на постоянен зърнометричен състав на продукта, при което се определя оптималното изменение на надлъжния профил на ролката в резултат на реализирането на работния процес. Във връзка с това е разработен алгоритъм за изчисляване на текущата височина на износената част на ролката. Той се състои от осем стъпки. В него са зададени начален радиус на масовия център, текущ радиус на износващата ролка и минимален допустим радиус. Освен това е разработен и алгоритъм за определяне на координатите на точки от крива, описваща износената част. Той се прилага при зададена височина на износената част и се състои от шест стъпки.
Първият алгоритъм е числено тестван с помощта на продукта Ексел. Това решение допълва аналитичните изрази от задачата за формоизменението. Предложените алгоритми могат да се използват от инженери за избор на оптимални размери на ролката от цилиндрично-ролкова мелница. Приложен е числен пример.

Ключови думи: центробежно-ролкова мелница, оптимален профил на ролката, напрежения.

Introduction

One of the most common grinding machines operating in inertia is the centrifugal roller mill. It guarantees higher performance than conventional gravity-based mills. This is accompanied by rapid wear of the rollers. The degree of grinding is proportional to the number of impacts. To increase their frequency, it is recommended that the work area at the height of the roller be increased. In this connection, the task of modulating the longitudinal profile of the roller is investigated.

One solution is described in Stoev et al. (1982). Based on the grinding theory, a detailed derivation of the analytical dependencies that determine the ultimate wear height of the rollers is described.

The main purpose of this work is to present an algorithm for determining the height and curve of the worn part of the roll. By using it and by using popular program tools, values for a real roller from a cylindrical roller mill are obtained in the article.

Exposition

1. Description of the task of the form modification

When studying the shape of the roller, the Rittinger theory of grinding is preferred. According to it, work in shredding should be proportional to the newly formed surface. According to this theory, the grinding of the material is realized after a sufficiently large elastic deformation, i. e. absorbing a certain amount of "elastic" energy from the body volume.

In recent years, new technologies, schemes and grinding machines have been developed. These are technologies (Parashkevov, 1969) in which high-speed machines and centrifugal forces are used for grinding. For these cases, the simple work of the deformations of a single piece will be proportional to the change in the volume of this piece, raised to the third degree. In order to maintain a constant grain size, it is necessary that the product of the number of deformation cycles of the roll at the intersecting force of the roller be constant.

In order to maintain the grain size composition, according to the Rittinger theory of grinding (Stoev et al., 1982), the condition must be fulfilled:

$$\left[\pi r^2 H + 2\pi \varphi(0)\right] R H =$$
$$\left[\pi y^2(x)(H + 2x) + 2\pi \varphi(x)\right](r_o - y)(H + 2x) \tag{1}$$

where $\varphi(x) = \int_x^h y^2(x)dx$; $\varphi(0) = \int_0^h y^2(x)dx$;

$r_o = R + r$.

The initial conditions are: $y(0) = r$ and $y(h) = r_k$.

Equation (1) is obtained by meeting the requirement of unchangeability of the product at the initial point and at an arbitrary point in time. Multipliers in this product are: the roll volume, the radius of the mass center, and the radius of the cylindrical part. In (1), the following symbols are defined, which are illustrated in Figure 1:

R - starting radius of the mass center;

H - initial height of the cylindrical section of the roll (working height);

r - current radius of the wear roll;

h - maximum height of the wearing roller;

$y(x)$ - function of the curve describing the worn portion of the roller (Fig. 1);
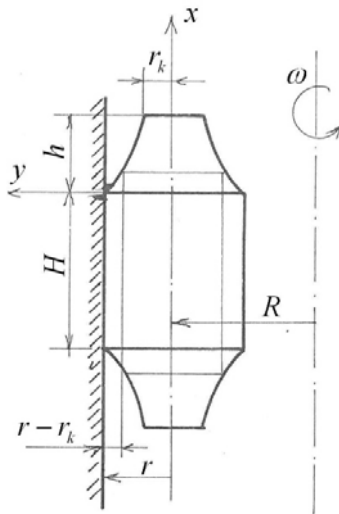
r_k - minimum tolerable radius.

Fig. 1. Roll of the mill

If $x = h$ и $y = r_k$ are substituted in (1), it is obtained:

$$D = r_k^2 B_1(H + 2h), \tag{2}$$

where

$B_1 = r_o - r_k$.

Equation (1) is processed and a Bernullium-type equation (Stoev et al., 1982) is reached:

$$t' = f_1(y)t + f_2(y)t^3, \tag{3}$$

where

$$f_1(y) = -(r_o - y)^{-1}; \qquad f_2(y) = -\frac{2(r_o - y)}{D};$$

$t(y) = H + 2x$.

Equation (3) integrates into squares (Korn, G., Korn, T, 1970). For this purpose, we exchange $\bar{t} = t^{-2}$ and receive:

$$\bar{t}' + 2f_1(y)\bar{t} = -2f_2(y), \tag{4}$$

which is a linear differential equation of first order.

The solution to (4) is equated to $(H + 2x)^{-2}$ and produces:

$$x = -\frac{H}{2} + \frac{B_4}{2(r_o - y)}, \tag{5}$$

where

$$B_4 = \frac{1}{\sqrt{B_2 + \dfrac{4}{D}\left[r - y + (r_o - y)\ln\left(\dfrac{R}{r_o - y}\right)\right]}};$$

$B_2 = H^{-2}R^{-2}$.

In this equation, $x = h$ and $y = r_k$ are replaced and after processing, this expression is to be solved:

$$(H + 2h)^2 = \frac{1}{B_2}\left(\frac{1}{B_1^2} - B_3\right), \tag{6}$$

where

$$B_3 = \frac{4}{r_k^2 B_1}\left[r - r_k + B_1 \ln\left(\frac{R}{B_1}\right)\right].$$

2. Algorithms for determining the height limit of the roll wear

The resulting expressions are used to determine the height of the worn part of the roller and the coordinates of points of that part at different heights. For this purpose, equations (5) and (6) need to be processed. The second equation determines the current height of the worn part h_i:

$$h_i = -\frac{H_i}{2} + \sqrt{\Delta B_i}, \tag{7}$$

where

$\Delta B_i = B_5 B_{2,i}^{-1}$; $B_5 = B_1^{-2}$; $B_{2i} = H_i^{-2}R^{-2}$.

In equation (7), the index i is an integer and takes an initial value of 0, and increases to a value n.

For specific values of h_i and H_i from equation (5), the coordinates of the points j, whose total number is m (Fig. 2), are determined. For this purpose, we replace x with x_i^j,

H with H_i and y with y_j. The following expression is obtained:

$$x_i^j = -\frac{H_i}{2} + \frac{B_{5,i}}{2B_{2,i}B_{6,i}^j}, \qquad (8)$$

where

$$B_{2,i} = H_i^{-2}R^{-2}; \qquad B_{5,i} = H_i + 2h_i;$$

$$B_{6,i}^j = \sqrt{B_{2,i}\left(B_{5,i}\right)^2 + B_{3,i}^j};$$

$$B_{3,i}^j = \frac{4}{r_k^2 B_1^j}\left[r - r_k + B_1^j \ln\left(\frac{R}{B_1^j}\right)\right]; \quad B_1^j = r_o - y_j.$$
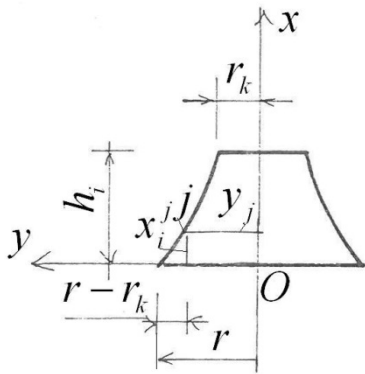

Fig. 2. Worn Roll View

In equation (8), the coordinate y_j participates, which is determined by

$$y_j = r - \Delta z_1 (r - r_k) j, \qquad (9)$$

where

$$\Delta z_1 = (m+1)^{-1}.$$

Equation (7) is basically in the algorithm for obtaining the limit value of the worn portion h_i. It sets the starting height of the cylinder H_o and the height increase ΔH. The algorithm is described in the following steps:

Step 1: Set the values of H_o, R, r, r_k, ΔH, n and m.

Step 2: Calculate the coefficients B_1, B_3 and B_5.

Step 3: The counter i is zero.

Step 4: Calculate $B_{2,i}$, ΔB_i and the height h_i.

Step 5: Activate a subroutine (Figure 4).

Step 6: The counter i is incremented by one.

Step 7: Check that the reading i is not greater than the set value n $(i > n)$. If this is the case, it ends with the first part of the algorithm (end).

Step 8: If the reading i is less than the set value n $(i < n)$ and the height is increased by ΔH, it goes to step 4.

The flow chart of the algorithm is given in Figure 3.
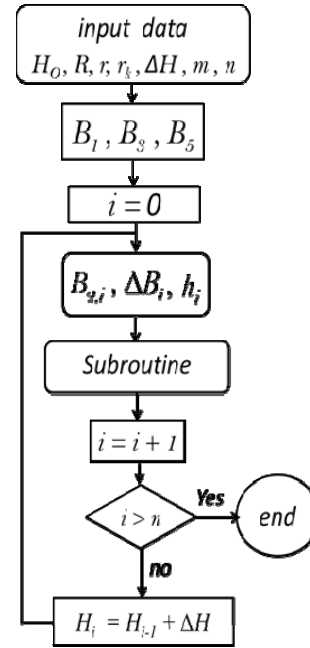
Fig. 3. Flow chart of the algorithm

Expression (8) is the basic in the subroutine algorithm described in the following steps:

Step 1: Set the counter j value 1.

Step 2: Set the value of m.

Step 3: Calculate y_j and x_i^j.

Step 4: The counter j is incremented by one.

Step 5: Verify that the counter value j is greater than m. If this is the case, the subroutine is finalized.

Step 6: If j is less than m, we assume that the roll is divided into layers Δz_j, grows with the next layer Δz_1 and passes to step 3.
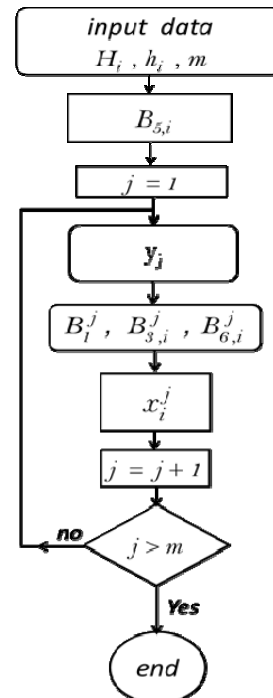
Fig. 4. Flow chart of subroutine program

The described algorithm applies to thirteen points and is illustrated by the flow chart given in Figure 4.

3. A numerical example

The roll with cross section from figure 1 is being considered. The input data are given in Table 1.

Table 1.
Input data

parameter	multiplier	dimension	value
H_o	–	mm	90
R	–	mm	120
r	–	mm	35
r_k	–	mm	15
B_1	–	mm	140
B_3	10^{-2}	mm	– 2.034
n	–	mm	3
m	–	mm	3
ΔH	–	mm	1

By observing the algorithm without the subroutine, the results obtained are presented in Table 2.

Table 2.
Results

| parameter → point i ↓	H_i	B_{2i}	ΔB_{1i}	h_i
multiplier		10^{-4}		
dimension	mm		mm	mm
0	70	1.42	179.539	32
10	80	1.09	234.500	37
20	90	0.857	296.789	41
30	100	0.694	366.407	46
40	110	0.574	443.352	50
50	120	0.482	527.625	55
60	130	0.411	619.227	59
70	140	0.354	718.157	64
80	150	0.309	824.415	69
90	160	0.271	938.001	73
100	170	0.240	1058.915	78
110	180	0.214	1187.157	82
120	190	0.192	1322.728	87

It can be seen from the table that a linear increase in the height of the cylindrical part of the roll H_i results in a non-linear increase in the worn portion of the roller h_i.

4. Key findings

The results of the work can be summarized as follows:
– the analytical expressions for determining the height of the worn part of the roller of a centrifugal mill are verified and refined;
– two algorithms are proposed for calculating the magnitudes described;
– the first algorithm is numerically tested.

The presented solution is a completed version of the developed analytical expressions from the task of changing the shape of the roll.

Conclusion

In order to find the optimum height of the worn part of the roll, a roll change task is formulated. An algorithm consisting of eight stages has been developed for it. The Excel application is used to produce numerical values. An algorithm for determining the wear curve is also given. It applies to a set height and is described in six steps.

The proposed analytical expressions and algorithms can be used by designers to select rolls in centrifugal roller mills.

References

Стоев С., П. Лалов, М. Чалашканов, Триботехнически аспект при оразмеряване на ролките в центробежно-ролкова мелница, *Рудодобив*, кн. 10, 1982, 9-11с. (Stoev S., P. Lalov, M. Chalashchanov, Tribotehnicheski aspekt pri orazmeryavane na rolkite v tsentrobezhno-rolkova melnitsa, Rudodobiv, kn. 10, 1982, 9-11s.)

Корн, Г., Т. Корн, Справочник по математике, Наука, М., 1970, 720с. (Korn, G., T. Korn, Spravochnik po matematike, Nauka, M., 1970, 720s.)

Парашкевов, Р., Механика на скалите, С., Изд. „Техника", 1969, 268с. (Parashkevov, R., Mehanika na skalite, S., Izd. "Tehnika", 1969, 268p.)

STRESSES AND DEFORMATIONS IN THE SHREDDING SHAFTS OF A TWO-SHAFT SHREDDER FOR CRUSHING OF CONCRETE, RUBBER, PLASTIC AND WOOD

Malina Vatskicheva[1], Irena Grigorova[1]

[1]*University of Mining and Geology "St. Ivan Rilski", 1700 Sofia, e-mail: malina_vatz@abv.bg*

ABSTRACT. The article focuses on stresses and deformations in the shredding shafts of a two-shaft shredder for concrete, rubber, plastic and wood crushing. A modeling study of the shredding shafts of such type of shredder has been performed in the present work. The studies of the mechanical load and behavior of the shredding shafts have been conducted through solving the equations describing the mechanical processes in working conditions under the finite element method. For this purpose a three-dimensional geometrical model of the shafts has been generated, which has been discretized (digitized) to a planned network of finite elements in the programming environment of ANSYS MECHANICAL APDL.

Keywords: stresses, deformations, two-shaft shredder.

НАПРЕЖЕНИЯ И ДЕФОРМАЦИИ В РАЗДРОБЯВАЩИТЕ ВАЛОВЕ НА ДВУВАЛОВ ШРЕДЕР ЗА РАЗДРОБЯВАНЕ НА БЕТОН, ГУМА, ПЛАСТМАСА И ДЪРВО

Малина Вацкичева[1], Ирена Григорова[1]

[1]*Минно-геоложки университет „Св. Иван Рилски", 1700 София, e-mail: malina_vatz@abv.bg*

РЕЗЮМЕ. Статията е посветена на изчисляване и проверка на раздробяващите валове на двувалов шредер за раздробяване на бетон, гума, пластмаса и дърво. Направено е моделно изследване на раздробяващите валове на такъв тип шредер. Изследванията на механичното натоварване и поведение на раздробяващите валове са проведени чрез решаване на уравненията, описващи механичните процеси при работни условия по метод на крайните елементи. За целта е генериран триизмерен геометричен модел на валовете, който е дискретизиран на планирана мрежа от крайни елементи в програмната среда на ANSYS MECHANICAL APDL.

Ключови думи: напрежения, деформации, двувалов шредер.

Introduction

The continuous process of production and use of products from rubber, plastic, and the intensified construction lead to a serious accumulation of waste, imbalance, and danger for the environment. In all industrial societies, the need appears for reducing the household and technogenic waste and their re-integration in the production process. As a process, the recycling of construction waste, as well as waste from rubber, plastic and wood, is extremely important both for the environment and the society.

The development of the recycling industry sees an increasing need for crushed materials with different composition and characteristics. The creation of new structures of crushing machines and their study through adequate mechanical and mathematical models, their engineering design, and their practical realization are a topical scientific problem (Vatskicheva, 2017).

The shredders are a relatively new group of machines, crushing refuse utility and waste materials. According to the number of the operating shafts, the shredders are classified intos single-shaft, two-shaft and four-shaft ones (Abadzhiev and Tonkov, 2007). Shredders are configured according to

each unique application, with the selection of different thicknesses and number of the cutting teeth, diameter of the shaft, thickness of the distance bushings, power of drive, and production capacity.

According to the technology of crushing, there is a choice between single-shaft, two-shaft, three-shaft, four-shaft, five-shaft shredders, with a different level of automation and control of the basic parameters, different noise level, different speed of rotation, supply, degree of sealing (pressurization), etc. (Abadzhiev and Tonkov, 2007).

The advantage of the two-shaft shredders is their high productive capacity. The disadvantages are related to the high price and the high maintenance cost of the machines.

The two-shaft hydraulic shredder consists of a feeder-conveyor, a receiving hopper, a crushing chamber, an output strip, an unloading strip, and a strip for the separation of metal particles.

In the present work, a model survey is carried out of the shredding shafts of such type of shredder for crushing of concrete waste.

Object of study

The object of study in the present development is the mechanical load and behavior of the shredding shafts of a two-shaft shredder for crushing of concrete, rubber, plastic and wood.

The shredding shafts are parallel, with length 900 mm, axle base 350 mm, and hexagonal cross-section. The crushing disks are mounted on the shafts. Between the disks, to the housing of the chamber, there are mounted counter-knives, serving for cleaning the space between the separate disks (Fig.1).
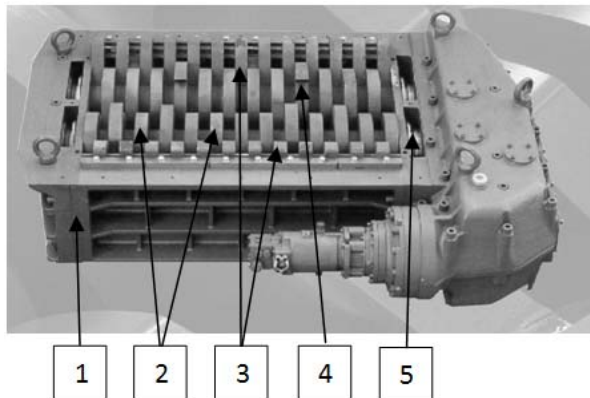

Fig.1. Shredding shafts
Legend: (1) Housing; (2) Crushing disks; (3) Counter-knives; (4) Removable cone; (5) Openings between the reducer and the crushing chamber

The disks intended for crushing are double-topped (two-pointed). On each top is mounted a removable cone (4) of tungsten carbide with a hardness HRC 60 - 64. The pressure exerted by the cone on the concrete must exceed the compressive strength of the concrete, which is 55 MPa. The excess or shortage of power for crushing is regulated through change of the number of simultaneously operating disks and the number of tops on each disk. In case of re-dimensioning of the drive it is possible to increase the crushing disks from two to three, with which the productive capacity will increase by about 50%.

Both crushing shafts are mounted in a common housing (1) by radial axial and radial roller bearings (Borshtev et al., 2000). The protection of the bearing units is three-stage:
- the first stage is through openings (5) between the reducer (reduction gear) and the crushing chamber. The powder and the particles, having penetrated on the side of the shafts, fall through the openings;
- the second stage is through double elastic sealants of the shafts axis;
- the third stage is through the lubrication of the bearings with oil under low pressure (3-5 bar), counteracting the penetration of particles into the bearing unit.

Drive (actuation) of the shredding shafts

The power W required for the propelling of the shredding shafts is determined on the basis of the formula:

$$W = \frac{P_b \cdot \mu \cdot S_t \frac{D_t}{2} \cdot Z \cdot N_v}{9554} = \frac{55.10^5 \cdot 2.6.10^{-4} \cdot 0.15.8.25}{9554} = 207 \, kW;$$

where:
P_b is the stress for the destruction of the concrete of the cross-ties - 55 MPa;
S_t is the maximum contact area of each destructive tooth ~20 x 30 mm or 6×10^{-4} m²;
Z is the number of simultaneously operating disks: 8 (4 from one of the shafts and 4 from the other shaft) with a total length along the axis of the shafts of 320 mm, which is greater than the maximum dimension of the cross-ties - 300 mm;
D_t is the diameter of the cutting disks: 300 mm (the distance of the teeth from the shaft axis);
N_v is the revolutions of the shafts: 25 min⁻¹;
µ is the coefficient of reserve of power, which is equal to 2.

The shredding shafts are mounted on the side of the reducers in paired roller radial axial bearings, and on the other side – in a needle-roller bearing with an inner ring (Borshtev, 2004).

The structure of the shredding shafts is verified for total strength /tension, compression, torsion/. Applied are the loads from the weight of the shaft, the knives with the destructive teeth, and the intermediate disks, as well as the support reactions in the bearings of the shafts. The studies have been conducted through the mathematical models and thenumerical procedures described below.

Model study concept

The studies of the mechanical load and behavior of the shredding shafts have been conducted by solving the equations that describe the mechanical processes in working conditions by the method of the finite elements (FAG Spherical roller bearings E1, 2011). For this purpose, a three-dimensional geometric model of the lower part (underpart) of the chamber has been generated. The model is discretized to a planned network of finite elements in the programming environment of ANSYS MECHANICAL APDL.

The end conditions, reflecting the mechanical load during the operation of the steel structure, include the following parameters (Tavakoli et al., 2008):

- input power: P_{ip} = 90 кW;
- revolutions of the working shaft: n_v= 25 min⁻¹;
- frequency of rotation of the working shaft:

$$\omega_v = \frac{\pi \cdot n_v}{30} = 2.62 \, rad/s;$$

- torque of the working shaft:

$$M_v = \frac{P_{ip}}{\omega_v \eta} = 35 \, kNm,$$

where η=0,98 is the efficiency of the transmission;
- stress of destruction of the concrete: t_s = 55 MPa;
- shear force from one knife:

$$F_s = \frac{M_v}{3.0,175} = 66.7 \, kN,$$

- moment of resistance of the crushing from one knife:

$$M_{S2} = F_s.l_s = 11.67 \, kNm.$$

The pressure that each carbide cone on the disk teeth exerts on the destructed railway sleeper is 94 MPa, which is nearly 2 times higher than the stress of destruction of 55 MPa. The disruptive pressure has been adopted as applied on an area of the tooth with a diameter of 30 mm. It is transformed into radial forces on the knives, respectively torques, on the shafts of the shredder. The condition is accepted about three simultaneously working "destructive" teeth. The nominal moment of rotation of each shaft for 25 rpm is determined: 40 kNm. In this case, the appropriate heliocentric-type reducer (reduction gear) is PG 5001 with gear ratio i = 5.1. Accordingly, the driving hydraulic motor is a radial piston with constant flow, of the type IAM 1600 H, with maximum revolutions (turnovers) 250 min^{-1}, and a moment of rotation equal to 7860 Nm at a pressure of 300 bar.

The mechanical load during operation of the structure is presented in Fig. 2.
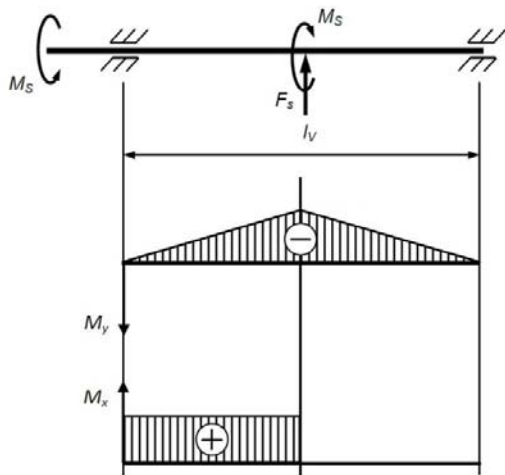
Fig. 2. Load

The system of equations has been solved with the parameters of the steel presented in Table 1.

Numerical results

The data for the material of the shafts accepted in the verification is summarized in Table 1.

Table 1.
Strength characteristics of the material for the shredding shafts

Name	Steel 42CrMo4	
General	Mass Density	7.85 g/cm^3
	Yield Strength	207 MPa
	Ultimate Tensile Strength	345 MPa
Stress	Young's Modulus	210 GPa
	Poisson's Ratio	0.3 ul
	Shear Modulus	80.7692 GPa
Stress Thermal	Expansion Coefficient	0.000012 ul/c
	Thermal Conductivity	56 W/(m K)
	Specific Heat	460 J/(kg c)

The figures below present a visualization of basic parameters characterizing the state of stress of the steel structure.

Fig. 3. Maximum stresses in the elements of the shaft

Fig. 4. Maximum deformations of the elements of the shaft

Fig. 5. Calculated safety factor for the elements of the shaft

Table 2.
Support reactions

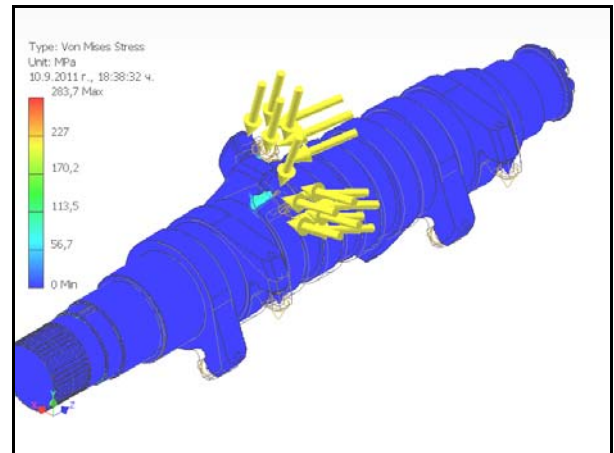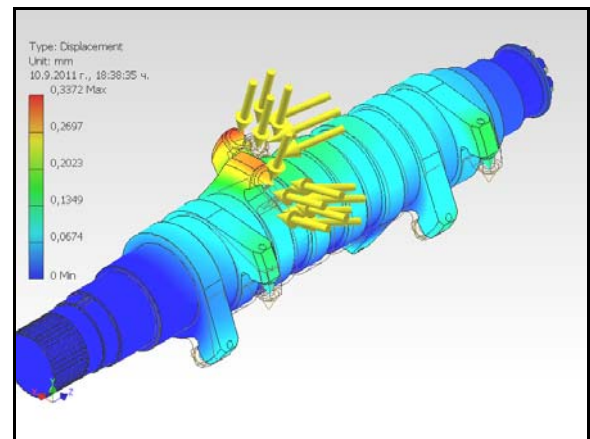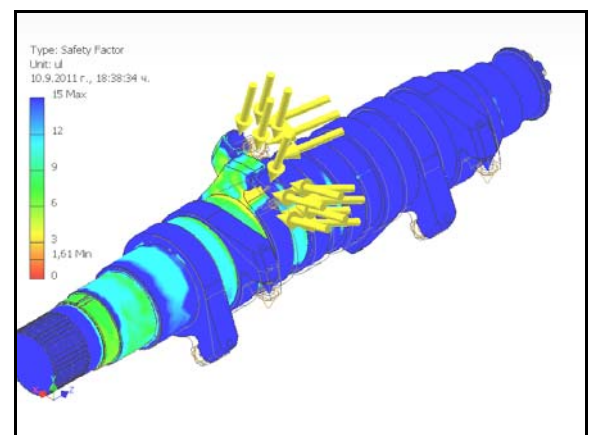| Constraint Name	Reaction Force		Reaction Moment	
	Magnitude	Component (X,Y,Z)	Magnitude	Component (X,Y,Z)
Pin Constraint:1	90793.,5 N	-90786.3 N	5917 N m	-73.9095 N m
		-1143.34 N		-5916.54 N m
		0 N		0 N m
Pin Constraint:2	0 N	0 N	4082.63 N m	-182.663 N m
		0 N		-4078.55 N m
		0 N		0 N m
Pin Constraint:3	49891.2 N	-49522.2 N	12149.7 N m	1378.84 N m
		6057.02 N		12071.2 N m
		0 N		0 N m
Pin Constraint:4	20872.4 N	20871.4 N	16536.2 N m	-21.0458 N m
		-207.16 N		238.686 N m
		0 N		16534,4 N m

Table 3 summarizes the maximum and minimum stresses and deformations.

Table 3.
Summarized stresses and deformations

Name	Minimum	Maximum
Volume	39292300 mm^3	
Mass	308.444 kg	
Von Mises Stress	0.00548071 MPa	65.7722 MPa
1st Principal Stress	-15.6595 MPa	28.8686 MPa
3rd Principal Stress	-83.2857 MPa	4.36874 MPa
Displacement	0 mm	0.127705 mm
Safety Factor	3.14722	15

The conducted study shows that the maximum stresses for the examined structure do not exceed the permissible values for the material of the shafts.

Conclusions

The results from the conducted model studies provide the basis for the following conclusions:
- A 3D model of the shredding shafts of a shredder for concrete railway sleeper is constructed;
- A power model of the load of the shaft from the technological forces during crushing is developed;
- The stresses and the deformations in the system shaft – knives – carbide teeth are studied;
- The coefficient of mechanical safety for the maximum load of the shafts of the shredder is determined;
- The mechanical reliability of the shafts is demonstrated;
- A suitable drive of each shredding shaft is selected – the heliocentric-type of reducer and the radial hydraulic motor.

The studied structure of shredding shafts may be used for the shredder-type of crushing machines.

References

Abadzhiev, V., G. Tonkov, About the synthesis of technological gears for disintegration processes, S., Industrial innovation forum "Machines, technologies, materials", 2007. - 123 p.

Borshchev, V.Y., Equipment for crushing of materials, State Technical University Tambovski, 2004. - 75 p.

Borshchev, V. Y., V. N. Dolgunin, G. S. Kormilitsin, A. N. Plotnikov, Technique of processing of brittle materials, State Technical University Tambovski, 2000. - 40 p.

Vatskicheva, M., Development of universal recycling machine for crushing of concrete, rubber, plastic and wood, Defensed Phd thesis, University of Mining and Geology "St. Ivan Rilski", Sofia, 2017.

Tavakoli, H., S. S. Mohtasebi, A. Jafari, A Comparison of Mechanical Properties of Wheat and Barley Straw, Engineering International: the CIGR Journal, Manuscript number CE12 002, Vol.10, 2008. -1-9.

FAG Spherical roller bearings E1, Schaeffer Technologies GmbH & Co.KG , 2011.

CAUSES OF MALFUNCTIONS WITH INSTALLATIONS FOR REFUSE DERIVED FUEL AND A NON-HAZARDOUS WASTE LANDFILL

Teodora Hristova[1], Nikolai Savov[1], Petya Gencheva[1]

[1] *University of Mining and Geology "St. Ivan Rilski", 1700 Sofia, e-mail: teodora@mgu.bg*

ABSTRACT. With the aim of avoiding future malfunctions and increasing the economic effect of installations for refuse derived fuel and of a non-hazardous waste landfill with an adjoining water-treatment plant for infiltrated water, a review is made of the failures and break-downs. The monitoring of the production process and the inspection carried out provide evidence of the observation of the adopted criteria for quality and faultless operation. Since the facilities have only operated for a short time since their inauguration and putting in service, the authors suggest an active monitoring, not reactive. After examining the faulty facilities on the territory of the plant, a classification is worked out for the various types of failure. The causes or the majority of faults and failures of the individual facilities are determined. Based on these, an analysis of the reasons for delays and interruptions of the working process is prepared. Recommendations are given. It has been established that there are constructional and technological errors that are impossible to correct. The mechanical problems are caused by the larger mass of the processed wastes. These problems can gradually be solved by replacing the driving equipment. As for the problems associated with the automation system, an adjustment of settings should be done that is connected with the power of the driving equipment and with the quality of the wastes recycled. Still, the reduction of the number of interruptions in the plant depends on the employees who need to be better educated and motivated by means of introducing clear criteria for career development. The authors believe that the introduction of the suggested measures for solving the problems that have arisen will help reduce production costs and will raise efficiency and the economic effect.

Keywords: accident, corrosion, electrical and mechanical damage failure, installation for refuse derived fuel

ПРИЧИНИ ЗА АВАРИИ ПРИ ИНСТАЛАЦИИТЕ ЗА МОДИФИЦИРАНО ГОРИВО И ДЕПО ЗА НЕОПАСНИ ОТПАДЪЦИ
Теодора Христова[1], Николай Савов[1], Петя Генчева[1]
[1] *Минно-геоложки университет "Св. Иван Рилски", 1700 София, e-mail: teodora@mgu.bg*

РЕЗЮМЕ. С цел предотвратяването на бъдещи аварии и повишаване на икономическия ефект е направен преглед на отказите и повредите на инсталациите за модифицирано гориво (RDF) и депо за неопасни отпадъци с прилежаща пречиствателна станция за инфилтратни води. Мониторингът и инспекцията предоставят доказателства за спазване на приетите критерии за качество и безаварийност на производствения процес. Тъй като предприятието е работило кратко време след пускането си в експлоатация, авторите препоръчват активен мониторинг, а не реактивен. След обследване на аварирали съоръжения на територията на завода е направена класификация на различните типове откази. Определени са причините за по-голямата част от авариите или отказите на отделни съоръжения. Въз основа на това е направен анализ на причините за забавяне или спиране на работния процес, дадени са препоръки. Установено е, че има конструктивни и технологични грешки, които не могат да бъдат променени. Механичните проблеми са причинени от по-голямата маса на преработваните отпадъци, които постепенно могат да се решат с подмяна на задвижващите съоръжения. Относно проблемите свързани със системата за автоматизация е необходима промяна на настройките съобразена с мощността на задвижващите съоръжения и с качествата на преработваните отпадъци. Все пак намаляването на броя на спиранията в завода зависят от персонала, който трябва да бъде по-добре обучен и мотивиран, чрез въвеждане на по-ясни критерии за кариерно израстване. Авторите вярват, че с внедряване на така предложените мерки за решаване на възникналите проблеми ще се намалят производствените разходи и ще повиши производителността и икономическия ефект.

Ключови думи: авария, корозия, електрически и механически повреди, инсталация за модифицирано гориво

Introduction

The rapidly evolving technologies, the high demands and the growing purchasing power of consumers are connected with the generation of more wastes, too. Natural resources are getting exhausted and this necessitates policies for a wiser management of wastes. These policies are associated with waste processing and re-use. With the development of the industry, an increasing number of enterprises is closing their work cycle in terms of generation and recovery of wastes. Therefore, waste management enterprises are in the service not only of the public but also of the industry to which they supply ready-made raw materials. Their own benefit is twofold - they work to minimise environmental pollution and produce resources for large processing companies, which is also associated with making profits. Effective waste management work requires the faultless operation of the working process and a low cost per unit of processing, which is achieved by meeting the criteria set in the technological cycle.

The purpose of this report is to examine malfunctions and to summarise the reasons for the necessity for early repairs in a newly-erected enterprise. The subject of the report is the premises and the adjoining facilities on the territory of a waste treatment plant.

The occurrence of malfunctions in the situation under consideration is a casual process despite the experience gained in the construction of such types of enterprise in other countries. This report aims at tracking the work of the structural units and analysing the trend of facility failures; both will lead to

taking timely actions to ensure the uninterrupted production process. Based on the problems identified and on the analysis of the causes, and following the generation of a sufficient amount of data, a risk assessment report can be produced for upcoming periods of time. Unfortunately, the experience of other authors can not be referred to since the conditions in every specific enterprise are individual and non-characteristic.

After a new plant has been constructed and commissioned, it is supposed to function flawlessly during the first years and no repairs are expected to be needed. Each plant like this has a specific structure and the adjoining facilities have a different operating period that depends on the construction and the functions they perform. In the course of the operation, each waste treatment facility is subjected to mechanical and physico-chemical peak loads.

Major structural units in a waste treatment plant

Non-hazardous waste landfill. The landfill is divided into two functional areas: first waste disposal area and a second waste pre-treatment area that incorporates a plant for mechanical and biological treatment. The block diagram of the non-hazardous waste landfill is presented in Figure 1.
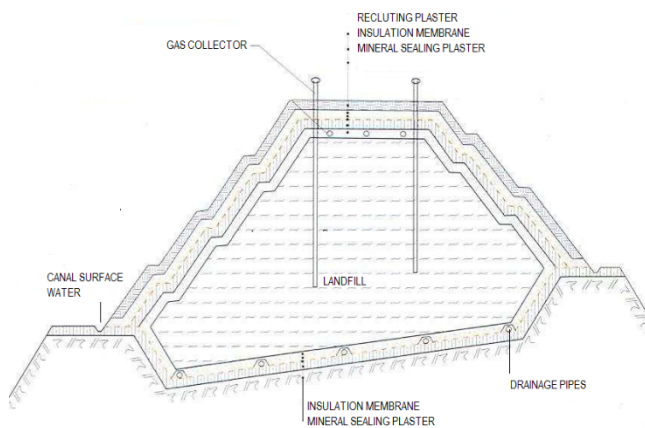

Fig. 1. Structure of the non-hazardous waste landfill

The landfill is constructed with an insulating screen at the bottom - to protect the soil and groundwater; collection and treatment of the infiltrate in a waste water treatment plant (WWTP) - to protect groundwater from pollution; biogas management - to prevent uncontrolled emissions into the atmosphere; placing wastes in cells - for operational control and reducing rainwater penetration; waste compacting - to limit pest access, to reduce the risk of fire, and to help stabilise the body of the landfill; daily and intermediate covering; final sealing.

Plant for mechanical and biological treatment (MBT) of wastes with the production of RDF fuel

The plant for mechanical and biological treatment is adjacent to a non-hazardous waste landfill. The plant processes household waste (except for the bio waste and the green waste that are collected separately). The process of mechanical and biological treatment includes the following steps: mechanical/manual separation and sorting, biological treatment of organic waste, and the production of refuse derived fuel (RDF)l. The origin of waste is: domestic waste (waste from households) and waste generated by shops, warehouses,

offices, and factories (industrial waste). The MBT facility consists of:

• Classification line for recyclable materials separated from specific suitable waste streams, such as paper, cardboard, plastics and metals.

• An RDF generating plant where high-calory fractions of bio-waste (some sorts of paper, cardboard, and mostly plastic) are released in the form of RDF. RDF is mainly released after drying the waste to a certain extent. Bio-waste drying is carried out as a combination of the stages of biological drying and thermal drying. The duration and the combination of processes take a minimum of 6 weeks, depending on the requirements posed to the products.

The article studies the individual processing units in a waste management plant. Each of these is analysed in terms of the problems that have arisen. The technology in the plant is given in the diagram in Fig. 2.
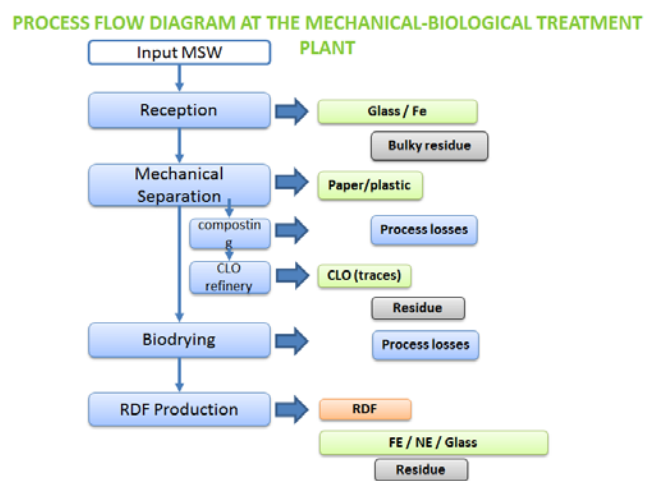
Fig. 2. Flowchart of the waste management process

The malfunction analysis involves exploring the causes of their occurrence. As a summary of the various problems, we offer the following groups:
- technological problems;
- constructive;
- building;
- mechanical - erosion, friction, pressure, vibration;
- chemical - corrosion;
- electrical;
- the human factor.

Monitoring and inspection

Monitoring and inspection provide evidence for the work performed in accordance with the adopted criteria. Concurrently, it allows for improvements to be made. Two types of inspection are possible to use - active and reactive monitoring (Brouwer, 1998). Based on the active monitoring, the risk for the system is predicted, feedback is provided related to the process management, and malfunctions are avoided. Reactive monitoring includes a "post-failure" record, reviews, repair incidents, and other evidences of the lack of adequate management. When managing a waste treatment plant, it is

necessary to ensure the efficient operation of the facilities. For the prevention of emergency situations, it is appropriate to apply active monitoring, which will determine the subsequent accumulation of a significant database. The subsequent analysis will result in the outlining of appropriate management policies and measures that aim at achieving the safety of both the installation and, as a leading requirement, the staff .

Technological problems / causes

The major problems in the plant are related to the project morphology of the waste, which differs from that of the currently incoming waste in the plant. Namely, the waste is of a higher humidity (up to 45% higher) and of a higher percentage of sand, dust, soil, building materials, and other inert materials. Over the heating period, an increased content of cinder and ash is observed, by up to 9%. The high content of dust, ash, and inert materials brings about clogging of the moving floors and heavier dust-loading in the buildings.

Trommel screening with a diameter of 200 mm is technologically inappropriate, since a significant proportion of PET bottles and other plastic materials that are of high cost if recycled fall out. Those do not go through manual separation; instead, they pass directly into the cells for bio-drying, which makes them impossible to be the objects of the recycling process, thus the recycling targets are not achieved. In bio-drying, there are 26 cells operating on a 7-day technological period of drying. Upon completion, the dried waste has a humidity of up to 20%. There is a tendency for a steady rise in humidity to 32-33%, with cells where humidity soars to 36-37%. This t is indicative of the fact that the technological scheme and the software do not allow for the waste to be dried in compliance with the requirements of the contracting authority. Adding to the problems of the heavy dust-loading, the poor performance of the taps, and the high incidences of cell fan failures, there is a clear indication as to the connectivity among electrical, mechanical and technological problems. The insufficiently dried material goes to the RDF (waste fuel) building. Excessive humidity and the high content of non-combustible inert materials in the incoming material lead to the wear of the vibration screens, the tear of the elastic membranes, congestion of the densitometric tables, blocking-up of other technological sieves. All of these result in ceasing of the operation of the production area for a long period of time in order to recover the electrical and mechanical systems.

Structural problems / reasons

In the present case, by a structural problem, we mean the design of the plant's processing lines. The RDF plant is designed after the model of enterprises with a similar object abroad. A special feature in this case is the presence of a sloping terrain that the designers have not taken into consideration because the processing line of the material goes from a lower to a higher point. This is related to the raising and movement of large masses of materials (recyclable raw materials), which is associated with economic losses. On the one hand, the introduction of engines and equipment for the lifting of these raw materials is required, and on the other hand, a huge amount of electricity is used for their operation. The economic effect would greater be if the production line moved from a higher to a lower level, whereby the materials would move by their own mass.

The manual classification lines are mounted at a higher level which poses difficulties for the workers and, similarly, makes attendance of the entire belt difficult. It is necessary to adjust the height of the floor from the manual sorting position. Another problem that violates the ergonomics of the working environment is the poor sealing of the windows in the control room, as a result of which polluted air from the hall penetrates into the manual sorting area.

We have also established the lack of shutters that open easily for access to various service premises. Besides, there are no rubber muffs on the ears through which the lighting cables pass and no railings along the bio-basins. To a large extent, these deficiencies incur risks for the employees of the enterprise. It is also imperative to put warning notices and information boards in Bulgarian.

Building problems

During the erection of the building, the contractor has overlooked some mistakes made, e.g. the concrete flooring around an expansion joint (between the concrete flooring and the asphalt pavement) at the exit from the mechanical and biological treatment plant was damaged; the cover of the W&S manhole in front of the electric substation 110/20 kV did not close tightly; there were no restrictive lines; the pavement around the transformer building was unfinished; newly formed cracks in the reinforced concrete pavement around switchboards were visible; the flooring in the pedestrian areas was missing or unfinished. All these problems have been resolved after a signal from the responsible bodies at the plant. In connection with the poor quality of the building work or with the fact that it was incomplete, the conclusion can be drawn that a number of rules and regulations related to the safety technique were violated, such as ORDINANCE № 5 of 21st May 2001, ORDINANCE № 8121z – 647 of the 1st October 2014, ORDINANCE № RD-07/8 of 20th December 2008, technical safety measures of the Safety and Health Regulations for the Operation of Eelectrical Equipment with Voltages of up to 1000V of 2014, requirements for safe use and operation of buildings, etc.

Mechanical problems

Mechanical problems have been found in all the buildings of the enterprise. Due to the poorly executed project in the reception building, material falls out on either side of the moving floor with a separating drum. This leads to the clogging of the bunker under the dosing drum. Cleaning itself is very labor-consuming and requires the participation of several workers. When belt conveyors were designed, no side guards and canvases were provided which is considered to be a disadvantage since part of the material falls out. A possible solution to the problem is to place a device to collect the pieces and take them aside. Due to the established structural peculiarities and the presence of raw materials to be processed that are heavier than the technologically set, a problem appears in various facilities mostly related to the leakages of oil in the following: the compressors; the chain conveyor with a de-compacting block where oozing of oil out of the gear box is seen; the feeding conveyor to the baling press. Overheating of some items of equipment has also been registered (for instance, the front bearing of the sleeve filter fan motor from the reception area gets excessively heated).

Another purely mechanical problem is the high level of dust in the RDF-production building which is the result of non-efficient operation of the dedusting system in the building. This poses considerable risks for the formation of explosive air-dust mixtures. The problem can be solved with the implementation of more powerful fans.

Also, non-efficient separation of glass from fraction 30-60 mm has been established which necessitates the installation of a separator functioning along a different principle.

Corrosion problems

Corrosion of the metal and concrete surfaces is a registered problem and at present the corrosion processes of the various facilities are monitored. The reasons are: the ill-painted protective coating on the metal elements and damages inflicted on them, the heavy mechanical loads they sustain, and, most of all, the aggressive environment

On the territory of the infiltrated water treatment plant, the most serious corrosion damage is the initiated corrosion of the drainage pipes. As a result of the analysis, it was established that a failure can occur due only to the advancement of corrosion processes, but not due to mechanical stress. The installed plant facilities are also subject to corrosion due to evaporation of infiltrated waters. With these facilities, faults can also occur due to mechanical reasons - friction of moving parts, erosion of the deposition of solids in the fluid, fluid pressure at the pumps. After analysing the infiltrated water and of the atmosphere around the equipment, it may be generalised that the causes of the corrosion are: the corrosive action of the agents in the environment (ammonium nitrogen (NH4-N), organic carbon, sulfates, chloride and oxygen), depolarisers from the air, temperature amplitudes due to seasonal changes, and an atmosphere rich in chlorine ions. These factors create conditions for accelerating the processes of oxidation and for the occurrence of oxide covering layer with weak protective properties that disintegrates under the action of chlorine ions. Consequently, uniform corrosion and pitting corrosion occur, and, due to the presence of anaerobic bacteria, microbiological corrosion is also possible.

To prevent the processes leading to failures, the following measures are recommended: the choice of a material suitable for the construction of the facilities and the pipes, the construction of protective gearboxes, placing the appropriate insulating coatings of the pipes, surface treatment of the equipment.

For facilities subjected to atmospheric corrosion, the suitable alloying elements are Sn, Cu, Ni, and some rare earth elements. Nitrogenation (doping with nitrogen) is suitable only for these facilities because it prevents the development of cracks. For the pipes, the recommended alloying elements are Cr, Si, Ni, and Mo or the so-called chromium-nickel steels or chromium-nickel-molybdenum steels. For all facilities on the territory of the WWTP, it is necessary to use a material with fine-grained structure, e.g. austenitic steel, and to avoid martensite (coarse-grained) structures. The following brands of steel can be recommended: 10H14G14N4T, 10H14AG15, and 07H13AG20 which are substitutes for steel type H18N10T in environments with relatively low aggressiveness.

Various laser and ultrasonic techniques are used to treat the pipe surfaces. Those lead to the removal of local dislocations, the hardening of materials, and the like. For example, laser decontamination or pre-treatment at high temperature or under high pressure contributes to the stability of the micro-grained structure of the steel, and in this case is recommended for both equipment and pipes. The formation of a passive layer under the influence of dynamic polarisation between hydrogen and oxygen, the exposure to UV light, or electropolishing, results in reduced development of local destruction. The materials used are argon, sodium nitrate or phosphate.

As a lining material for the walls of new pipes, in view of the composition of the corrosive environment, polystyrene, fiberglass, epoxy polymers, laminated fabric, silicone rubber, rubber with inhibiting substances in its composition, etc. are offered. As the facilities are operative and their premature replacement is economically unprofitable, in order to extend their operating life, it is recommended to cover them with boxes equipped with blowing fans. The same materials that were listed for pipe insulations, without the rubber, can be used for the boxes.

The use of an inhibitor in this case is inappropriate. On the one hand, there is a large flow of water along the tubes, and the inhibitors can only act in a limited volume. In addition, there are anaerobically active bacteria in the pipes that can also be affected, with the resulting negative effect produced on the production process. Devices operating in the workshop and above it can be treated with the compound 0.5 mM $SnCl_2$ (Kamimura, 2012), but there are chlorine ions in the medium, and further research is needed to determine the concentration and its effectiveness.

All these recommendations can be carried out after replacing the facilities. At this stage, the main tools for process control and for failure prevention remain the continuous inspection and the additional processing. Running facilities can be laser-cleaned: laser melting (LSM), laser alloying, or laser annealing. Laser Peening (Hackel, Rankin) is suitable for the processing of blades, fans, motors, and other moving parts, thus the risk of crack formation will be diminished. With respect to friction, laser transformation hardening needs to be carried out with moving parts for improving the wear resistance (Brown, 2010). Laser beating (Peyre, 2000) increases resistance to pitting corrosion that is obvious in all units in the shop.

Another important measure is building of additional monitoring systems. For this purpose, sensors operating on a resistive principle were installed in the infiltration tube section and the SBRs section to monitor the corrosion growth. The sensors measure levels of 1 mm, 2 mm, 4 mm, and 5 mm (Stefanov, Hristova, 2009). The material for making the sensors and the measured thicknesses are consistent with the material and thickness of the tubes. At present, corrosion growth has been reported in bio-basins and in SBRs, and none the infiltrated water section. Ultrasonic measurement is another suitable method for the non-destructive tracking of corrosion damage and cracks in the depth of the monitored objects. The level of corrosion in the equipment and in the pipes was inspected by means of the OLYMPUS company ultrasound thickness gauge 45 MG. The model provides options for recording previous measurements.

Electrical problems and such associated with the controlling and measurement equipment and automation

At the reception building, failures of the SCADA system for controlling and measurement equipment and automation are more serious. The system does not take into account the data from the scale integrators. There is a problem with their setup as the instruction is incomplete. For the time being, it is recommended to train the staff for: working with the software for setting-up the integrators, and monitoring for disconnected electrical cables that might lead to possible failures.

In the mechanical separation building, part of the material falls out of the 2nd rotary drum and under the floor. The problem is not mechanical, but is also related to the SCADA system. It is recommended to change the settings of the SCADA automatic system for the performance of the feeding conveyor in such a manner that the sieve is not overfilled. Naturally, a change of setting in the system for controlling and measurement equipment and automation goes with the requirement for new data. For instance, in the mechanical separation building, this necessitates the installation of a sensor that monitors the level of feeding the containers with recyclable materials.

Problems have been identified that are due to poor connection between electrical wires, or a problem in the software of the SCADA control system: e.g. there is no visualisation of the electric power in Transformer substation 1, Transformer substation 3, and Transformer substation 4 in electrical sub-station 110/20 kV.

Because of unfinished or incomplete setup of the SCADA control system, other serious problems have been identified as well. Some of them are as follows:
- in the reception building, some of the integrators are not connected to the SCADA system;
- in the reception building and in the bio-drying building, the unfinished adjustment of the SCADA control system causes problems to the function of the Valtorta bridge cranes, with all consequences for the operation of the above in automatic mode; besides, the Valtorta command console system is not translated into the Bulgarian language, thus hindering staff operation;
- in the reception building, communication errors between the entrance weighbridge and the SCADA system have been registered that impose manual operation; this leads to delays in the technological process;
- in the mechanical separation building, no information in SCADA is available as to the feeding of the reception bunker;
- in the mechanical separation building, upon starting the process line, the shredder indicates an error;
- in the mechanical separation building, the information is not entered in MOTION SCADA; troubles in the whole system have been established;
- in the biological drying building, the information from MOTION SCADA does not read the real periods of time set by the operator, thus restricting the opportunities to check the quantities of incoming and outgoing material to/from the building;
- when changing the direction of the belt conveyor (reversible) that feeds ferrous metals to two containers, the SCADA system makes it possible to change the direction only from container 2 to container 1, but not from container 1 to container 2.
- in the biological drying building, while the crane operates in manual mode, it is not possible to record the quantity of the material that is being fed to the cells and from the cells to the movable floors;
- in the RDF-production building, interruptions are frequent due to activation of the overload protection of the belt conveyor; the problem may as well be mechanical because of the heavier material;
- there is a problem with the automatic switching and adjustment of the belt conveyor (collective for PVC); a new control system for the engine revolutions is needed.

There are also a number of problems that result from sensor malfunctioning. For example, in the bio-drying building, the water level sensor in the tub of the cooling tower is mounted but does not work properly. Baling presses cause incessant interruptions of the technological process due to problems with the sensors for the waste level in the bunkers, as well as to problems with the devices for the wire tightening. To solve these problems, calibration of the sensors measuring various indicators is advisable to be carried out and the required documents to be presented by the manufacturing company.

Problems have been identified that relate to the presence of higher current and voltage harmonics, as well as to losses in transformers. Variable active filters to suppress harmonics are installed to improve network characteristics, as well as a variable anti-resonant harmonic filter. Those are connected in parallel to the respective modules and are controlled by a controller. Theoretically, when introducing them, electrical energy savings should be reported, along with an increase in the reserve and the power capacity charge of the electrical installation, and hence a reduction in maintenance costs. In practice, however, the realisation of the estimated benefits has not been proven.

To achieve an efficient and fault-free process, it is necessary to install such automation tools as:
- emergency stop buttons on the magnetic separators;
- an emergency stop button for the movable floors in the reception hall; this might speed up the operators' reaction in an emergency situation (e.g. if waste that has is not intended for the mechanical and biological treatment (MBT) plant falls on the movable floor.

It can be seen that the major problems are related to the automatic control system that does not always work properly. A conclusion can be drawn that the problems found are three - interrupted cables, sensors that are out of order, or inappropriate SCADA settings. Therefore, it is necessary to introduce wireless data transmission.

Problems associated with the human factor

A complete documentation is provided to change the settings of the control system. It is imperative that the personnel who handle the individual modules be well-trained to work properly with the software that is currently causing problems. Inscriptions in the Bulgarian language should be placed on for various objects. Besides, clear criteria for career prospects must be introduced that will bring about self-training initiatives.

This, in turn, will optimise the process of working with the SCADA system.

To sum up:

Only after the problems have been classified is it possible to take differential measures to solve them. It is clear that constructive features can not be changed. What matters in this case is that this problem should be taken into account by constructors when building similar plants on other premises. Construction waste and unfinished objects have been removed. Mechanical problems are caused by the larger mass of the processed waste. Those can gradually be resolved by replacing the driving equipment. For the time being, each separate engine requires inspection by a specialist who can offer adequate solutions.

Problems related to the automation system are the result of the waste morphology and of the presence of mechanical problems. To fix them, it is necessary to change the settings in accordance with the power of the drive equipment and the quality of the waste processed. Because of the distributed structure of the enterprise, a modular system for measurement and control is appropriate. Modules in all workshops must be compatible with the overall system and be capable of wireless data transmission. According to the significance of the measured value, data can be transmitted on a continuous basis, once a day, or when a value has been measured whose magnitude deviates from the standard value. Continuous data submission is required for all engines, pumps, and dispensers. With corrosion monitoring, switching on is only necessary when deviation has been measured.

Conclusion

It can be concluded that the problems in the enterprise are caused by the incorrect design of the facilities, the morphology of the waste generated by the respective region, and the lack of well-trained staff. This also generates the deficiencies in the automatic control system and brings about machine failures. The measures recommended are prompted by the expertise of the specialiststhat has been gained as a result of the inspections carried out and measurements made. The human factor, supported by an adequate monitoring system, is essential for the prevention of malfunctions. In this manner, unnecessary repairs are avoided and the outcome is a better economic result. No risk assessment has been performed which is due to the lack of accumulated data on the failures of the various facilities and systems. In order to achieve the quality of management of the production process and to reduce the risk of malfunctions, after accumulating data about accidents and subsequent repairs, the reliability theory can be applied for each site on the premises of the enterprise.

References

Стефанов С., Т. Христова, Използване на резистивни датчици за следене на корозията по подземни тръбопроводи, Минно дело и Геология, бр.10, 2009, стр. 42-44 (Stefanov S., T. Hristova, Izpolzvane na rezistivni datchitsi za sledene na koroziata po podzemni traboprovodi, Minno delo I geologia, br. 10, 2009, str. 42-44).

Brown M. S., C. B. Arnold, Fundamentals of Laser-Material Interaction and Application to Multiscale Surface Modification, book, http://www.princeton.edu/.

Brouwer, R. C. Corrosion Management in PDO, Proc. 8th Middle East Corrosion Conference, pp 239–244, Bahrain, Pub.The Bahrain Soc. of Engineers & NACE International, 1998.

Hackel L., J. Rankin, M .Hill., Production Laser Peening of High Strength Metals, Metal Improvement Company, Livermore, California, http://www.metalimprovement.com/.

Kamimura T., K. Kashima, K. Sugae, H. Miyuki, T. Kudo, The role of chloride ion on the atmospheric corrosion of steel and corrosion resistance of Sn-bearing steel, Corrosion Science, Volume 62, p. 34–41, 2012.

Peyre, P., X. Scherpereel, L. Berthe, C. Carboni, R. Fabbro, G. Beranger, and C. Lemaitre, Surface Modifications Induced in 316L Steel by Laser Peening and Shot Peening. Influence on Pitting Corrosion Resistance, Materials Science and Engineering A, 280, 294-302, 2000.

http://www.hse.gov.uk/landuseplanning/failure-rates.pdf accessed 2 May 2017.